Oxidation Communications 33, No 3, 485–501 (2010)

SUPRAMOLECULAR REACTION OF LAUROYL PEROXIDE WITH TETRAALKYLAMMONIUM BROMIDES

N. A. TUROVSKIJ[a]*, E. N. PASTERNAK[b], E. V. RAKSHA[a],
N. A. GOLUBITSKAYA[a], I. A. OPEIDA[b], G. E. ZAIKOV[c]

[a]*Donetsk National University, 24 Universitetskaya Street, 83 055 Donetsk, Ukraine*; *Ukrainian-American Laboratory of Computational Chemistry, Kharkov, Ukraine, Jackson, USA*
[b]*Institute of Physico-organic and Coal Chemistry, National Academy of Sciences of Ukraine, 70 R. Luxemburg Street, 83 114 Donetsk, Ukraine*
[c]*Institute of Biochemical Physics, Russian Academy of Sciences, 4 Kosygin Street, 117 334 Moscow, Russian Federation*
E-mail: *turov@dongu.donetsk.ua*; *chembio@sky.chph.ras.ru*

ABSTRACT

Activated decomposition of lauroyl peroxide in the presence of tetraalkylammonium bromides (Alk_4NBr) has been studied. The ammonium salts show catalytic properties in the system. The initiation efficiency of the binary system lauroyl peroxide – Alk_4NBr has been studied. The causes of peroxide bond chemical activation are considered on the basis of experimental results and results of molecular modelling of the activated peroxide decomposition. The supramolecular mechanism is proposed for the peroxide decomposition in the presence of tetraalkylammonium bromides.

Keywords: lauroyl peroxide, quaternary ammonium salts, catalysis, supramolecular mechanism, initiation efficiency, molecular modelling.

AIMS AND BACKGROUND

Peroxide compounds are widely used as initiators of radical-chain processes[1]. Presence of –O–O– bond in peroxide structure provides the thermal instability of the peroxide compounds. Chemical activation of the homolytical peroxides decomposition allows to create new effective initiating systems for radical processes. In radical-chain reactions the initiation stage determines the process rate and thus the process efficiency. The initiation stage rate is significantly dependent on the rate of initiator decomposition and efficiency of the initiator. The characteristic feature of the activated decomposition of peroxides in the presence of onium salts is providing of radical-chain reactions initiation at 293–303 K (Refs 2–4).

* For correspondence.

Lauroyl peroxide (LPO) is a representative of diacyl peroxides and it is widely used for initiation of radical processes[1,5,6]. In the present work the results of activated decomposition of lauroyl peroxide in the presence of tetraalkylammonium bromides are presented. The initiation efficiency of the binary system LPO–Alk_4NBr has been studied. The causes of peroxide bond chemical activation are considered on the basis of experimental results and results of molecular modelling of the activated peroxide decomposition.

EXPERIMENTAL

The peroxides purity (98.9%) was controlled by iodometry method. Tetraalkylammonium bromides were recrystallised from acetonitrile solution by addition of diethyl ether excess. The salt purity (99.6%) was determined by argentummetric titration with potentiometric fixation of the equivalent point. Acetonitrile (CH_3CN) was purified according to Ref. 7. Its purity was controlled by electroconductivity χ value, which was within $(8.5 \pm 0.2) \times 10^{-6}\ \Omega^{-1}\,cm^{-1}$ at 303 K. Isopropylbenzene (IPB) was subjected to acid-alkali purification with subsequent desiccation under calcium chloride and distillation according to Ref. 8. Reactions of LPO decomposition were carried out in glass soldered ampoules in argon atmosphere. To control the proceeding of peroxide thermolysis and their decomposition in the presence of Alk_4NBr the iodometric titration with potentiometric fixation of the equivalent point was used. IPB oxidation was carried out in acetonitrile in the glass reactor placed into thermostat. The reactor was shaking up with a frequency which provided mixing sufficient for the reaction proceeding in the kinetic region. Accuracy of the determination of the absorbed oxygen amount is 5%.

Quantum chemical calculations of peroxide molecule and corresponding radicals were carried out by AM1 semi-empirical method implemented in MOPAC2007™ package[9]. The RHF method was applied to the calculation of the wave function. Optimisation of peroxide structure parameters was carried out by Eigenvector following procedure. The molecular geometry parameters were calculated with boundary gradient norm 0.01. The peroxide bond homolysis has been followed by the reaction coordinate method, taking the internuclear distance corresponding to the peroxide bond as the reaction coordinate.

RESULTS AND DISCUSSION

KINETICS OF LAUROYL PEROXIDE DECOMPOSITION ACTIVATED BY TETRAALKYLAMMONIUM BROMIDES

Study of the kinetic features of lauroyl peroxide decomposition in the presence of tetraalkylammonium bromides is necessary for the quantitative estimation of the initiating activity of the system in radical reactions.

The kinetics of the LPO decomposition activated by Alk_4NBr has been studied at 313–333 K, and the peroxide thermal decomposition has been studied at 343–363 K. The peroxide decomposition was carried out in isopropyl benzene (IPB) – acetonitrile (CH_3CN) (1:1) solution in argon atmosphere. The LPO decomposition activated by Alk_4NBr (Et_4NBr, Et_2Benz_2N, Pr_4NBr, and Bu_4NBr) was carried out at equimolar reagents concentration. The LPO decomposition kinetics has been investigated up to 40–50% of peroxide conversion. The reaction kinetic parameters obtained are listed in Table 1.

Table 1. Kinetic parameters of lauroyl peroxide thermolysis and decomposition activated by Alk_4NBr CH_3CN – IPB (1:1); $[Alk_4NBr]_0 = [LPO]_0 = 2\times10^{-2}$ mol dm^{-3}

Alk_4NBr	T (K)	$k\times10^3$ (dm^3 mol^{-1} s^{-1})	E_a (kJ mol^{-1})	lg$A$ (A, dm^3 mol^{-1} s^{-1})
Thermolysis	343	$(2.13 \pm 0.08) \times 10^{-5}$, s^{-1}	129 ± 2	14.9 ± 0.4
	353	$(7.38 \pm 0.07) \times 10^{-5}$, s^{-1}		
	363	$(2.74 \pm 0.09) \times 10^{-4}$, s^{-1}		
Et_4NBr	313	4.0 ± 0.2	81 ± 1	11.1 ± 0.2
	323	10.1 ± 0.4		
	333	26.0 ± 0.9		
Et_2Benz_2NBr	313	3.2 ± 0.1	89 ± 2	12.4 ± 0.3
	323	8.8 ± 0.3		
	333	25.0 ± 1		
Pr_4NBr	313	2.59 ± 0.07	96 ± 1	13.4 ± 0.2
	323	8.3 ± 0.2		
	333	23.6 ± 0.3		
Bu_4NBr	313	1.68 ± 0.05	110 ± 4	15.7 ± 0.7
	323	7.0 ± 0.1		
	333	21.4 ± 0.5		

The rate constants of the activated LPO decomposition (k) listed in Table 1 decrease in the following way: $Et_4NBr > Et_2Benz_2NBr > Pr_4NBr > Bu_4NBr$. They are drawing nearer with temperature increase. In this reaction series an isokinetic relationship is observed (Fig. 1) with isokinetic temperature of 338 K. The compensation relationship can be due to the effect of the tetraalkylammonium cation.

Investigation of the LPO thermal decomposition has revealed that thermolysis kinetics was not complicated by decomposition products up to 50% peroxide conversion. The rate constants and activation parameters of LPO thermal decomposition in CH_3CN – IPB (1:1) solution are also listed in Table 1. Thus, tetraalkylammonium bromides activate the lauroyl peroxide and decrease the activation barrier of the peroxide decomposition reaction.

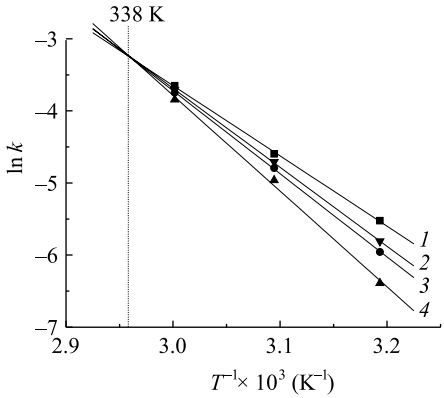

Fig. 1. Temperature dependence of the rate constant of LPO decomposition activated by Alk_4NBr CH_3CN – IPB (1:1), *1* – Et_4NBr**,** *2* – Et_2Benz_2NBr , *3* – Pr_4NBr, *4* – Bu_4NBr

ISOPROPYLBENZENE OXIDATION INITIATED BY LAUROYL PEROXIDE – TETRAALKYLAMMONIUM BROMIDE SYSTEM

Processes of radical-chain oxidation of hydrocarbons by molecular oxygen in liquid phase proceed usually according to the scheme of branched chain reaction. Products with branched chains (hydroperoxides) provide the rate of radicals formation near 10^{-9}–10^{-8} mol dm^{-3} s^{-1} (Ref. 10). In the presence of peroxide initiators the hydrocarbons oxidation proceeds as chain reaction[1,9] according to reactions (1)–(8). Chains are generated with initiation rate W_i. At high temperature rate W_i is large and hydroperoxide radical decomposition makes insignificant contribution into initiation, and during the reaction constant value of W_i is observed. Oxidation process develops as chain flat reaction.

$$\mathrm{ROOR} \xrightarrow{k_0} 2\mathrm{RO}^{\cdot} \qquad \text{(1) initiation stage}$$

$$\mathrm{RO}^{\cdot} + \mathrm{PhCH(CH_3)_2} \longrightarrow \mathrm{ROH} + \mathrm{PhC}^{\cdot}\mathrm{(CH_3)_2} \qquad \text{(2) initiation stage}$$

$$\mathrm{PhC}^{\cdot}\mathrm{(CH_3)_2} + \mathrm{O_2} \xrightarrow{k_1} \mathrm{PhC(CH_3)_2OO}^{\cdot} \qquad (3)$$

$$\mathrm{PhC(CH_3)_2OO}^{\cdot} + \mathrm{PhCH(CH_3)_2} \xrightarrow{k_p} \mathrm{PhC(CH_3)_2OOH} + \mathrm{PhC}^{\cdot}\mathrm{(CH_3)_2} \qquad (4)$$

$$\mathrm{PhC(CH_3)_2OOH} \xrightarrow{k_3} \mathrm{PhC(CH_3)_2O}^{\cdot} + {}^{\cdot}\mathrm{OH} \qquad (5)$$

$$\mathrm{PhC}^{\cdot}\mathrm{(CH_3)_2} + \mathrm{PhC}^{\cdot}\mathrm{(CH_3)_2} \xrightarrow{k_4} \qquad \text{(6) chain termination}$$

$$\mathrm{PhC}^{\cdot}\mathrm{(CH_3)_2} + \mathrm{PhC(CH_3)_2OO}^{\cdot} \xrightarrow{k_5} \qquad (7)$$

$$\mathrm{PhC(CH_3)_2OO}^{\cdot} + \mathrm{PhC(CH_3)_2OO}^{\cdot} \xrightarrow{k_t} \qquad (8)$$

Reaction of PhC$^{\bullet}$$(CH_3)_2$ radicals with O_2 proceeds very fast and in the presence of dissolved oxygen ($[O_2] > 10^{-4}$ mol dm^{-3}) the relationship $[R^{\bullet}] << [RO_2^{\bullet}]$ is observed. Thus, reaction (4) limits chain propagation, chain termination proceeds practically only by reaction (8), whereas reactions (6) and (7) are negligible. In the presence of the initiator (I) the hydroperoxide $PhC(CH_3)_2OOH$ decomposition (reaction (5)) is not of great importance and thus $W_i = k_i$ [I]. If the chains terminate only by reaction (8) stationary radical concentration in the system sets in time $(W_i\, k_t)^{-1/2}$. Usually $W_i = 10^{-7}$–10^{-5} mol dm^{-3} s^{-1}, and $(W_i k_t)^{-1/2} = 0.1$–10 s, so stationary radical concentration sets quickly. In conditions of long chains the present relations are accomplishable $\nu = W/W_i \geq 10$, $k_1[O_2][R^{\bullet}] = k_p[RH][RO_2^{\bullet}]$, and $[R^{\bullet}]/[RO_2^{\bullet}] = k_p[RH]/k_1[O_2]$, i.e. at high oxygen concentrations the oxidation rate does not depend on the O_2 concentration and can be described by the following equation:

$$W_0 = \frac{k_p}{\sqrt{2k_t}}\,[RH]\,\sqrt{W_i} \qquad (9)$$

where k_p (dm^3 mol^{-1} s^{-1}) is the rate constant of chain propagation reaction; k_t (dm^3 mol^{-1} s^{-1}) – the rate constant of chain termination reaction; W_i (mol dm^{-3} s^{-1}) – rate of the initiation reaction; W_0 (mol dm^{-3} s^{-1}) – initial rate of the oxidation reaction. Initiation rate can be obtained from the oxidation rate on the basis of known value of constants ratio $k_p/(2k_t)^{1/2}$ that depends on the solvent and temperature.

The investigated system LPO–Alk_4NBr can be used for radical generation in the processes of liquid phase hydrocarbons oxidation in mild conditions. The isopropylbenzene oxidation by O_2 initiated by LPO in the presence of Alk_4NBr has been studied ($[IPB]_0 = 3.58$ mol dm^{-3}, $[LPO]_0 = 2 \times 10^{-2}$ mol dm^{-3}, $[Alk_4NBr]_0 = 2 \times 10^{-3}$ mol dm^{-3}). The IPB oxidation initiated by LPO only ($[LPO]_0 = 2 \times 10^{-2}$ mol dm^{-3}) at 313 K in CH_3CN – IPB (1:1) for 2 h was not observed. Addition of catalytic amounts of tetraalkylammonium bromides ($[Alk_4NBr]_0 = 2 \times 10^{-3}$ mol dm^{-3}) leads to the system activation, and in these conditions the initiated IPB oxidation is now observed. The kinetic data analysis has shown that in the initial period of oxidation reaction the oxygen consumption is linearly dependent on time (Fig. 2). It allows to calculate the initial rate of initiated oxidation W_0 (Table 2) as the slope of experimental curves ($r = 0.99$).

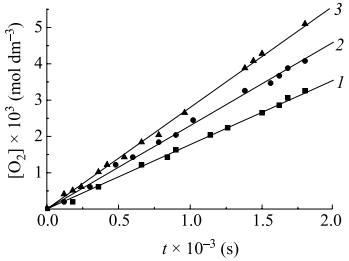

Fig. 2. Kinetic curves of IPB oxidation initiated by LPO in the presence of Alk_4NBr at 313 K

CH_3CN – IPB (1:1); $[IPB]_0 = 3.58$ mol dm^{-3}, $[LPO]_0 = 2\times 10^{-2}$ mol dm^{-3}, $[Alk_4NBr]_0 = 2\times 10^{-3}$ mol dm^{-3}; *1* – Bu_4NBr; *2* – Pr_4NBr; *3* – Et_4NBr

The rate of initiation (W_i) was estimated according to equation (10), where W_0 is the initial rate of the IPB oxidation; k_p, k_t are the rate constants of chain propagation and termination, correspondingly.

$$W_i = \frac{W_0^2}{\left(\frac{k_p}{\sqrt{2k_t}}\right)^2 [RH]^2} \tag{10}$$

$k_p/(2k_t)^{1/2}$ values were estimated by inhibitor method. Temperature dependence of $k_p/(2k_t)^{1/2}$ was determined within 303–339 K at IPB oxidation in acetonitrile (CH_3CN: IPB = 1:1) initiated by benzoyl peroxide in the presence of quaternary ammonium halides and by AIBN (Ref. 2). It is described by the following equation:

$$\ln (k_p/(2k_t)^{1/2}) = (5.1 \pm 1.4) - (3.5 \pm 0.5)\ T^{-1} \tag{11}$$

The obtained values of the initiation rate of radical-chain IPB oxidation initiated by LPO in the presence of Alk_4NBr are listed in Table 2. Initial rates of IPB oxidation initiated by LPO–Alk_4NBr system decrease in the following way: $Et_4NBr > Pr_4NBr > Bu_4NBr$. Thus the rate of initiated IPB oxidation depends significantly on the structure of the tetraalkylammonium cation.

Table 2. Initiation rates of IPB oxidation initiated by LPO–Alk_4NBr system at 313 K $[LPO]_0=2\times 10^{-2}$ mol dm^{-3}; $[Alk_4NBr]_0=2\times 10^{-3}$ mol dm^{-3}; CH_3CN – IPB (1:1); $[IPB]_0 = 3.58$ mol dm^{-3}

Alk_4NBr	$W_0 \times 10^6$ (mol dm^{-3} s^{-1})	$W_i \times 10^8$ (mol dm^{-3} s^{-1})
Et_4NBr	2.8	13.7
Pr_4NBr	2.3	9.27
Bu_4NBr	1.8	5.68

The effect of the system components concentration on the kinetic parameters of IPB oxidation initiated by LPO in the presence of Bu_4NBr at 313 K has been studied. Increasing of components commensurable concentration by a factor of one order leads to corresponding tenfold increase in oxidation rate. Increasing of only one component concentration by a factor of one order leads to threefold increase in oxidation rate (Table 3). Since the oxidation rate is proportionate to $(W_I)^{1/2}$, the dependence of initiation rate from the concentrations of initiating system components can be described by the following equation:

$$W_i = k[LPO][Alk_4NBr] \tag{12}$$

Temperature dependence of the rate of IPB initiated oxidation (Fig. 3) in CH_3CN – IPB (1:1) was studied at equimolar concentration ratio of LPO and Et_4NBr. W_0 and W_i values for the oxidation reaction at different temperatures are listed in Table 4.

The temperature dependence of the initial oxidation rate is described by the following equation:

$$\ln W_0 = (15.0 \pm 0.5) - (70 \pm 1)\, R^{-1}\, T^{-1} \qquad (13)$$

Table 3. Kinetic parameters of initiated IPB oxidation at 313 K
CH_3CN – IPB (1:1); $[IPB]_0 = 3.58$ mol dm^{-3}

$[LPO]_0 \times 10^2$ (mol dm^{-3})	$[Bu_4NBr]_0 \times 10^2$ (mol dm^{-3})	$W_0 \times 10^6$ (mol dm^{-3} s^{-1})	$W_i \times 10^8$ (mol dm^{-3} s^{-1})	$[O_2]_t \times 10^2$ (mol dm^{-3})
2.0	2.0	6.12	65.6	5.6
0.2	2.0	1.73	5.25	2.6
2.0	0.2	1.80	5.68	2.8
0.2	0.2	0.57	0.57	0.90

Table 4. Initiating activity of LPO in the presence of Et_4NBr in IPB oxidation
$[IPB]_0 = 3.58$ mol dm^{-3}, $[LPO]_0 = [Et_4NBr]_0 = 2 \times 10^{-2}$ mol dm^{-3}; CH_3CN – IPB (1:1))

T (K)	$W_0 \times 10^5$ (mol dm^{-3} s^{-1})	$W_I \times 10^6$ (mol dm^{-3} s^{-1})
313	0.82	1.2
328	2.70	4.6
339	6.40	12.8

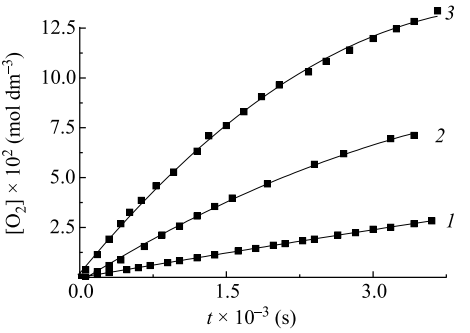

Fig. 3. Kinetics of oxygen consumption in IPB oxidation initiated by LPO–Et_4NBr system
CH_3CN – IPB (1:1); $[IPB]_0 = 3.58$ mol dm^{-3}, $[LPO]_0 = [Et_4NBr]_0 = 2 \times 10^{-2}$ mol dm^{-3}, temperature, K: *1* – 313; *2* – 328; *3* – 339

ESTIMATION OF THE INITIATION EFFICIENCY OF LPO – Alk_4NBr SYSTEM IN ISOPROPYLBENZENE RADICAL OXIDATION

The efficiency of initiating systems, i.e. radical yield on one decomposed peroxide molecule has been estimated on the basis of the following relationship:

$$e = W_i / W_p, \qquad (14)$$

where W_i, mol·dm^{-3} s^{-1} – initiation rate of oxidation reaction; W_p, mol dm^{-3} s^{-1} – rate of the peroxide initiator decomposition; e – initiation efficiency. Experimental data

obtained for IPB oxidation initiated by LPO in the presence of Bu_4NBr at 313 K are listed in Table 5. Initiation rates of isopropylbenzene oxidation reaction at different components ratio have been calculated according to equation (10). Value of $(k_p/(2k_t)^{1/2})$ at 313 K estimated according to relationship (11) was 2.11×10^{-3} $(dm^3\ mol^{-1}\ s^{-1})^{1/2}$. The rate of activated LPO decomposition (W_p, $mol \cdot dm^{-3}\ s^{-1}$) was estimated according to relationship (12) using k values, calculated from data listed in Table 1. Thus initiation efficiency of LPO in the presence of Bu_4NBr in the reaction of liquid phase IPB oxidation by O_2 is 0.86 ± 0.06.

Table 5. Kinetic parameters of initiated IPB oxidation at 313 K
CH_3CN – IPB (1:1), $[IPB]_0 = 3.58$ mol dm^{-3}

$[LPO] \times 10^2$ (mol dm^{-3})	$[Bu_4NBr] \times 10^2$ (mol dm^{-3})	$W_i \times 10^8$ (mol $dm^{-3}\ s^{-1}$)	$W_p \times 10^8$ (mol $dm^{-3}\ s^{-1}$)	e
2.00	2.00	65.6	67.2	0.98
0.20	2.00	5.25	6.72	0.78
2.00	0.20	5.68	6.72	0.84
0.20	0.20	0.569	0.672	0.85

Experimental results obtained have shown that temperature dependence of initiation rate of IPB oxidation initiated by LPO in the presence of Et_4NBr (Table 6) is described by equation (15). This equation can be used for the next estimations of initiation rate values at different temperatures. Initiation efficiency of LPO–Et_4NBr system in the reaction of initiated IPB oxidation is 0.75 ± 0.02 and does not depend on temperature.

$$\ln W_i = (16.9 \pm 0.6) - (80 \pm 2)\ (RT)^{-1} \qquad (15)$$

Table 6. Initiation efficiency of LPO in the presence of Et_4NBr in IPB oxidation
CH_3CN – IPB (1:1), $[IPB]_0 = 3.58$ mol dm^{-3}, $[LPO]_0 = [Et_4NBr]_0 = 2 \times 10^{-2}$ mol dm^{-3}

T (K)	$W_i \times 10^6$ (mol $dm^{-3}\ s^{-1}$)	$*W_p \times 10^6$ (mol $dm^{-3}\ s^{-1}$)	e
313	1.2	1.56	0.77
328	4.6	6.48	0.71
339	12.8	16.9	0.76

* W_p – rates of LPO decomposition activated by Et_4NBr were calculated on the basis of results listed in Table 1.

Rates of LPO decomposition activated by Alk_4NBr have been calculated for CH_3CN – IPB (1:1) solution at 313 K. Obtained values are listed in Table 7. The initiation rate values for the systems have been calculated on the basis of rates of IPB oxidation initiated by LPO in the presence of Alk_4NBr. Results listed in Table 7 show that the nature of tetraalkylammonium cation influences the initiation rate but has no effect on the initiation efficiency.

Table 7. Initiation afficiency of LPO in the presence of Alk_4NBr in IPB oxidation

CH_3CN – IPB (1:1), 313 K, $[LPO]_0 = 2 \times 10^{-2}$ mol dm^{-3}, $[Alk_4NBr]_0 = 2 \times 10^{-3}$ mol dm^{-3}

Alk_4NBr	$W_i \times 10^8$ (mol dm^{-3} s^{-1})	$W_p \times 10^8$ (mol dm^{-3} s^{-1})	e
Et_4NBr	13.74	16.00	0.86
Pr_4NBr	9.27	10.36	0.89
Bu_4NBr	5.68	6.72	0.85

The initiation rate and initiation efficiency of the LPO and binary system LPO–Alk_4NBr can be estimated. Initiation rates of IPB oxidation have been calculated by equation (10) and on the basis of data listed in Table 1. Initiation efficiency of the LPO in the reaction of IPB oxidation is 0.6. Initial rates of oxidation initiated by LPO calculated according to equation (10) are listed in Table 8.

Table 8. Kinetic parameters of initiated IPB oxidation
$[LPO]_0 = 2 \times 10^{-2}$ mol dm^{-3}, CH_3CN – IPB (1:1)

T (K)	$k_p \times 10^7$ (s^{-1})	$W_p \times 10^8$ (mol dm^{-3} s^{-1})	$W_i \times 10^8$ (mol dm^{-3} s^{-1})	$^{T}W_0 \times 10^6$ (mol dm^{-3} s^{-1})	$^{act}W_0 \times 10^6$ (mol dm^{-3} s^{-1})
298	0.198	0.040	0.048	0.094	2.13
303	0.478	0.096	0.115	0.18	3.3
313	2.56	0.511	0.614	0.59	8.2
318	5.68	1.14	1.36	1.05	12.5
328	26.1	5.21	6.26	1.16	27.9
339	125.6	25.1	30.1	9.83	63.7

Comparison of the oxidation rates of IPB oxidation initiated by binary system ($^{act}W_0$) calculated from equation (13) and oxidation rates of IPB oxidation initiated by LPO ($^{T}W_0$) has shown that the rate of oxidation reaction was 20 times higher in the presence of binary system at 298 K and only 5 times higher at 339 K (Table 8). Thus, using of the binary system is rational at low temperatures.

QUANTUM CHEMICAL MODEL OF THE LAUROYL PEROXIDE ACTIVATED DECOMPOSITION IN THE PRESENCE OF TETRAALKYLAMMONIUM BROMIDES

To investigate the role of chemical structure of the tetraalkylammonium cation in the chemical activation of the LPO the quantum chemical modelling of the investigated system has been carried out in the approximation of the substrate separated ion pair. This model has been proposed recently for the activated decomposition of benzoyl peroxide[11,12], dihydroxydicyclohexyl peroxide and hydroxycyclohexyl hydroperoxide[13], cumene hydroperoxide[14] in the presence of the quaternary ammonium salts. Complex formed in the system includes besides peroxide or hydroperoxide molecule also anion and cation of the ammonium salt (Fig. 4).

We proceed from the conception that the decomposition of peroxide is possible if ion–molecular bonding of peroxide molecule by onium salt leads to molecule configuration changes and brings the peroxide structure to the structure of the decomposition reaction transition state. It leads to decreasing of activation energy. For

peroxide complex construction the model of the LPO has been used (Fig. 5) for which the calculated value of dipole moment 0.96 D was in accordance with experimental one 1.32 D (Ref. 15).

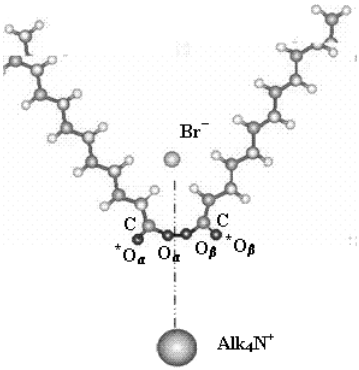

Fig. 4. Model of the complex between LPO and Alk_4NBr

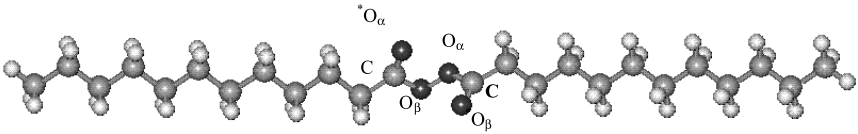

Fig. 5. Molecular model of the LPO

Associative interactions of LPO with cation and anion are accompanied by reorganisation of the peroxide structure. In the peroxide complex an elongation of peroxide bond is observed in comparison with non-bonded peroxide molecule, conformations of peroxide (COOC) and peroxyacyl torsion fragments changes significantly in the complex bonded peroxide as compared with free peroxide (Table 9). The extent of these changes depends on structure of quaternary ammonium cation that takes part in the complex formation. Such conformation changes of the peroxide structure are the determinative factor of peroxide bond activation. It clearly can be shown by changes in peroxide bond energy (i.e. total of electronic and nuclear energies of two-center term of O–O atom pair) $E_{\text{–O–O–}}$ and bond order value ($p_{\text{–O–O–}}$) (Table 9). Stable peroxide structure has the lowest O–O bond energy (–11.78 eV for free LPO) and less stable (or activated) peroxide conformation has the highest one (–11.05 eV for Et_4N^+…ROOR…Br^- complex). Difference between –O–O– bond energy in stable and activated peroxide structure ($\Delta E_{\text{–O–O–}}$) increases in the catalyst row: Bu_4NBr, Pr_4NBr, and Et_4NBr indicating weakening of the O–O bond in the ROOR–Alk_4NBr complex. The stable structure of free peroxide molecule has the highest bond order value whereas the lowest values are observed for complex-bonded peroxide structure (Table 9).

Table 9. Structural parameters of the free LPO and peroxide complexes

Object	r_{-O-O-} (Å)	E_{-O-O-} (eV)	p_{-O-O-}	Torsion angle (°)	
				COOC	OOC(O)
ROOR	1.29	–11.78	0.985	90.2	–4.8
Et_4N^+…ROOR	1.29	–11.68	0.983	134.9	26.0
ROOR…Br^-	1.31	–11.31	0.968	154.1	30.5
Et_4N^+…ROOR…Br^-	1.31	–11.05	0.961	157.6	30.3
$Et_2Benz_2N^+$…ROOR…Br^-	1.31	–11.13	0.964	145.6	25.1
Pr_4N^+…ROOR…Br^-	1.31	–11.20	0.966	140.3	27.2
Bu_4N^+…ROOR…Br^-	1.30	–11.34	0.970	125.5	28.3

Investigation of the peroxide complexes which includes only cation or anion (Fig. 6) has shown that individual cation effect is not large and formation of this complex leads to the weak chemical activation of the peroxide reaction centre. Individual anion effect is proponent as compared with cation effect. In this case the activation of peroxide bond is now observed. But significant effect of peroxide bond activation is observed only for combined action both of anion and tetraalkylammonium cation. In semi-logarithmic coordinates a linear dependence between rate constants of lauroyl peroxide decomposition activated by tetraalkylammonium bromides (k, l mol^{-1} s^{-1}) and ΔE_{-O-O-} values is observed (Fig. 7) where ΔE_{-O-O-} can be evaluated according to the following equation:

$$\Delta E_{-O-O-} = E_{-O-O-}(Q^+\ldots ROOR\ldots Br^-) - E_{-O-O-}(ROOR) \qquad (16)$$

The ΔE_{-O-O-} values define the effect of the peroxide bond activation by combined action of bromide anion and tetraalkylammonium anion. Similar dependence is observed between rate constants of LPO decomposition activated by Alk_4NBr (k, l mol^{-1} s^{-1}) and peroxide bond order p_{-O-O-} values for peroxide complex (Fig. 7). Linear dependences between experimental activation parameters and ΔE_{-O-O-} values are also observed (Fig. 8).

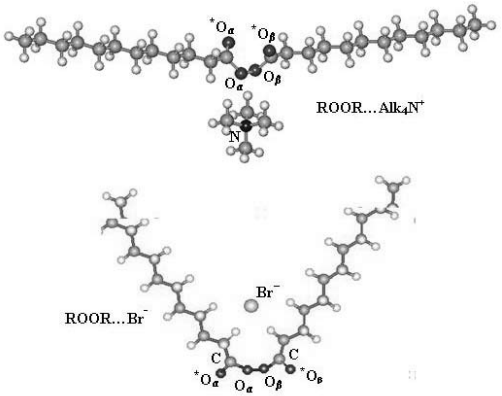

Fig. 6. Peroxide complexes with bromide anion and tetraethylammonium cation

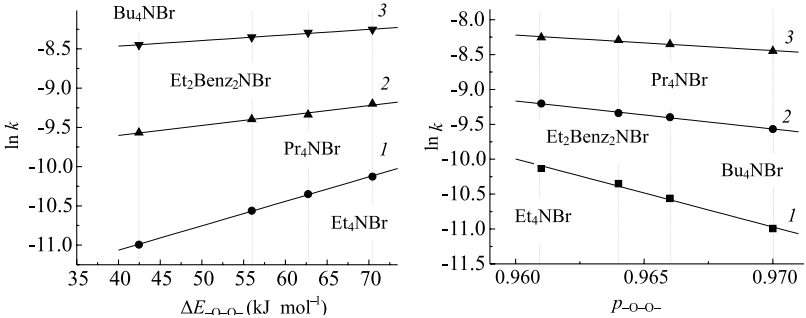

Fig. 7. Semi-logarithmic dependence between rate constants of LPO decomposition activated by Alk_4NBr and ΔE_{-O-O-} (*a*) and peroxide bond order (*b*) values
1 – 313 K, *2* – 323 K, *3* – 333 K

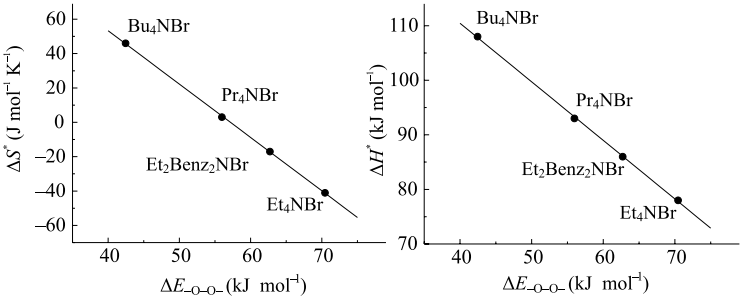

Fig. 8. Dependence between activation parameters of LPO decomposition activated by tetraalkylammonium bromides Alk_4NBr and ΔE_{-O-O-} values

The obtained dependences can be used for estimation of the kinetic parameters of the LPO decomposition activated by Alk_4NBr in CH_3CN – IPB solution and rates of the IPB oxidation initiated by binary system LPO–Alk_4NBr. For more correct conclusions and evaluations parameters of the transition state of the reactions should be taken into account. Thus, the molecular modelling of the peroxide complex decomposition has been carried out in the approximation of the least energy path. There is a maximum on the minimum energy reaction path (Fig. 9) even in one determinant approximation. Appearance of the maximum is due to the electrone transfer from bromide-anion to the peroxide. We assume that the complex configuration in transition state (TS) of the reaction of peroxide complex decomposition with the O–O bond rupture. The maximum localised in the curve corresponds to the 1.5-fold elongation of the peroxide bond.

Similar investigations have been carried out for the homolytic cleavage of peroxide bond in free lauroyl peroxide and also for the binary complexes with tetraalkylammonium cations and bromide anion. The minimum energy reaction path of peroxide bond cleavage is a smooth curve (Fig. 10) that passes through a maximum. We assume that crucial peroxide complex configuration in that point corresponds to the reaction transition state. It should be mentioned that for the free peroxide homolysis

and for the ROOR...Br complex decomposition the localised maximum is observed more later on the path curve as compared with peroxide complexes decomposition (Fig. 11). Consequently the mentioned structural reorganisation of the peroxide fragment resulting from complexation leads to the reaction centre structure close to the reaction transition state. Similar effects are typical for the supramolecular reactions proceeding[15].

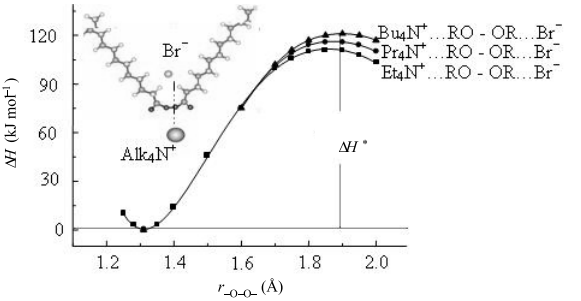

Fig. 9. Minimum energy reaction path of peroxide bond cleavage in the reaction of the peroxide complex decomposition

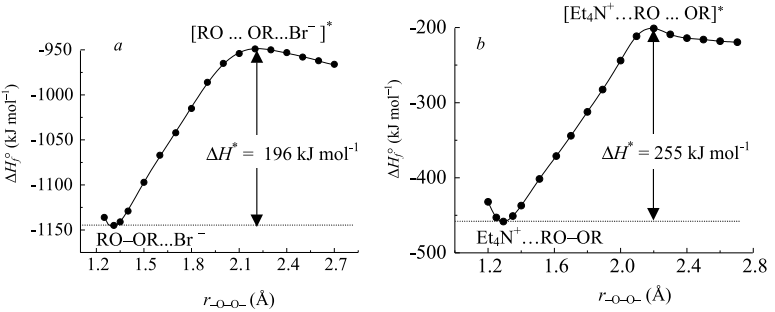

Fig. 10. Minimum energy reaction path of peroxide bond cleavage for the lauroyl peroxide complex with bromide anion (*a*) and tetraethylammonium cation (*b*)

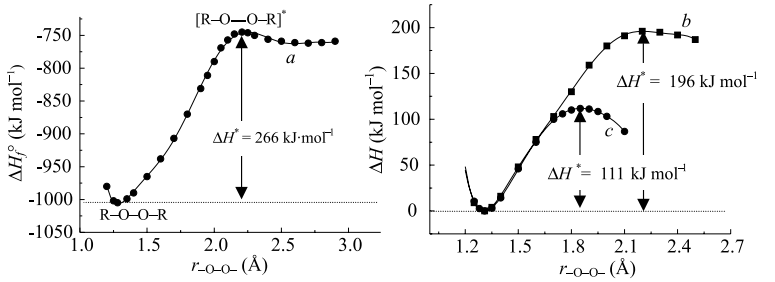

Fig. 11. Minimum energy reaction path of peroxide bond cleavage for the LPO (*a*) and peroxide complex with bromide-anion (*b*) and substrate separated ion pair (*c*)

On the basis of the obtained data the values for activation enthalpy ($\Delta_{AM1}H^*$) of the peroxide complex decomposition have been calculated. They are listed in Table 10. $\Delta_{AM1}H^*$ values for complexes of combined ions action nearly two times less as compared with corresponding values for complexes with anion only, and for complexes with cation only, and for free peroxide decomposition. For complexes Q^+…ROOR…Br^- with different the $\Delta_{AM1}H^*$ value increases in the following way for cations: $Et_4N^+ < Pr_4N^+ < Bu_4N^+$. This is in agreement with experimental results. There is a linear dependence between initiation rate of the isopropylbenzene oxidation initiated by lauroyl peroxide in the presence of the Alk_4NBr at 313 K and calculated values of activation enthalpies of complex-bonded peroxide (Fig. 12). It should be mentioned the linear dependence between calculated heats of formation of peroxide complexes and the corresponding values for transition state of the peroxide complex decomposition reaction (Fig. 13). Such a correlation can be used for preliminary estimation of the formation enthalpy of the transition state peroxide complex configuration. Thus, on the basis of the results of simple calculations of the formation enthalpy of the peroxide complex the reaction activation enthalpy can be estimated.

Table 10. Standart formation enthalpies of LPO, peroxide complexes in ground state (GS) and transition state (TS) and activation enthalpies of peroxide complexes decomposition

Q^+…ROOR…Br^-	ΔH_f° (kJ mol^{-1})		$\Delta_{AM1}H^*$ (kJ mol^{-1})
	GS	TS	
Et_4N^+…ROOR…Br^-	–776	–665	111
Pr_4N^+…ROOR…Br^-	–890	–776	116
Bu_4N^+…ROOR…Br^-	–1001	–879	122
ROOR…Br^-	1145	–950	195
Et_4N^+…ROOR	–456	–201	255
Pr_4N^+…ROOR	–575	–316	259
Bu_4N^+…ROOR	–687	–432	255
ROOR	–1007	–741	266

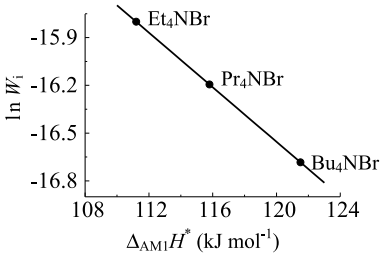

Fig. 12. Dependence between initiation rate of the IPB oxidation initiated by LPO–Alk_4NBr system (313 K) and calculated values of activation enthalpies of complex decomposition

The experimentally determined values of activation enthalpy and entropy of the LPO decomposition activated by Alk_4NBr are linear dependent on the calculated activation enthalpy of the complex-bonded peroxide decomposition (Fig. 14). Thus,

calculation of the activation enthalpy of the peroxide complex in system LPO–Alk_4NBr allows estimating of the experimental activation parameters of the chemically activated peroxide decomposition in CH_3CN – IPB solution.

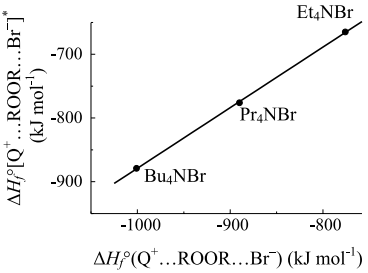

Fig. 13. Dependence between calculated heats of formation of peroxide complexes and corresponding values for transition state of the peroxide complex decomposition reaction

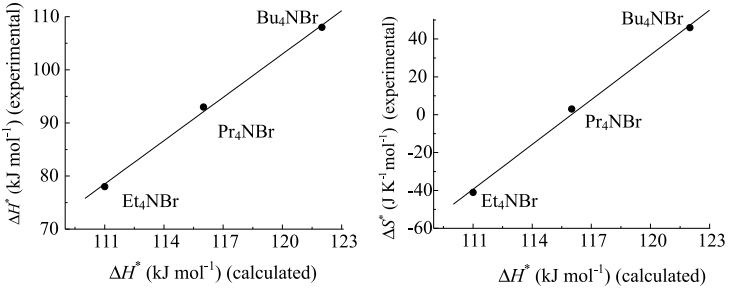

Fig. 14. Relationship between experimental activation enthalpy and entropy of the LPO decomposition activated by Alk_4NBr and calculated activation enthalpy of the complex-bonded peroxide decomposition

The stage of complex formation in the reaction of the LPO decomposition in the presence of Alk_4NBr should be taken into consideration. Quantum-chemical modelling of the complex-bonded lauroyl peroxide decomposition according to reactions (17)–(19) has shown that the largest effect of chemical activation can be obtained in the case of combined action of bromide anion and tetraalkylammonium cation. This effect is in correspondence with experimental results of the activated LPO decomposition.

$$Alk_4N^+\ldots ROOR \rightarrow [Alk_4N^+\ldots RO\text{---}OR]^* \quad (17)$$

$$ROOR\ldots Br^- \rightarrow [ROOR\ldots Br^-]^* \quad (18)$$

$$Alk_4N^+\ldots ROOR\ldots Br^- \rightarrow [Alk_4N^+\ldots ROOR\ldots Br^-]^* \quad (19)$$

In the case of complex formation according to equation (20) the estimated reaction enthalpies for complexation stage ($\Delta_r H_{ass}$) are very large and total heat efficiency ($\Delta_\Sigma H^*$) is then negative, so total decomposition reaction may be exothermal (Table 11). This is inconsistent with experimental results.

$$Alk_4N^+ + Br^- + ROOR \rightleftharpoons Alk_4N^+\ldots ROOR\ldots Br^- \quad (20)$$

Table 11. Reaction enthalpies of some stages of activated LPO decomposition

Complex	$\Delta_r H$ (kJ mol^{-1})			
	ΔH_{ass}	ΔH^*	$\Delta_\Sigma H^* = \Delta H_{ass} + \Delta H^*$	$\Delta_{exp} H^*$
$Et_4N^+ \ldots ROOR \ldots Br^-$	–249	111	–138	78
$Pr_4N^+ \ldots ROOR \ldots Br^-$	–246	116	–130	93
$Bu_4N^+ \ldots ROOR \ldots Br^-$	–239	122	–117	108

In the case of alternative model of peroxide complex formation (equation (21)) the reaction enthalpies for complex formation stage are 5–6 times less as compared with the model of reaction (20) (Table 12).

$$Alk_4N^+ \ldots Solv \ldots Br^- + ROOR \rightleftharpoons Alk_4N^+ \ldots ROOR \ldots Br^- + Solv \qquad (21)$$

The experimentally obtained values for the activation enthalpy ($\Delta_{exp} H^*$) of the activated LPO decomposition in the presence of Alk_4NBr is the effective value. It can be represented as a sum of two values – reaction enthalpy of complex formation stage ΔH_{ass} (exothermal stage) and activation enthalpy of the peroxide complex decomposition ΔH^* (endothermic stage). Therefore, these two stages of the reaction should be taken into account, namely reactions (21) and (19). Such an approach leads to values consistent with experimental data (Table 12). Experimentally observed values of the reaction activation enthalpy and activation entropy are linearly dependent on calculated activation enthalpy taking into consideration the complexation stage and stage of peroxide complex decomposition (Fig. 15).

Table 12. Reaction enthalpies of some stages of activated LPO decomposition

Alk_4NBr	$\Delta_r H°$ (kJ mol^{-1})			
	ΔH_{ass}	ΔH^*	$\Delta_\Sigma H^* = \Delta H_{ass} + \Delta H^*$	$\Delta_{exp} H^*$
Et_4NBr	–46	111	65	78
Pr_4NBr	–43	116	73	92
Bu_4NBr	–39	122	83	108

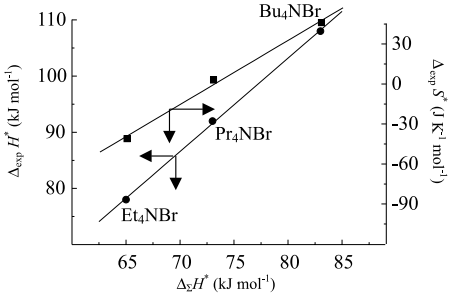

Fig. 15. Relationship between experimentally observed values of the reaction activation enthalpy and activation entropy and calculated total activation enthalpy

CONCLUSIONS

Combined consideration of the experimental and quantum chemical modelling results revealed that anion nature and cation structure determine the catalytic activity of the tetraalkylammonium salt in the reaction of lauroyl peroxide decomposition. In the case of peroxide–Alk_4NBr complex formation peroxide geometry and electron structure changes bring it to the configuration close to that of transition state. The assumed mechanism of lauroyl peroxide decomposition in the presence of tetraalkylammonium bromides can be regarded as one of the supramolecular reactions[15].

REFERENCES

1. E. T. DENISOV, T. G. DENISOVA, T. S. POKIDOVA: Handbook of Free Radical Initiators. John Wiley & Sons Inc. Hoboken, New Jersey, 2003.
2. M. A. TUROVSKYJ, I. O. OPEIDA, O. M. TUROVSKAYA, O. V. RAKSHA, N. O. KUZNETSOVA, G. E. ZAIKOV: Kinetics of Radical Chain Cumene Oxidation Initiated by α-oxycyclohexyl Peroxides in the Presence of Et_4NBr. Oxid. Commun., **29**, 249 (2006).
3. N. A. TUROVSKYJ, I. O. OPEIDA, O. V. KUSH, E. L. BARANOVSKIJ: Initiation of the Methyl Methacrylate Polymerization by the Systems Benzoyl Peroxide – Onium Salt and Benzoyl Peroxide – Aminostyryl Pyridine. J. Appl. Chem., **77**, 1887 (2004).
4. I. A. OPEIDA, N. M. ZALEVSKAYA, E. N. TUROVSKAYA: Oxidation of Cumene in the Presence of the Benzoyl Peroxide–Tetraalkylammonium Iodide Initiator System. Petroleum Chemistry, **44**, 358 (2004).
5. J. C. BEVINGTON, B. J. HUNT: The Use of Stabilized Radicals with Monomers and Lauroyl Peroxide. Eur. Polym. J., **40**, 103 (2004).
6. C. H. KENNEDY, J. M. DYER, D. F. CHURCH, G. W. WINSTON, W. A. PRYOR: Radical Production in Liver Mitochondria by Peroxidic Tumor Promoters. Biochem. Biophys. Research Commun., **160**, 1067 (1989).
7. A. VAISBERGER, E. PROSKAUER, J. RUDDIK, E. TUPS: Organic Solvents. Izd. Inostr. Lit., Moscow, 1958 (in Russian).
8. A. J. GORDON, R. A. FORD: The Chemist's Companion. Mir, Moscow, 1976 (in Russian).
9. J. J. STEWART: MOPAC2007, Stewart Computational Chemistry, Colorado Springs, CO, USA, http://OpenMOPAC.net (2007).
10. E. T. DENISOV, O. M. SARKISOV, G.I. LIKHTENSHTEIN: Chemical Kinetics. Khimija, Moscow, 2000 (in Russian).
11. N. A. TUROVSKYJ, I. A. OPEIDA, E. N. TUROVSKAYA, N. A. GOLUBITSKAYA, E. V. RAKSHA: Supramolecular Model of the Initiation Reaction of Low-temperature Radical Polymerization of Methyl Methacrylate by the Benzoyl Peroxide and Onium Benzoates. In: Proc. of the Scientific Conference Review 'The Polymers of Special Application', Ukraine, Dnepropetrovsk, 2006, p. 38.
12. M. A. TUROVSKYJ, I. O. OPEIDA O. M. TUROVSKAYA, O. V. RAKSHA, N. O. KUZNETSOVA, G. E. ZAIKOV: Kinetics of Activated by Et_4NBr Alfa-oxycyclohexylperoxides Decomposition: Supramolecular Model. In: Order and Disorder in Polymer Reactivity (Eds G. E. Zaikov, B.A. Howell). Nova Science Publishers, Inc., New York, 2006, p. 37.
13. V. M. SHUFLET'UK, M. A. TUROVSKYJ: Quantum-chemical Model of Cumylhydroperoxide Activation by Tetraethylammonium Halides. Visnyk Donetskogo Universytetu, A, (1), 146 (2001) (in Russian).
14. V. L. ANTONOVSKY, S. L. KHURSAN: Physical Chemistry of Organic Peroxides. Academkniga, Moscow, 2003 (in Russian).
15. J.-M. LEHN: Supramolecular Chemistry: Concepts and Perspectives. Nauka, Novosibirsk, 1998 (in Russian).

Received 30 June 2008
Revised 21 August 2008

SODIUM HYPOCHLORITE PREPARATION BY ELECTROCHEMICAL OXIDATION OF CHLORIDE SOLUTIONS

L. PETKOV*, I. DARDANOVA

University of Chemical Technology and Metallurgy, Sofia, Bulgaria
E-mail: *l.petkovv@abv.bg*

ABSTRACT

The investigation considers the process of sodium hypochlorite production by electrochemical oxidation of chloride solutions. The experiments are carried out with different electrode materials, concentrated and diluted solutions, direct and impulse current. It is found that among all anode materials the highest current efficiency, 72%, occurs when using oxide ruthenium-titanium anodes. However, at low concentrations, 0.5 g/l, the current efficiencies do not exceed 8–10%. The use of Zr–Ce–Y cathodes increases the current efficiency by 5–6%. These electrodes possess better corrosion resistance compared to steel in concentrated Na–Cl solutions, 10–250 g/l. The electrolysis by impulse current at low concentration solutions provides possibility to accelerate the process; the current usability is increased by 1–2% and the energy consumption is decreased by 25–30%.

Keywords: electrochemical oxidation, overpotential, current efficiency.

AIMS AND BACKGROUND

The sodium hypochlorite is a very significant oxidising agent. It finds wide application in the treatment of waste and natural waters, in the organic synthesis, etc. In view of that fact the study of the process of its electrochemical production is of undoubted interest.

During the electro-oxidation of sodium chloride solutions the following reactions run on the electrodes:

Anode:

$$2Cl^- + 2e = Cl_2 \quad (1)$$

$$H_2O - 2e = 0.5O_2 + 2H^+ \quad (2)$$

Cathode:

$$2H_2O + 2e = H_2 + 2OH^- \quad (3)$$

* For correspondence.

The obtained chlorine hydrolyses and hypochlorous acid is formed:

$$Cl_2 + OH^- = HClO + Cl^- \quad (4)$$

The hypochlorous acid is weak acid and the hydrolysis process quickly ceases. However, if the acid interacts with the NaOH, formed around the cathode, sodium hypochlorite (NaClO) is formed. The latter is strong electrolyte, the balance of the hydrolysis reaction will shift from the left to the right hand side and in consequence of that there will be dissolution of more and more Cl_2 quantities.

$$HClO + NaOH = NaClO + H_2O \quad (5)$$

The produced NaClO can subsequently oxidise to chlorate $NaClO_3$:

$$ClO^- - 4e + 4H_2O = ClO_3^- + 4H^+ \quad (6)$$

The oxidation to chlorate may go also chemically, in the solution volume, by the formed during the hydrolysis process HClO:

$$NaClO + 2HClO = NaClO_3 + HCl \quad (7)$$

Besides, NaClO can be reduced on the cathode to the initial Cl^- ions:

$$2NaClO + 4e + H_2O = 2Cl^- + 2NaOH \quad (8)$$

As seen in the above presented data, NaClO is produced as a result of electro-oxidation of the chloride ions (1) and subsequent reactions (4) and (5) in the solution volume. As far as the volume reactions go fast, the quantity of the produced hypochlorite shall be determined by the rate of the run of the Cl^- ions electro-oxidation reaction (1). In addition, the hypochlorite quantity and the connected with it current efficiency of the preparation process will be determined by the extent of the oxidation reactions (6) and (7) run. The reaction of cathode reduction (8) shall be of importance, too.

Many sources in the publications present data about the hypochlorite preparation on the base of electrolysis of NaCl solutions. There is studied the effect of the anode material on the preparation process, i.e. graphite[1], ruthenium-platinum alloy[2], oxide-ruthenium titanium[3], ferro oxides[4], the so-called spinels[5] or compounds of the $A(A,B)O_4$ type, where A-bivalent ion (Mn, Zn, Mg, Fe, Cr and Ti), and B-trivalent ion (Al, Fe and Cr). Other publications treat experiments with cobalt-oxide electrodes[6] manganese-oxide electrodes alloyed with palladium[7], oxide-ruthenium titanium (ORTA) with tin additive[8]. Main method for the production of these anodes is the thermal dissociation of their salts at high temperatures on inert substrate, most often titanium.

The use of NaClO in the treatment of waste and natural waters has provided the prerequisites for the investigation of the process of its preparation from diluted solutions of NaCl or by the direct electrolysis of water[9–12]. Publication[13] considers investigation of the effects of additives to NaCl, bivalent ions – Ca^{2+} and Mg^{2+}. It is found that they increase the NaClO solution stability by decreasing the rate of the oxidation reaction to chlorate. Besides, the most stable are the solutions of the electrochemically prepared NaClO of concentrations 2–3 g/l.

Publications[14–17] present data concerning the process of cathode reduction. It is found[14] that addition of $K_2Cr_2O_7$ in quantity 1–5 g/l to the initial solutions impedes the reduction process. Reason for this is the Cr^{6+} reduction to Cr^{3+} and the formation of inhibition film of oxide on the cathode surface.

Publication[16], on the basis of the carried out experiments, presents the conclusion that ZrO_2 cathode prepared electrochemically is not suitable as electrode material in the chloride solution electrolysis because of the oxide reduction and the decrease of selectivity with respect to the basic concurrent reaction – hydrogen evolution. Publication[17] considers study of steel cathodes. It is found that after certain period of time the steel effectiveness decreases compared to the effectiveness of the fresh cathodes.

In spite of the large number of data in the publications concerning the process of NaClO preparation, it should be noted that there are no sufficient results related to the effect of the anode material under compared conditions – initial solution concentration, current density and process duration. The possibility is not investigated also to a sufficient extent for replacement of the cathode material (steel) by another which to provide possibility to increase the current efficiency as regards to NaClO with no use of additives of $K_2Cr_2O_7$, that are ecologically inexpedient. Interest would present as well the data about the effect of the hydrodynamics, the shape of the electric current (direct, impulse) on the characteristics of the electrolysis process from concentrated and diluted solutions. Providing additional experimental data in the said aspect appears the purpose of the present paper.

EXPERIMENTAL

The investigations were carried out in a glass cell of 400 cm^3 volume. Current power was preset by direct current source, which permits maintenance of constant current power during the electrolysis process (TEC – 7M). 'Sewast' generator was used in the experiments by impulse current. The constant temperature was maintained by a thermostat UTU-2. The anodes of appropriate dimensions for the laboratory cells ($60 \times 25 \times 1$ mm) were prepared of industrial specimens – graphite, platinised titanium, oxide-ruthenium titanium anodes, the anodes of cobalt oxide – by thermal decomposition of cobalt salts at high temperatures and those of lead oxide – by anode formation during electrolysis of lead salts solutions on nickel base. Steel was used as cathode in the studies on the effect of the anode material.

The initial solutions were prepared by distilled water and sodium chloride, p.a. The concentration of the prepared hypochlorite was determined by volumetric iodometric method. The quantitative relationships based on the Faraday laws for the electrolysis were used in the calculations of the current efficiency.

RESULTS AND DISCUSSION

Figure 1 presents the dependence of the current efficiency on the duration of the NaClO production process at different current densities for graphite anode. As seen in the figure the dependence has non-linear character and with the progress of the process time the current efficiency decreases. That is more strongly expressed in the initial moments of the process after which the effect is less expressed and tending to constant values. With the increase of the current density the character of the dependence does not change but the current efficiency decreases. Thus, for instance at process duration of 1 h and current densities of 2.5, 5.0 and 10 A/dm^2 the current efficiencies are 52, 36 and 32%, respectively.

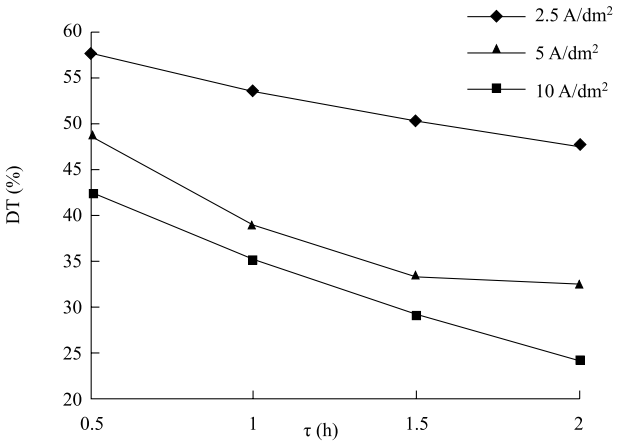

Fig. 1. Current efficiency–time dependence of electrolysis for different current densities (anode – graphite, CNaCl = 100 g/l, temperature 22°C)

The observed dependences can be explained by the change of the correlations of the main reaction speeds (equation (1)) and those of the side ones (equations (3) and (6)). With the progress of the electrolysis time and the corresponding formation of more significant hypochlorite quantities the speed of the oxidation reaction (6) to chlorate grows. In case of prolonged electrolysis the speeds of reactions (4) and (6) equalise and the current efficiency remains constant. On the other hand, the increased current densities favour the oxidation of water (2) on the account of the oxidation of the Cl^- ions.

As the graphite is a classical anode material and can be used for comparative analysis with other systems, interest present the investigations related to the effect of the initial solution (NaCl) concentration and of the electrolysis temperature with such anode. The dependences of the current efficiency on the concentration and temperature are presented in Fig. 2 and Fig. 3, respectively. As seen in Fig. 2 the increase of the NaCl concentration in the range 25–250 g/l results in current efficiency increase. However, the observed effect is well expressed up to concentrations of 100 g/l, after

which is insignificant. Conclusion could be made that the greater Cl^- ion quantity affects the rate of their oxidation (equation (1)) to definite value.

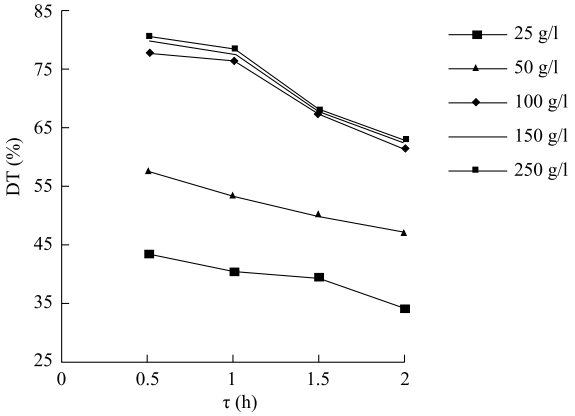

Fig. 2. Current efficiency–time dependence of electrolysis for different solution concentrations (anode – graphite, cathode – steel, current density – 10 A/dm^2, temperature 22°C)

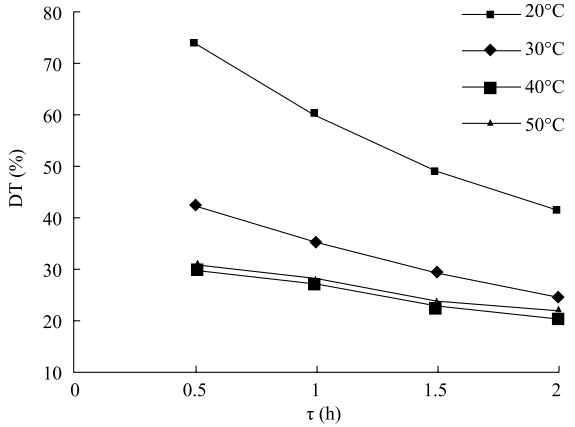

Fig. 3. Current efficiency–time dependence of electrolysis for different temperatures (anode graphite, cathode – steel, CNaCl – 100 g/l)

The obtained result has significant practical importance because the final compound, NaClO, does not dissociate from the solution, hence from the not reacted NaCl quantity, and the operation with strongly concentrated initial solutions could lead to losses.

The temperature dependence presents interest with a view of the circumstance that in the electrolysis of the NaCl solutions there is increase of the temperature during the process run. Decrease of the current efficiency is observed (Fig. 3) when the temperature is increased, this being well expressed up to temperature of 40°C.

As noted above, the NaClO oxidation to $NaClO_3$ goes both electrochemically on the anode (equation (5)) and chemically in the volume of the solution (equation (6)).

The rate of the chemical oxidation depends strongly on the temperature and its accelerated run will lead to decrease of the produced hypochlorite quantity. Obviously the mentioned effect exceeds considerably the favourable effect of the temperature on the overpotential of the chlorine reaction (1) and consequently on the subsequent reaction of chlorine hydrolysis (3).

Figure 4 presents the dependences of the current efficiency on the electrolysis time at one and the same temperature, 20°C, and current density, 10 A/dm^2, for anodes of graphite, oxide-ruthenium titanium, platinised titanium, lead oxide and cobalt oxide. As seen from the results obtained, the character of the dependence is the same for the different anodes – there is a decrease of the current efficiency for the produced hypochlorite with time, the effect being better expressed in the initial moments of the electrolysis. However, the values of the current efficiency differ. They are the highest with ORTA and the lowest with graphite. As far as the reactions in the solution volume go almost instantly, these values to the greatest extent shall be determined by the speed of the reaction (1). In this case it is the highest on ORTA, a result of the low overpotential of the oxidation reaction on this anode material.

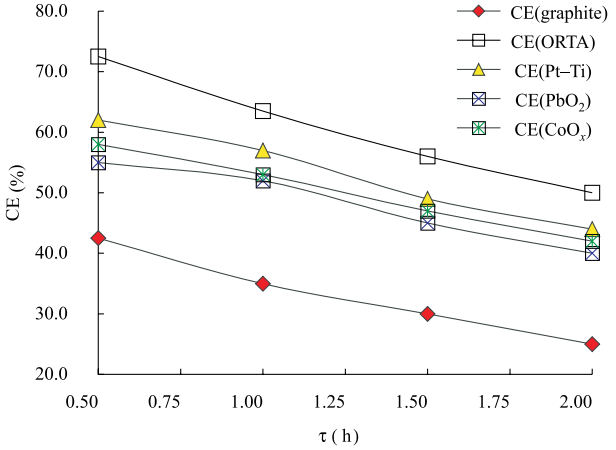

Fig. 4. Current efficiency–time dependence of electrolysis (anodes – ORTA (*1*), Pt–Ti (*2*), CoO (*3*), PbO (*4*), graphite (*5*); current density i – 10 A/dm^2; CNaCl – 100 g/l; temperature 22°C)

Effect of the cathode material. In the introductory part of the present paper it is noted that the NaClO, produced in the electro-oxidation of the chloride ions, takes part in the reduction reaction (8). In order to prevent this reaction usually bi-chromate ions $Cr_2O_7^-$ in quantity to 5 g ion/l are added to the initial solutions. They increase the current efficiency by about 5–6%; the mechanism of their effect is explained by their reduction on the cathode to Cr^{3+} and subsequent formation of inhibition film from its oxide. This method is connected with ecological inconveniencies. An alternative of it appears the replacement of the commonly used cathode material, steel, by another. Preliminary investigations ascertain that the use of Zr–Ce–Y-coated (thickness 1–2 μm)

steel cathodes in the process of NaClO preparation provide current efficiencies that are higher by 5–6% compared to current efficiencies with steel cathode. Or else, the obtained values are commensurate with the effects when using Cr^{6+} ions.

Figure 5 presents the current density-potential dependences for NaCl concentration of 10 g/l for steel specimen (the dependence for more positive potentials) and Zr–Ce–Y (for two different proportions of the components). On the basis of the obtained analogical dependences for NaCl concentrations of 30 and 200 g/l there is determined the corrosion rate or corrosion current I_{cor} (Table 1). As seen in Table 1 for the steel specimen with the increase of the NaCl concentration the corrosion current grows. Thus for instance, at concentrations of 10 and 200 g/l its values are 10.43 and 24.37 μA, respectively.

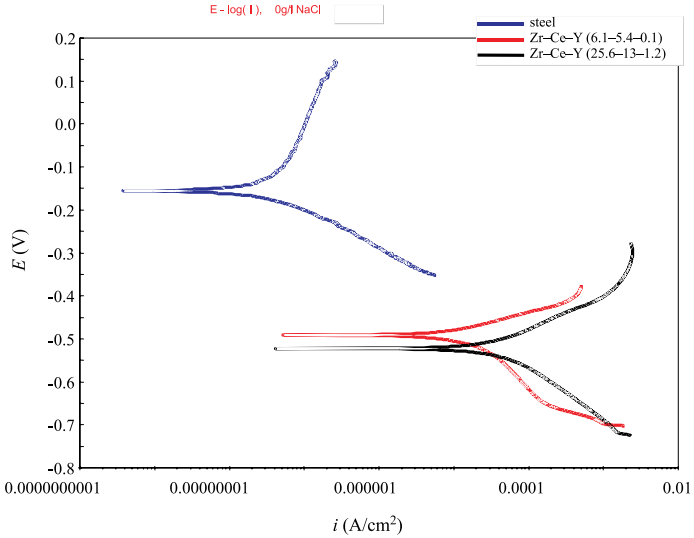

Fig. 5. Potential–current densities dependence (cathode – Zr–Ce–Y, anode – Pt, NaCl – 10 g/l)

Table 1. Dependence between the corrosion current and NaCl concentration

Specimens	10 g/l NaCl $I_{corr.}$ (μA)	30 g/l NaCl $I_{corr.}$ (μA)	200 g/l NaCl $I_{corr.}$ (μA)
Steel	10.43	15.01	24.37
Zr–Ce–Y (6.1–5.4–0)	13.99	10.78	8.657
Zr–Ce–Y (25.6–13–1.2)	38.33	27.09	20.19

Unlike the steel, with the Zr–Ce–Y specimens a reverse effect is observed – the corrosion current decreases when the chloride concentration is increased in the studied range – the obtained values for example for the first specimen are 14 and 8.65 μA, respectively. The obtained results show the reliable chemical endurance of the Zr–Ce–Y coatings in the NaCl environment, in which the electrolysis process is performed.

Conclusion could be made that the increase of the current efficiency for coated specimens is due to the facilitation of the hydrogen evolution process (the increase of the electrode selectivity with respect to the hydrogen reaction). As it is known, in compliance with the Taffel equation in the electrochemical kinetics ($\eta = a + b \lg i$, where η is the overpotential of the cathode process, a – constant, equal to the value of η for current density i =1 A/cm^2), the rate of the gas evolution reaction is determined by the constant b or by the tangent of the angle of the right-linear dependence slope. The experiments with 10 g/l NaCl show values for this constant for the steel and Zr–Ce–Y specimens 98.3, 146.7 and 115.8 mV, respectively, i.e. acceleration of the reaction.

NaClO preparation from low-concentrated chloride solutions. The process of NaClO preparation from low-concentrated chloride solutions is important for the direct electrolysis of water with the purpose of its disinfection. Generally in these cases the NaCl concentration does not exceed 0.5–0.7 g/l. Figure 6 presents the dependence of the current efficiency on the current density in the preparation of NaClO from NaCl solutions of concentration 0.5 g/l. As seen in the presented dependence, the process is characterised by very low current efficiencies that do not exceed 8–9%. Besides, it is characterised by a maximum whose value for the examined anodes (ORTA) corresponds to current density 0.75 A/dm^2 and amounts to about 8.5%. The comparison of Fig. 6 with the dependences for concentrated solutions (Figs 1–4) shows that they have different character. The observed result can be explained by the much higher speed of running of the water oxidation reaction (2) for low concentrated solutions. With the increase of the current density the speed of the chloride ions oxidation reaction also increases but in a very narrow density range and under further increase of the current density reaction (2) begins to prevail again.

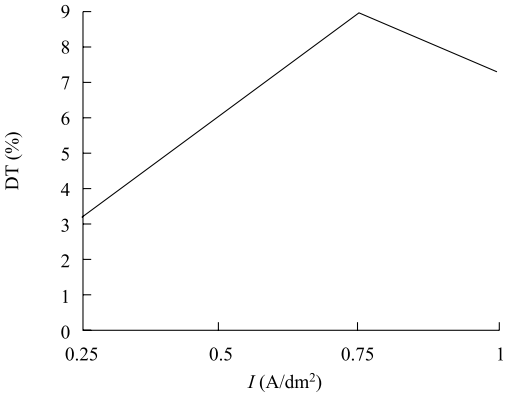

Fig. 6. Current efficiency–time dependence of electrolysis (anode – ORTA; cathode – steel, NaCl – 0.5 g/l; temperature 22°C)

Table 2. Dependence between the current efficiency and hydrodynamic conditions

NaCl (g/l)	Current efficiency (%) without stirring	Current efficiency (%) with stirring
50	57.5	5.2
0.5	8.9	7.3

Table 2 presents the values of the current efficiencies for high- and low-concentrated chloride solutions in the presence and absence of stirring. The presented results show that in conditions of stirring the current efficiencies decrease in both cases (the NaClO access to the anode is facilitated and therefore its oxidation to $NaClO_3$). However, for the low concentrated solutions the effect is more strongly expressed. Thus for instance, the corresponding decrease is from 57.5 to 52.9% (about 1/11) and from 8.9 to 7.3 % (or 1/5). Obviously, the negative effect of the hydrodynamics is more strongly expressed in the processes of direct electrolysis where the oxidation of the chlorine ions and the formation of hypochlorite go at very low rates.

Table 3. Influence of pulsating current on the current efficiency and energy consumption

NaCl (g/l)	Constant current		Pulsating current	
	CE (%)	*W* (Wh/g)	CE (%)	*W* (Wh/g)
25	54.5	7.4	49.5	10.0
0.5	6.0	120.8	8.9	68.8

Table 3 presents comparative data for the current efficiency when using direct and impulse current. The results obtained show that the effect of the impulse current is different. With the concentrated solutions there is observed a decrease of the current efficiency compared to the case of direct current (49.55 and 54.5%, respectively) while with the low concentrated solutions there is increase of the current efficiencies (8.95 and 6%). On that basis, carrying out electrolysis in conditions of impulse current leads to decrease of the specific electric energy consumption – from 120.77 to 68.82 Wh/g. The values of the specific energy consumption for concentrated solutions are 10 Wh/g (impulse current) and 7.31 Wh/g (direct current), respectively. The obtained result may have practical importance for the processes of chloride systems electro-oxidation.

The effects related to impulse current can be explained by the circumstance that through the time of pause there runs the recovery of the concentration of the reacting ions around the electrodes and particularly around the anode. Obviously, this has favourable effect in the case of low concentrated solutions and with them the recovery of the concentration of the chloride ions is also the greatest (hence the increase of the chlorine reaction speed) compared to the concentration variations of the other ions – ClO^-.

In the cases of concentrated solutions, obviously the concentration of the chloride ions around the anode is high so the increase of the quantities of ions participating in the side reactions has greater importance, i.e. they decrease the current efficiency.

CONCLUSIONS

There are carried out investigations of the process of NaClO preparation by electrochemical oxidation of NaCl solutions. It is found that the process goes at the highest effectiveness when ORTA is used. The replacement of the steel cathodes by Zr–Ce–Y increases the current efficiency by 5–6%. Performing the electrolysis of low concentrated (0.5 g/l NaCl) solutions in conditions of impulse current provides the possibility to accelerate the electro-oxidation process and to decrease the consumed electrical energy.

REFERENCES

1. L. A. KULSKII, B. D. GREBENIUK, O. O. SAWLUK: Electrochemistry in Water Treatment Processes. Tekhnika, Kiev, 1987 (in Russian).
2. S. TRASATI, G. LODI: Electrodes of Conductive Metallic Oxides. Part A (Ed. S. Trasati). Elsevier, Amsterdam, 1980, p.301.
3. C. C. HU, C. H. LEE, T. C. WEN: Oxygen Evolution and Hypochlorite Production on Ru-Pt Binary Oxides. J.of Appl. Electrochem., **26**, 72 (1996).
4. F. V. KUPOVICH, A. M. VIRNIK, V. I. EBERI: Iron-Oxide-Titanium Anode for Electrolysis of Chloride Solutions. Russ. J. of Electrochem., **37**, 1157 (2001).
5. B. I. LIUBUSHKIN, B. A. SMIRNOV, E. T. LIUBUSHKINA: Electrosynthesis of Sodium Hypochloride in Spinel-coated Electrodes. Elektrokhimiya, **37**, 828 (1981) (in Russian).
6. S. Iu. BASHTAN, V. V. GONCHARUK, R. D. CHEBOTAREVA, V. M. LINKOV: Sodium Hypochlorite Production in an Electrolyzing Cell with a Ceramic Membrane. Russ. J. of Electrochem**.**, **37**, 913 (2001).
7. B. C. SOROKEDAIA, P. U. BONDAR, O. G. KLUSHKINA, Iu. G. OLESOV: Titan-manganese Anodes Doped with Palladium Oxide. Elektrokhimiya, **27**, 1133 (1991) (in Russian).
8. CHIEN-HSING YANG: Hypochloryte Production on Ru-Sn Binary Oxide Electrode and Its Application in Treatment of Dye Wastewaters. Can. J. of Chem. Ing., **77**, 1161 (1999).
9. A. CRAFT, M. STADELMANN, M. BLASCHKE, D. KREYSIG, B. SANDT, F. SCHRODER, J. RENNAU: Electrochemical Water Dysinfection. Part 1. Hypochlorite Production from Fey Dilute Chloride Solutions. J. of Appl. Electrochem., **29**, 861 (1999).
10. A. CRAFT, M. BLASCHKE, D. KREYSIG, F. SCHRODER, J. RENNAU: Electrochemical Water Dysinfection. Part 2. Hypochlorite Production from Portable Water, Chloride Consumption and the Problem of Calcareous Deposits. J. of Appl. Electrochem., **29**, 895 (1999).
11. C. H. YANG, C. C. LEE, T. C. WEN: Hypochlorite Generation on Ru-Pt Binary Oxide for Treatment of Dye Wastewater. J. of Appl. Electrochem., **30**, 1043 (2000).
12. V. A. GRINBERG, A. M. SKUNDINA, E. K. TUSEEVA: Electrochemical Production of Medicinal Sodium Hypochlorite Solutions in Flow-through Electrolyzing Cell. Russ. J. of Electrochem., **37**, 500 (2001).
13. S. Iu. BASHTAN, B. B. GONCHARUK, R. D. CHEBOTAROVA: Effect of Sodium Chloride Qualities on the Parameters of Electrochemical Synthesis of Sodium Hypochlorite.Ghim. i tekhnolog. Wodi, **23**, 364 (2001) (in Russian).
14. T. NAGAI, T. TAKEI: Effect of Chromate Addition on Cathode Process in Chloride Solutions. J. Electrochem. Soc.of Japn., **25**, 333 (1957).
15. G. G. LINDBERGH, D. SIMANSSON: The Effect of Chromate Addition on Cathodic Reduction of Hypochlorite in Hydroxide and Chlorate Solutions. J. of Electrochem.Soc., **137**, 3094 (1990).
16. F. HERLITZ: Inhibiting Effect of Oxidized Zirconium on Parasitic Cathode Reaction in the Sodium Chlorate Process. Part 1. Hypochlorite Reduction. J. of Appl. Electrochem., **31**, 207 (2001).
17. J. WULFF, A. CORNELL: Cathodic Current Efficiency in the Chlorate Process. J. of Appl. Electrochem., **37**, 181 (2007).

Received 9 February 2009
Revised 18 March 2009

RUTHENIUM(III)-CATALYSED OXIDATION OF SOME SUGARS (D-GLUCOSE AND D-GALACTOSE) IN THE PRESENCE OF ALKALINE POTASSIUM BROMATE

SH. SRIVASTAVA*, SH. SINGH, P. SRIVASTAVA

Spectrokinetic Laboratories, Feroze Gandhi College, 229 001 RaeBareli, U.P., India
E-mail: *she_ila72@yahoo.com*; *shalinisingh_chem@yahoo.co.in*

ABSTRACT

The kinetics of oxidation of two aldoses (D-glucose and D-galactose) by potassium bromate ($KBrO_3$) in the presence of an alkaline solution of $RuCl_3$ as a catalyst and $Hg(OAc)_2$ as a scavenger for bromide ion have been investigated in the temperature range of 30–45°C. The main products of the oxidation are the corresponding aldonic acids. The reaction rate is zero order with respect to aldoses and [Cl^-]. The reaction follows first order dependence of the reaction both on $KBrO_3$ and Ru(III). A negative effect on the rate of reaction has been found on the successive addition of [OH^-]. Insignificant influence of ionic strength of the medium was observed. A possible mechanism from the results of kinetic studies, reaction stoichiometry and product analysis has been proposed. Various activation parameters have been calculated.

Keywords: kinetics, oxidation, Ru(III) chloride, D-glucose, D-galactose, alkaline potassium bromate.

AIMS AND BACKGROUND

The utility of ruthenium(III) chloride as a non toxic and homogeneous catalyst has been reported[1,2]. Potassium bromate ($KBrO_3$) has been used to oxidise various compounds in acidic medium[3–7]. This prompted us to undertake the present investigation which is focused on the kinetics and mechanism of Ru(III)-catalysed oxidation of some aldoses by potassium bromate in alkaline medium, in the presence of mercuric acetate as a scavenger.

EXPERIMENTAL

Materials. Sodium perchlorate, potassium bromate, sodium hydroxide, D-glucose, D-galactose, mercuric acetate (E. Merck) were used as supplied without further

* For correspondence.

purification by preparing their solutions in doubly distilled water. A stock solution of Ru(III) chloride (Johnson Metthey) was prepared by dissolving the sample in hydrochloric acid of known strength. All other reagents used were of analytical grade. The reaction vessels were coated from outside with black paint to avoid any photochemical reaction.

Kinetic procedure. A thermostated water bath was used to maintain the desired temperature within ± 0.1°C. Requisite volume of all reagents, including substrate, were taken in a reaction vessel and thermostated at 35°C for thermal equilibrium. A measured volume of sodium periodate solution also maintained separately at the same temperature, was rapidly poured into the reaction vessel. The kinetics was followed by iodometric estimation of unconsumed bromate at regular time intervals.

Stoichiometry and product analysis. The stoichiometry of the reaction was determined by equilibrating varying ratios of [$KBrO_3$] to [reducing sugars] at 35°C for 48 h under kinetic conditions. The estimation of unconsumed bromate showed that 1 mol of sugars is oxidised by 1 mol of bromate. The result showed 1:1 stoichiometry according to equations (A) and (B) for glucose and galactose, respectively.

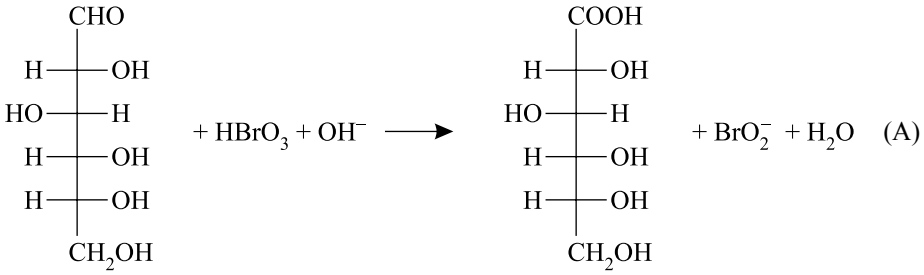

D-glucose gluconic acid

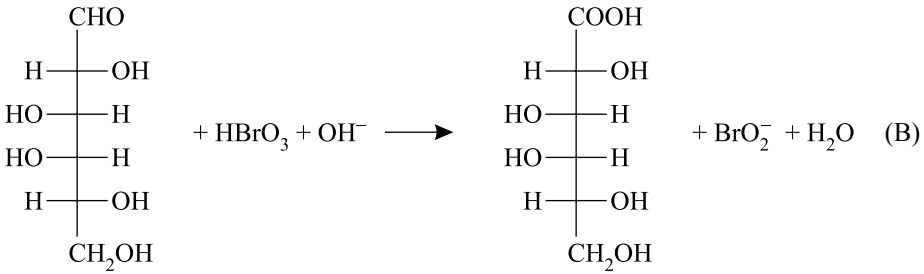

D-galactose galactonic acid

The formation of corresponding acids was identified by conventional methods[8].

RESULTS AND DISCUSSION

The kinetic results were collected at several initial reactant concentrations (Table 1). First order kinetics was observed with respect to the oxidants ($KBrO_3$) in both aldoses. Insignificant effect of increase in concentration of glucose and galactose was observed. First order kinetics was observed in case of catalyst Ru(III) chloride. A plot of $(-dc/dt)$ versus [Rh(III)] (Fig. 1) gave a slope of 5.71 s^{-1} for glucose, 5.45 s^{-1} for galactose, which is close to the average value of first order rate constants, i.e. k_1 = 5.46 s^{-1} and 5.86 s^{-1} for glucose and galactose, respectively, at 35°C. k_1 values were obtained by dividing the $-dc/dt$ value by [Ru(III)]. A fair degree of closeness in the first order rate constants obtained graphically and obtained values of $(-dc/dt)$/[Ru(III)] clearly confirms the first order dependence on [Ru(III)]. A negligible effect of change in [KCl] was observed.

Table 1. Effect of variation of reactants on the reaction rate at 35°C
[Ru(III)] = 4.80 ×10⁶ mol dm⁻³, [NaOH] = 1.00 ×10³ mol dm⁻³, [$Hg(OAc)_2$] = 1.67 × 10³ mol dm⁻³

$[KBrO_3] \times 10^3$ (mol dm⁻³)	[S] ×10³ (mol dm⁻³)	[KCl] ×10³ (mol dm⁻³)	$(-dc/dt) \times 10^7$ (mol dm⁻³ s⁻¹)	
			(glu.)	(gal.)
0.83	10.00	1.00	1.90	1.80
1.00	10.00	1.00	2.60	2.75
1.25	10.00	1.00	3.00	2.90
1.67	10.00	1.00	3.75	3.65
2.50	10.00	1.00	5.90	5.84
5.00	10.00	1.00	11.60	11.68
1.00	3.33	1.00	2.80	2.60
1.00	4.00	1.00	3.00	3.00
1.00	5.00	1.00	3.00	3.10
1.00	6.66	1.00	2.65	3.00
1.00	10.00	1.00	2.60	2.75
1.00	20.00	1.00	2.80	2.60
1.00	10.00	0.83	2.35	2.22
1.00	10.00	1.00	2.60	2.75
1.00	10.00	1.25	2.65	2.80
1.00	10.00	1.67	2.40	2.35
1.00	10.00	2.50	2.75	2.25
1.00	10.00	5.00	2.50	2.40

The kinetic results show a negligible effect of ionic strength (μ) of the medium and [$Hg(OAc)_2$] variation on the reaction rate (Table 2).The negligible effect of mercuric acetate indicates its role as a scavenger[9,10] for any bromide ion formed in the reaction. Kinetic results obtained on varying concentration of hydroxide ions indicate negative effect of [OH^-] variation, which means rate of the reaction decreases with increase in [OH^-].

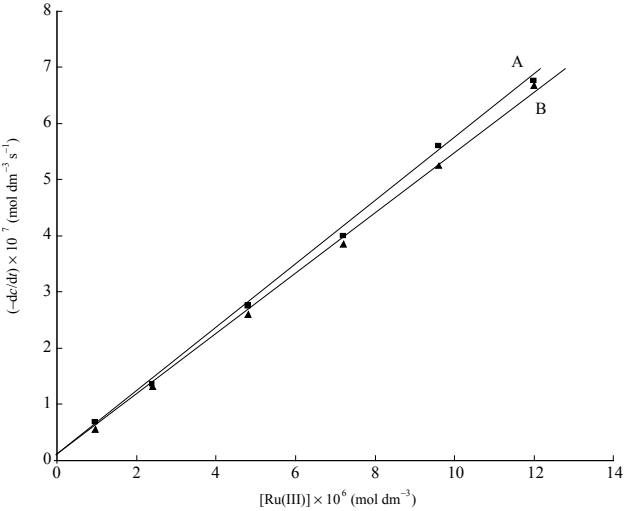

Fig. 1. Plot between [Ru(III)] and (–d*c*/d*t*) for oxidation of D-glucose (A) and D-galactose (B) at 35°C

Table 2. Effect of variation of hydroxide ion, mercury(II) acetate and sodium perchlorate on the reaction rate at 35°C

[Ru(III)] = 4.80 ×10^6 mol dm^{-3}, [$KBrO_3$] = 1.00 × 10^3 mol dm^{-3}, [KCl] = 1.00 ×10^3 mol dm^{-3}, [S] = 10.00 × 10^3 mol dm^{-3}

[NaOH] ×10^3 (mol dm^{-3})	[$Hg(OAc)_2$] ×10^3 (mol dm^{-3})	[$NaClO_4$] ×10^3 (mol dm^{-3})	(–d*c*/d*t*) × 10^7 (mol dm^{-3} s^{-1})	
			(glu.)	(gal.)
0.83	1.67	–	3.15	3.10
1.00	1.67	–	2.60	2.75
1.25	1.67	–	2.50	2.40
1.67	1.67	–	2.33	2.25
2.50	1.67	–	1.95	2.00
5.00	1.67	–	1.70	1.80
1.00	0.83	–	2.50	2.65
1.00	1.00	–	2.75	2.60
1.00	1.25	–	2.70	2.65
1.00	1.67	–	2.68	2.75
1.00	2.50	–	2.65	2.68
1.00	5.00	–	2.70	2.70
1.00	1.67	0.83	2.65	2.60
1.00	1.67	1.00	2.60	2.75
1.00	1.67	1.25	2.65	2.68
1.00	1.67	1.67	2.70	2.75
1.00	1.67	2.50	2.60	2.76
1.00	1.67	5.00	2.65	2.65

The rate measurements were taken at 30–45°C and specific rate constants were used to draw a plot of lg (–dc/dt) versus 1/T, which was linear (Fig. 2, glucose (A) and galactose (B)). The values of activation energy (ΔE^*), the Arrhenius factor (A), entropy of activation (ΔS^*) and free energy of activation (ΔG^*) were calculated from the rate measurements at 30, 35, 40 and 45°C and these values are recorded in Table 3.

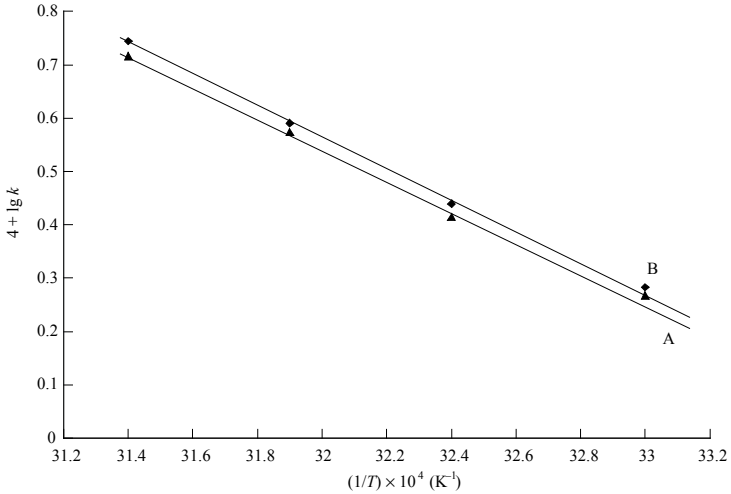

Fig. 2. Plot of 1/T versus lg k for oxidation of D-glucose (A) and D-galactose (B) at 35°C

Table 3. Activation parameters for alkaline bromate oxidation of glucose and galactose

Parameters	Temperature (°C)	Glucose	Galactose
$k_r \times 10^4$ (s^{-1})	30	1.85	1.92
$k_r \times 10^4$ (s^{-1})	35	2.60	2.75
$k_r \times 10^4$ (s^{-1})	40	3.75	3.90
$k_r \times 10^4$ (s^{-1})	45	5.20	5.55
lg A	–	9.66	10.17
ΔE^* (kJ mol^{-1})	–	54.58	57.45
ΔG^* (kJ mol^{-1})	–	74.25	74.08
ΔH^* (kJ mol^{-1})	–	69.55	73.78
ΔS^* (J K^{-1} mol^{-1})	–	–15.23	–12.86

$[RuCl_2(H_2O)_3OH]$ has been earlier reported as a reactive species in alkaline medium[11].

The following reaction steps are suggested on the basis of the above discussion for the Ru(III)-catalysed oxidation of aldoses by $KBrO_3$ in alkaline medium.

$$\underset{[C_1]}{[RuCl_2(H_2O)_3OH]} + H_2O \rightarrow \underset{[C_2]}{[RuCl_3(H_2O)_4]} + OH^-$$

$$[RuCl_3(H_2O)_4] + BrO_3^- \xrightarrow[\text{slow}]{k_1} [\ RuCl_3\ (H_2O)_4 \ldots\ldots BrO_3]^-$$

$$[RuCl_3\ (H_2O)_4 \ldots\ldots BrO_3]^- + S \rightarrow [RuCl_3\ (H_2O)_4] + P + BrO_2^-$$

where S is glucose and galactose and P – gluconic acid and galactonic acid.

Considering the above steps and applying the steady-state treatment with reasonable approximation, the rate law may be written in terms of rate of consumption of $[BrO_3^-]$ as follows:

$$-d[BrO_3]/dt = k_2\,[C_2]\,[BrO_3^-]$$

$$-\frac{d[BrO_3]}{dt} = \frac{k_2\,K_1\,[Ru(III)]_T\,[BrO_3^-]}{K_1 + [OH^-]}\ .$$

CONCLUSIONS

The experimental results reveal that the reaction doubles when the concentration of the catalyst Ru(III) is doubled. The rate law is in conformity with all kinetic observations and the proposed mechanistic steps are supported by the negligible effect of ionic strength. The high positive value of change in free energy of activation (ΔG^*) indicated highly solvated transition state, whereas fairly high negative values of change in entropy of activation (ΔS^*) suggest the formation of an activated complex with reduction in the degree of freedom of molecules. From this investigation is concluded that $[RuCl_2(H_2O)_3OH]$ and BrO_3^- are the reactive species of Ru(III) chloride and potassium bromate in alkaline medium, respectively.

ACKNOWLEDGEMENTS

One of the authors, Shalini Singh, thanks UGC for financial support.

REFERENCES

1. Sh. SRIVASTAVA, P. KHARE: Ru(III) and Ir(III) Catalysed Oxidation of Malic Acid by N-bromosuccinimide. A Comparative Kinetic Study. Oxid. Commun., **29** (1), 48 (2006).
2. Sh. SRIVASTAVA, A. AWASTHI, K. SINGH: Ruthenium(III) Catalyzed Oxidation of Cyclopentanol and Cyclohexanol by N-bromo Acetamide. Intern. J. of Chemical Kinetics, **37** (5), 275 (2005).
3. Sh. SRIVASTAVA, R. K. SHARMA: Kinetics and Mechanism of Iridium(III) Catalysed Oxidation of Some Cyclic Ketones by Acid Bromate. Oxid. Commun., **29** (2), 343 (2006).
4. Sh. SRIVASTAVA, S. SINGH: Kinetic Study of Ru(III) Catalyzed Oxidation of Proline by Potassium Bromate in Perchloric Acid Medium. J. Indian Chem. Soc., **81**, 295 (2004).
5. Sh. SRIVASTAVA, A. KUMAR, P. SRIVASTAVA: A Kinetic Study of Ru(III) Catalyzed Oxidation of Maltose by Potassium Bromate in Alkaline Medium. J. Indian Chem. Soc., **83**, 347 (2006).
6. Sh. SRIVASTAVA, R. K. SHARMA, S. SINGH: Kinetics and Mechanism of Iridium(III) Catalyzed Oxidation of Some Cyclic Alcohols by Potassium Bromate in Acidic Medium. J. Indian Chem. Soc., **84**, (2006).

7. A. SINGH, S. SINGH, A. SINGH, B. SINGH: Mechanistic Study of Osmium(VIII) Promoted Oxidation of Crotonic Acid by Aqueous Alkaline Solution of Potassium Bromate. Trans. Metal Chem., **30** (5), 610 (2005).
8. F. FIEGL: Spot Test in Organic Analysis. Elsevier, New York, 1996, p. 325.
9. N. VENKATASUBRAMANIAN, V. THIAGARAJAN: Mechanism of Oxidation of Alcohols with N-bromo Succinimide. Can. J. Chem., **47**, 694 (1969).
10. J. C. BAILER: Chemistry of Coordination Compound. Reinhold, New York, 1964, p. 4.
11. A. KUMAR, VIDHI, Y. ARAFAT: Ruthenium(III) Catalyzed Oxidation of D(+) Galactose and Lactose by Alkaline Potassium Bromate. Bull. of the Catalysis Society of India, **8**, 96 (2009).

Received 10 October 2008
Revised 19 January 2009

KINETICS AND MECHANISM OF PERIODATE OXIDATION OF *p*-ANISIDINE IN ACETONE–WATER MEDIUM

R. D. KAUSHIK[a]*, MANILA[a], D. KUMAR[a], P. SINGH[b]

[a]*Department of Chemistry, Gurukul Kangri University, 249 404 Haridwar* (*U. K.*), *India*
[b]*Department of Chemistry, D.A.V. College, Muzaffarnagar* (*U. P.*), *India*
E-mail: *rduttkaushik@yahoo.co.in*

ABSTRACT

Main reaction product of the periodate oxidation of *p*-anisidine (PMA) in acetone–water medium, 4-methoxy-1,2-benzoquinone, was isolated and characterised. The kinetics of the reaction has been followed by monitoring the increase in the absorbance of reaction intermediate, C. The reaction followed second order, being first order in each reactant. Results under pseudo-first order conditions, $[IO_4^-] >> [PMA]$, are in agreement with the derived rate law. Also in agreement with the rate law the $1/k_2$ versus $[H^+]$ profile passes through the minimum. Increase in ionic strength increases the rate of reaction. Further, the rate of reaction increases with increase in dielectric constant of the medium. Free radical scavengers do not affect the reaction rate. Thermodynamic parameters evaluated are: E_a = 3.46 kcal mol^{-1}, A = 114.6 dm^3 mol^{-1} s^{-1}; $\Delta S^* = -51.2$ cal K^{-1} mol^{-1}, ΔG^* = 18.7 kcal mol^{-1} and ΔH^* = 2.9 kcal mol^{-1}.

Keywords: kinetics, mechanism, periodate oxidation, *p*-anisidine, 4-methoxy-1,2-benzoquinone.

AIMS AND BACKGROUND

The kinetic and mechanistic studies on the periodate oxidation of *p*-anisidine have been aimed at elucidating the mechanism of the reaction and rate law particularly for seeking an explanation for the unique rate-pH profile observed.

The kinetic studies reported for the non-Malapradian periodate oxidation of aromatic amines are rather few[1–6] and contradictory in regard to the ionic or free radical mechanism being followed. Recent reports include the periodate oxidation of 3,3′,5′,5′-tetramethylbenzidine and oxidation of L-proline by bis(hydrogen periodato) argentate(III) complex anion[7]. In continuation to our earlier studies[8–11], the results of

* For correspondence.

periodate oxidation of *p*-anisidine in acetone–water medium are being presented and discussed in the present communication.

EXPERIMENTAL

Reagents and chemicals. Sodium meta periodate (Loba Chemie), *p*-anisidine (Sigma–Aldrich), acetone (E. Merck) and all other chemicals of analytical reagent/guaranteed reagent grade were used after redistillation/recrystallisation. Triply distilled water was used for preparation of the solutions. Thiel, Schultz and Koch buffer[12], consisting of different volumes of 0.05 M oxalic acid, 0.02 M boric acid, 0.05 M succinic acid, 0.05 M sodium sulphate and 0.05 M borax, was used for maintaining the pH, measured on a Systronics digital pH-meter-802. The reactions were studied in a spectrophotometric cell and initiated by adding temperature equilibrated $NaIO_4$ solution of known concentration to the reaction mixture containing the *p*-anisidine and buffer and maintained at the desired temperature (± 0.1°C).

Kinetics procedure. The progress of the reaction was followed by recording the absorbance on a Schimadzu double beam spectrophotometer (UV Pharmaspec-1700), at 475 nm, i.e. the λ_{max} of the orange colour reaction mixture. λ_{max} was not found to change with change in pH. High-precision thermostatically controlled water bath with an accuracy of ± 0.1°C was employed for maintaining the desired temperature.

Product analysis. Reaction mixture containing oxidant in excess was left overnight to ensure completion of the reaction. Initially the solution turned light orange, thereafter dark red and finally the product was precipitated on standing. It was filtered and the filtrate was extracted with petroleum ether (40–60°C). The extract was evaporated at room temperature to get a scarlet coloured product, which was found to be TLC single. It was recrystallised in ether and characterised as 4-methoxy-1,2-benzoquinone on the basis of positive test for quinone[13], m.p. 87°C (literature value 88°C (Ref. 14)), UV spectrum (in $CHCl_3$ giving absorption maxima at 400 nm, which suggested the presence of quinonoid structure in the compound (literature values 406.5 nm for 4-methoxy-1,2-benzoquinone[15]). The IR spectrum of compound (in KBr) showed the presence of bands at 2976 cm^{-1} (s) (due to ring C–H stretch), 1674 cm^{-1}(s) (indicating the presence of C=O on benzoquinone pattern with the possibility that the position of this band got lowered due to +I effect of methoxy group[16]), 3280 cm^{-1}(s) (may be due to overtone of C=O stretch). Further, the bands at 1520 cm^{-1} (s), 1400 cm^{-1}(s) may be due to C=C ring stretch. The bands at 1238 cm^{-1} (m) to 1040 cm^{-1} (m) may be due to the asymmetric and symmetric C–O–C stretch and at 746 cm^{-1} (s) (m) and 824 cm^{-1} (m) (due to out of plane C=C and C–H bending modes). The observed values are in a good agreement with those reported/ expected for 4-methoxy-1,2-benzoquinone.

The NMR spectrum of this compound in $CDCl_3$ showed the peaks at δ= 7.266, s, (1H); at δ = 7.046, d, (1H), δ = 7.286, d, (1H) and at δ = 4.08, s, (3H). A singlet at δ =

4.08 may be due to $-OCH_3$ group attached to the ring. The other signals in spectrum may be due to the three protons of the ring.

Stoichiometry. Stoichiometry of the reaction was determined by allowing a known excess of $NaIO_4$ to react with substrate. After completion of the reaction, the precipitated product was filtered out and in the filtrate unconsumed $NaIO_4$ was determined iodoimetrically. The results indicate the stoichiometry to be 1 mol PMA : 2 mol periodate as in the following equation:

$$CH_3OC_6H_4NH_2 + 2IO_4^- + 2H^+ \rightarrow CH_3OC_6H_3O_2 + 2HIO_3 + NH_3 \quad (1)$$

RESULTS

Preliminary observations. On mixing the reactants, the solution becomes light orange which later changes into dark red. On keeping for long time it finally gives the product. These observations indicate the formation of more than one intermediate prior to the formation of final reaction product. The rapid scan of the wine red solution showed the λ_{max} of the intermediate C to be 475 nm. The UV-vis. spectra of IO_4^- and *p*-anisidine indicated these to show no absorption in visible region. Hence for following the kinetics the absorbance changes were recorded at 475 nm at which only the intermediate C absorbs. Plane mirror and the Guggenheim methods, respectively, were used for evaluation of initial rates in terms of change in absorbance with time, (dA/dt), and pseudo-first order rate constants, k_{obs}.

Rate law. The kinetics was studied under pseudo-order conditions, viz. $[IO_4^-]_0 >> [S]$ and $[S]_0 >> [IO_4^-]$. Under both these conditions the reaction displayed first order. Under the condition, $[S]_0 >> [IO_4^-]$, the results (Table 1) were defined by equation (2) and pseudo-first order rate constant, k_{obs}, was equal to $k_2 [S]_0$.

$$d[C]/dt = k_2 [IO_4^-] [S]_0 \quad (2)$$

where k_2 is a pH-dependent second order rate constant.

On the other hand, under the condition $[IO_4^-]_0 >> [S]$, the rate was defined by equation (3) and k_{obs} was equal to $k_2 [IO_4^-]_0$.

$$d[C]/dt = k_2 [IO_4^-]_0 [S]. \quad (3)$$

In equations (2) and (3) $[IO_4^-]_0$ and $[S]_0$ represent the initial concentrations of reactants in excess. The values of k_2 determined from k_{obs} values clearly indicate a clear cut first order in each of periodate and anisidine.

Table 1. Effect of variation of concentration of reactants, ionic strength, dielectric constant and pH on the reaction rate at 35 ± 0.1°C

$[NaIO_4]$ (M)	[PMA] (M)	Acetone (%)	[NaCl] (M)	pH	$k_{obs} \times 10^4$ (s^{-1})	k_2 ($dm^3\ mol^{-1}\ s^{-1}$)
0.0001	0.0010	10	–	7.0	4.0	0.40
0.0001	0.0012	10	–	7.0	5.8	0.48
0.0001	0.0014	10	–	7.0	6.5	0.47
0.0001	0.0016	10	–	7.0	7.7	0.48
0.0001	0.0018	10	–	7.0	8.4	0.47
0.0010	0.0001	5.0	–	7.0	8.4	0.84
0.0012	0.0001	5.0	–	7.0	10.2	0.85
0.0014	0.0001	5.0	–	7.0	11.5	0.82
0.0016	0.0001	5.0	–	7.0	13.4	0.84
0.0018	0.0001	5.0	–	7.0	15.4	0.85
0.0010	0.0001	10	–	5.0	3.1	0.31
0.0010	0.0001	10	–	5.5	3.5	0.35
0.0010	0.0001	10	–	6.0	3.8	0.38
0.0010	0.0001	10	–	6.5	4.4	0.44
0.0010	0.0001	10	–	7.0	5.0	0.50
0.0010	0.0001	10	–	7.5	3.7	0.37
0.0010	0.0001	10	–	8.0	2.9	0.29
0.0010	0.0001	10	–	8.5	2.7	0.27
0.0010	0.0001	10	–	9.0	2.6	0.26
0.0001	0.0010	10	0.003	7.0	5.8	0.58
0.0001	0.0010	10	0.004	7.0	6.3	0.63
0.0001	0.0010	10	0.005	7.0	6.9	0.69
0.0001	0.0010	10	0.006	7.0	7.7	0.77
0.0001	0.0010	10	0.007	7.0	8.4	0.84
0.0001	0.0010	10	0.008	7.0	9.4	0.94
0.0001	0.0010	2.5	–	7.0	10.0	1.00
0.0001	0.0010	5.0	–	7.0	7.2	0.72
0.0001	0.0010	10	–	7.0	5.8	0.58
0.0001	0.0010	15	–	7.0	3.3	0.33

The effect of pH was examined in the range 5.0–9.0. Rate-pH profile indicates a maximum at pH = 7.0 (Table 1), which could be due to change in the nature of species and their relative reactivity when the pH is changed.

Effect of ionic strength, dielectric constant of medium, free radical scavengers and temperature. An increase in ionic strength, μ, led to an increase in the rate and the plot of lg k_2 versus μ was almost linear. An increase in dielectric constant increased the rate of reaction as indicated by a linear plot between lg k_2 versus $1/D$, where D is the dielectric constant of the medium. Both these effects (Table 1) indicate an ion–dipole type interaction in the rate-determining step, and that the reacting ion is

possibly an anion. Free radical scavengers acrylamide and allyl alcohol had no effect of on the reaction rate.

By determining the rate constants at four different temperatures (30.0 to 45.0°C), the values of different thermodynamic parameters were found to be: E_a = 3.46 kcal mol^{-1}, A = 114.6 dm^3 mol^{-1} s^{-1}, ΔS^*= –51.2 cal K^{-1} mol^{-1}, ΔG^* = 18.7 kcal mol^{-1} and ΔH^* = 2.9 kcal mol^{-1} at [PMA] = 0.001 mol dm^{-3}, [$NaIO_4$] = 0.0001 mol dm^{-3}, pH = 7.0 and acetone = 10.0 % (v/v).

DISCUSSION

Some important features of this reaction, which provide clue to the possible mechanism, are as follows:

Firstly, there is appearance of orange colour which continues to darken with increase in the concentration of the intermediate, C and finally the product settles on standing for long time. Obviously, the coloured intermediate is formed on a time scale of minutes and the final product on a time scale of hours. In reality the overall reaction involves several steps and possibly several transient intermediates, in addition to comparatively stable one C, are formed during the oxidation of *p*-anisidine into benzoquinone.

Secondly, the kinetic order of one in periodate but requirement of the two periodate molecules for each anisidine molecule as per stoichiometry indicates the involvement of only one periodate in the rate-determining step and second IO_4^- ion is consumed in a fast reaction in the formation of the intermediate, C. It also indicates the orange coloured intermediate is quite stable, and its concentration is not in steady state. Had this been so, there should have been no change in its concentration with time. On the contrary, concentration of C increases continuously with time and reaches a limiting value. And this has been used in following the kinetics of this reaction.

Thirdly, k_2 – pH profile indicates the presence of at least three differently reactive reactant species in the pH region chosen for study.

Before presenting a mechanism, it is necessary to discuss the speciation of anisidine and periodate species in aqueous solutions. In aqueous solutions, periodate exists in three forms governed by the following equilibria:

$$H_5IO_6 \rightleftharpoons H_4IO_6^- + H^+ , \; K_1 = 2.3 \times 10^{-2} \quad (4)$$

$$H_4IO_6^- \rightleftharpoons H_3IO_6^{2-} + H^+ , \; K_2 = 4.35 \times 10^{-9} \quad (5)$$

The value of K_1 indicates that in the pH range 5–9 the species H_5IO_6 shall be practically non-existent and hence only species $H_4IO_6^-$ and $H_3IO_6^{2-}$ need to be considered for explaining the observed pH-dependence. In case of *p*-anisidine[17], in aqueous solution the following acid-base equilibrium with $K_b = 20 \times 10^{-10}$ operates.

$$CH_3OC_6H_4NH_2 + H_2O \rightleftharpoons CH_3OC_6H_4N^+H_3 + OH^- \quad (6)$$

In the studied pH-range, both $CH_3OC_6H_4NH_2$ and $CH_3OC_6H_4N^+H_3$ shall exist and both of these have been considered.

Based on the observed kinetic rate laws (2)–(3) and pH-dependence, the following mechanism, which assumes $CH_3OC_6H_4NH_2$ and $H_4IO_6^-$ to be the reactive species, is proposed:

$$CH_3OC_6H_4NH_2 + [IO_4^-] \overset{K}{\rightleftharpoons} [A] \quad (7)$$

$$[A] \overset{k}{\longrightarrow} \text{intermediate [B] (slow)} \quad (8)$$

$$[B] + IO_4^- \longrightarrow \text{intermediate [C] (fast)} \quad (9)$$

The intermediate, C, appears to undergo very slow reorganisation/hydrolysis to yield the reaction product:

$$\text{intermediate [C]} \longrightarrow \text{product [D]} \quad (10)$$

In the mechanism for simplicity, $H_4IO_6^-$ has been written as IO_4^-. Since the elementary reactions in liquid phase are a rarity, the formation of a transient intermediate [C], which could be a collisional complex/reactant pair in a rapid step having a low value of equilibrium constant, K, is assumed in the proposed gross mechanism.

The mechanistic steps (8)–(9) lead to the following rate law:

$$d[C]/dt = k\,[A] \quad (11)$$

$$= kK[CH_3OC_6H_4NH_2]\,[IO_4^-]. \quad (12)$$

Since the observed kinetics shows first order in each of $[CH_3OC_6H_4NH_2]$ and $[IO_4^-]$, the value of K must be low.

At a fixed pH, under the condition $[S]_0 >> [IO_4^-]$, the rate of formation of intermediate, C, is given by equation (13) as follows:

$$d[C]/dt = kK\,[IO_4^-]\,[S]_0/(1+K[S]_0). \quad (13)$$

Likewise, under the condition $[IO_4^-]_0 >> [S]$

$$d[C]/dt = kK\,[IO_4^-]_0[S]\,/\,(1+K[IO_4^-]_0). \quad (14)$$

Since the reaction shows a clean-cut first order in each of [S] and $[IO_4^-]$, the inequalities $K[S]_0 << 1$ and $K[IO_4^-]_0 << 1$ should operate in equations (13) and (14), respectively leading to the rate laws in equations (2) and (3).

On substituting the values of concentrations of the reactive species $[CH_3OC_6H_4NH_2]$ and $[IO_4^-]$ in terms of equilibria (4)–(5) and (6), respectively, in equation (12), the complete rate law including $[H^+]$-dependence becomes:

$$d[C]/dt = kK\,(([S]\,[OH^-]\,/(\,[OH^-] + K_b))(([IO_4^-]_0\,[H^+]\,/(K_2 + [H^+])) \quad (15)$$

On replacing $[OH^-]\,[H^+]$ by K_w and $[OH^-]$ by $K_w/\,[H^+]$ in denominator and on rearranging, we get:

$$d[C]/dt = k\,KK_w\,[S]\,[IO_4^-]_0\,[H^+]\,/\,\{K_2\,K_w + (K_w + K_b K_2\,)\,[H^+] + K_b\,[H^+]^2\} \quad (16)$$

where kK is the empirical composite rate constant; K_w – ionic product of water; K_2 – acid dissociation constant of $H_4IO_6^-$; K_b – base dissociation constant of PMA and $[IO_4^-]_0$ represents the concentration of periodate that has been taken in excess.

On comparing equations (3) and (16), we get

$$k_2 = kK\,K_w\,[H^+]\,/(K_2\,K_w + (K_w + K_b K_2)\,[H^+] + K_b\,[H^+]^2). \quad (17)$$

Equation (17) on rearranging becomes equation (18) as follows:

$$1/k_2 = (K_2\,/kK[H^+]) + \{(K_w + K_b K_2)\,/kKK_w\} + K_b\,[H^+]\,/kKK_w. \quad (18)$$

The nature of the rate law shows that a plot of $1/k_2$ versus $[H^+]$ shall pass through a minimum as discussed in detail in a review by Gupta and Gupta[18]. On differentiating $1/k_2$ with respect to $[H^+]$ in equation (18), we get the values of $d^2[1/k_2]/d[H^+]^2$. The value of second derivative is found to be positive showing the plot of $1/k_2$ versus $[H^+]$ to pass through a minimum. Thus, on setting $d[1/k_2]/d[H^+]$ equal to zero for obtaining hydrogen ion concentration at which the $1/k_2$ versus $[H^+]$ profile will pass through minimum, we obtain:

$$[H^+]_{min} = (K_2\,K_w/K_b)^{1/2}$$

On substituting the values of K_2, K_w and K_b, we get

$$[H^+]_{min} = 1.48 \times 10^{-7}\ \text{mol dm}^{-3}.$$

It is gratifying to note that the calculated value of $[H^+]_{min.}$ is in excellent agreement with the experimental value of $[H^+]_{min}$ of 1.0×10^{-7} mol dm^{-3} obtained from $1/k_2$ versus $[H^+]$ plot (Fig. 1).

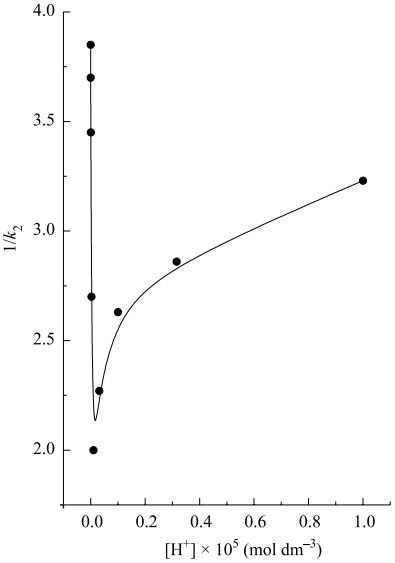

Fig. 1. Effect of $[H^+]$ on reaction rate at $[NaIO_4] = 0.0001$ M, [PMA] = 0.001 M, acetone = 10% (v/v), temperature 35 ± 0.1°C

It is necessary and interesting to discuss the possible molecular mechanism of the reaction. Mechanism proposed in Scheme 1 shows the first step as a reversible bimolecular reaction between PMA and [IO_4^-]. The formation of a charged intermediate complex [A] taking place by the attack of [IO_4^-] on the nitrogen of anilino group and stabilisation of positive charge on this nitrogen are well supported by our earlier LFER studies on this type of reaction series[19]. The high negative value of entropy of activation supports the involvement of solvation effects in this reaction. The formation of another intermediate [B] followed by its reaction with another IO_4^- to form quinoneimine [C] in a fast step are the expected steps of the mechanism involved.

Scheme 1

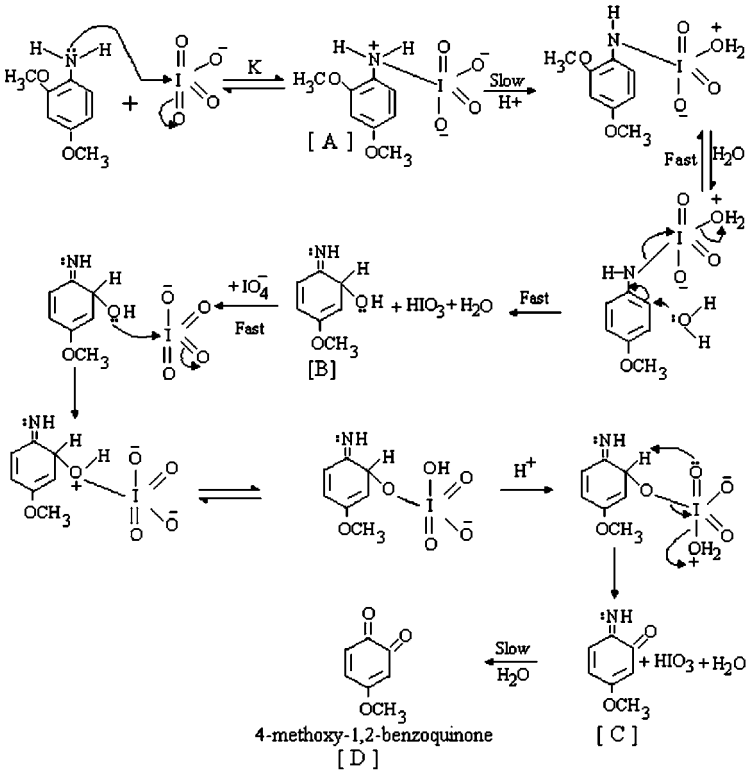

The last step (10) seems to be the slow hydrolysis and rearrangement of (C) to give 4-methoxy-1,2-benzoquinone (D), i.e. the main product of the reaction that has been isolated, separated and characterised.

CONCLUSIONS

The kinetics of the reaction between *p*-anisidine (PMA) and periodate ion in acetone–water medium has been followed by monitoring the increase in the absorbance of reaction intermediate, C. The reaction followed second order behaviour, being first order in each reactant. Results under pseudo-first order conditions, $[IO_4^-] >> [PMA]$, are in agreement with the derived rate law. The rate law matches the $1/k_2$ versus $[H^+]$ profile that passes throught a minimum.

Increase in ionic strength increases the rate of reaction. Further, the rate of reaction increases with increase in dielectric constant of the medium. Free radical scavengers do not affect the reaction rate. Main reaction product was isolated and characterised as 4-methoxy-1, 2-benzoquinone.

REFERENCES

1. G. DRYHURST: Periodate Oxidation of Diols and Other Functional Groups, Analytical and Structural Applications. Pergamon Press, N. Y., 1970.
2. V. E. KALININA: Kinetics and Mechanism of Periodate Oxidation Reactions Catalysed by Ruthenium Compounds. Kinet. Katal., **12**, 100 (1971) (in Russian).
3. V. K. PAVOLVA, Ya. S. SEVCHENKO, K. B. YATSMIRISKII: Kinetics and Mechanism of Oxidation of Diethylaniline with Periodate. Zh. Fiz. Khim., **44**, 658 (1970) (in Russian).
4. M. P. RAO, B. SETHURAM, T. N. RAO: Kinetics of Oxidation of Aniline and Substituted Anilines by Periodate. Indian J. Chem., **17 (A)**, 52 (1979).
5. S. P. SRIVASTAVA, G. BHATTACHARJEE, V. K. GUPTA, SATYA PAL: Kinetics and Mechanism of Oxidation of Sulfanilic Acid by Periodate Ion in Aqueous Medium. React. Kinet. Catal. Letters, **13**, 231 (1980).
6. M. K. BEKLEMISHEV, E. N. KIRYUSHCHENKOV, E. K. SKOSYRSKAYA, A. M. PETRENKO: Periodate Ion as an Oxidant in Indicator Reactions with Aromatic Amines. J. Anal. Chem., **61**, 1067 (2006).
7. H. W. SUN, H. M. SHI, S. G. SHEN, Z. F. GUO: Kinetics and Mechanism for Oxidation of L-proline by Bis(hydrogen periodato)argentate(III) Complex Anion. Chinese J. Chem., **26**, 615 (2008).
8. S. P. SRIVASTAVA, M. C. JAIN, R. D. KAUSHIK: Kinetics and Mechanism of Periodate Oxidation of Aromatic Amines – Oxidation of N,N-dimethylaniline. Nat. Acad. Sci. Letters, **2**, 63 (1979).
9. V. K. GUPTA, R. BHUSHAN, R. D. KAUSHIK, M. C. JAIN, S. P. SRIVASTAVA: Kinetics and Mechanism of the Oxidation of Aromatic Amines by Periodate Ion – Oxidation of Aniline and N,N-dimethylaniline. Oxid. Commun., **7**, 409 (1984).
10. R. D. KAUSHIK, R. P. SINGH, SHASHI: A Kinetic-mechanistic Study of Periodate Oxidation of *p*-chloroaniline. Asian J. Chem., **15**, 1485 (2003).
11. R. D. KAUSHIK, AMRITA, M. DUBEY, R. P. SINGH: Periodate Oxidation of *p*-bromoaniline in Acetone-water Medium: A Kinetic-mechanistic Study. Asian J. Chem., **16**, 831 (2004).
12. H. T. S. BRITTON: Hydrogen Ions. D. Von Nostrand Co., 1956, p. 354.
13. B. S. FURNISS, A. J. HANNAFORD, P. W. G. SMITH, A. R. TATCHELL: Vogel's Textbook of Practical Organic Chemistry. 5th ed. Addison-Wesley Longman Ltd., 1998, p.1221.
14. J. BUCKINGHAM (Ed.): Dictionary of Organic Compounds. 5th ed. Chapman and Hall, N. York, 1982, Vol. 3, p. 3002.
15. J. P. PHILLIPS, R. E. LYLE, P. R. JONES (Eds): Organic Electronic Spectral Data. Interscience Publishers, N. York, 1960–1961, Vol. 5, p. 91.

16. P. S. KALSI: Spectroscopy of Organic Compounds. 2nd ed. New Age International Ltd., N. Delhi, 1996.
17. R. T. MORRISON, R. N. BOYD: Organic Chemistry. 6th ed. Prentice Hall of India Pvt. Ltd., N. Delhi, 1996, p. 824.
18. K. S. GUPTA, Y. K. GUPTA: Hydrogen-ion Dependence of Reaction Rates and Mechanism. J. Chem. Educ., **61**, 972 (1984).
19. S. P. SRIVASTAVA, V. K. GUPTA, M. C. JAIN, M. N. ANSARI, R. D. KAUSHIK: Thermodynamic and LFER Studies for the Oxidation of Anilines by Periodate Ion. Thermochimica Acta, **68**, 27 (1983).

Received 22 May 2009
Revised 23 August 2009

KINETICS OF OXIDATION OF GLYCINE BY ALKALINE HEXACYANOFERRATE(III)

D. LALOO[a], M. K. MAHANTI[a,b]*

[a]*Department of Chemistry, North-Eastern Hill University, 793 022 Shillong, India*
E-mail: *m.mahanti@yahoo.com*
[b]*National Institute of Science Education and Research, 751 005 Bhubaneswar, India*

ABSTRACT

The reaction between glycine and potassium hexacyanoferrate(III), in alkaline medium, at constant ionic strength, gave glyoxylic acid. The rate of the reaction was dependent on the first powers of the concentrations of substrate and oxidant, but was independent of the concentration of alkali in the range studied. The slow step of the reaction involved the formation of a radical intermediate, which was detected by ESR spectroscopy as a 7-line spectrum with peak intensity ratios of 1:5:11:14:11:5:1.

Keywords: kinetics, oxidation, glycine, alkaline hexacyanoferrate(III).

AIMS AND BACKGROUND

Amino acids are the building blocks in protein synthesis. The fact that all of the more important naturally occurring amino acids have α-hydrogens, suggests that the biosynthesis and degradation of amino acids occur by way of α-keto acids and α-imino acids, thus:

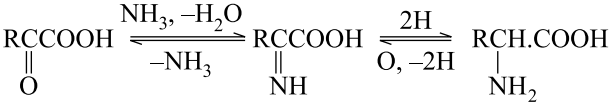

In metabolism, amino acids are subjected to many reactions, and can supply precursors for various endogeneous substances, as for example, hemoglobin in blood. Amino acids undergo various kinds of reactions depending on whether the particular amino acid contains nonpolar groups, polar substituents, acidic, or basic substituents. Amino acids have been oxidised by diverse oxidising agents[1–7].

Glycine is one of the major constituents of silk fibroin and collagen. The formation of δ-aminolevulinic acid from succinyl CoA (coenzyme A) and glycine is the first step leading specifically to the biosynthesis of porphyrins, which are present in

* For correspondence.

chlorophyll, hemoglobin and cytochromes. In continuation of our work on the oxidation of amino acids by hexacyanoferrate(III) in alkaline medium[8], we report the kinetics of oxidation of glycine by alkaline hexacyanoferrate(III), at constant ionic strength, under nitrogen.

EXPERIMENTAL

Materials, *methods and stoichiometry*. Glycine (Loba Chemie) was recrystallised (m.p. 262°C). Potassium hexacyanoferrate(III), potassium hexacyanoferrate(II), sodium hydroxide and sodium perchlorate were E. Merck samples. The ionic strength was kept constant using sodium perchlorate (0.001 mol dm^{-3}). All reactions were performed under nitrogen.

For the kinetic studies, pseudo-first order conditions, [amino acid] >> [oxidant] were used. The methods used for the preparation of solutions, and for the kinetic determinations for the disappearance of hexacyanoferrate(III) at 420 nm, have been described earlier[8].

The stoichiometry of the reaction was determined[8] to be:

$$C_2H_5O_2N + 2Fe(CN)_6^{3-} + 2OH^- \rightarrow C_2H_2O_3 + 2Fe(CN)_6^{4-} + NH_3 + H_2O \quad (1)$$

Product analysis. Reaction mixtures containing glycine (0.01 mol dm^{-3}) and excess of oxidant (0.1 mol dm^{-3}) were mixed in the presence of 0.5 mol dm^{-3} NaOH (ionic strength adjusted to 0.001 mol dm^{-3} by the addition of $NaClO_4$), and allowed to react at 328 K for 24 h, under nitrogen.

(i) The evolution of ammonia was shown by partial distillation of the reaction mixture. The ammonia formed was absorbed in an excess of standard acid (0.5 mol dm^{-3} HCl). The excess of acid was then back-titrated (against base) in the presence of methyl red indicator[9];

(ii) The reaction mixture was extracted with ether, washed with water, dried over anhydrous $MgSO_4$, and then concentrated. The product obtained was confirmed as glyoxylic acid[10] (yield ≈ 75%);

(iii) The product was treated with an acidic solution of sodium hydrogen sulphite, and cooled in ice. A solution of 2,4-dinitrophenylhydrazine (0.05 mol dm^{-3}) was added and the mixture allowed to stand overnight at 0°C. The solid compound formed was filtered off, dried, recrystallised from ethyl acetate, and weighed as the 2,4-dinitrophenylhydrazone derivative (m.p. 125°C).

RESULTS AND DISCUSSION

Kinetic results. Under pseudo-first order conditions, the reaction showed first order dependence in $[Fe(CN)_6^{3-}]$, as seen from the near constancy in the values of the pseudo-first order rate constant (k_1), over a 10-fold range of $[Fe(CN)_6^{3-}]$. The reaction exhibited first order dependence on the concentration of glycine (20-fold range).

The rate of the reaction was independent of the concentration of NaOH in the range studied (0.01 to 0.10 mol dm^{-3}). The kinetic results are shown in Table 1. Under the present experimental conditions, the rate law was expressed as follows:

$$\text{rate} = -\text{d}\,[\text{Fe(CN)}_6^{3-}]/\text{d}t = k\,[\text{glycine}]\,[\text{Fe(CN)}_6^{3-}] \quad (2)$$

Effect of temperature. The reaction was temperature dependent (Table 1), and the activation parameters were evaluated: $E = 15 \pm 2$ kJ mol^{-1}; $\Delta H^{*} = 12 \pm 2$ kJ mol^{-1}; $\Delta S^{*} = -180 \pm 4$ J K^{-1} mol^{-1}. The values of ΔH^{*} and ΔS^{*} were both favourable for electron abstraction processes[11].

Table 1. Rate data for oxidation of glycine at 328 K ($\mu = 0.001$ mol dm^{-3})

[Glycine] × 10^2 (mol dm^{-3})	[$K_3Fe(CN)_6$] × 10^3 (mol dm^{-3})	[NaOH] (mol dm^{-3})	$k_1 \times 10^3$ (s^{-1})
1.0	1.0	0.1	1.90
5.0	1.0	0.1	9.6
10.0	1.0	0.1	19.5
20.0	1.0	0.1	39.2
1.0	0.75	0.1	1.92
1.0	0.50	0.1	1.94
1.0	0.25	0.1	1.88
1.0	0.10	0.1	1.85
1.0	1.0	0.25	1.96
1.0	1.0	0.5	1.93
1.0	1.0	0.75	1.94
1.0	1.0	1.0	1.95
1.0	1.0	0.1	1.10[a]
1.0	1.0	0.1	1.41[b]
1.0	1.0	0.1	2.60[c]
1.0	1.0	0.1	3.42[d]

[a]318 K; [b]323 K; [c]333 K; [d]338 K; all temperatures ± 0.1 K.

Effect of ionic strength. Variations in the ionic strength of the medium using $NaClO_4$ ($\mu = 0.001$ to 0.01 mol dm^{-3}) did not affect the rate of the reaction, since the high concentration of alkali dominated over the ionic strength of the medium.

Effect of hexacyanoferrate(II). The addition of hexacyanoferrate(II) ions in the concentration range 1×10^{-4} to 1×10^{-3} mol dm^{-3} did not have any effect on the rate of the reaction, indicating that the reaction between the substrate and oxidant (the electron abstraction step) was irreversible.

Radical intermediate. The ESR spectrum (E-4, varian) of the radical generated from the oxidation of glycine by alkaline hexacyanoferrate(III), in a flow system, gave a 7-line spectrum. The number of lines was accounted for by a radical species consisting of 4

equivalent protons and a nitrogen atom, all having nearly equal coupling constants. The 7-line spectrum had relative intensities of 1:5:11:14:11:5:1.

Mechanism. Potassium hexacyanoferrate(III) is a one-electron oxidant, and hence it would be justified to postulate that the reaction between the substrate and oxidant would give rise to a radical intermediate (**1**), analogous to enzymatic oxidation reactions which are also known to proceed via radical species[12].

It is well known that amino acids exist as zwitterions in aqueous solution. In strongly acidic or alkaline media, the following equilibria exist:

$$\underset{\text{cation}}{RCH(\overset{+}{N}H_3)COOH} \underset{H^+}{\overset{OH^-}{\rightleftharpoons}} \underset{\text{zwitterion}}{RCH(\overset{+}{N}H_3)COO^-} \underset{H^+}{\overset{OH^-}{\rightleftharpoons}} \underset{\text{anion}}{RCH(NH_2)COO^-} \qquad (3)$$

In alkaline solution, the zwitterion would be converted into the anion, $RCH(NH_2)COO^-$, which is the reactive species under the present experimental conditions. The pK_a value for $RCH(NH_3)COO^- \rightleftharpoons RCH(NH_2)COO^- + H^+$ has been reported, with the dissociation constant[13] for glycine at 298 K being 1.67×10^{-10} (pK = 9.87). Since the kinetic studies were carried out at high concentrations of NaOH, it may be assumed that glycine would be completely dissociated into the anion, $RCH(NH_2)COO^-$ (**A**).

The kinetic isotope effect caused by deuterating the α-carbon atom gave a k_H/k_D value of 8.2, indicating that, in the rate-determining step, the C–H bond underwent fission to give the radical species.

The slow step was the direct reaction of the substrate with the oxidant, giving the radical intermediate (**1**). The subsequent rapid reaction was via the imino compound (**2**), which underwent hydrolysis to give the product (**3**):

$$\underset{\mathbf{A}}{RCH(NH_2)COOH + OH^- \rightleftharpoons RCH(NH_2)COO^-} + H_2O$$

$$\mathbf{A} + Fe(CN)_6^{3-} \rightarrow \underset{\mathbf{1}}{RC^{\bullet}(N^+H_3)COO^-} + Fe(CN)_6^{4-} \qquad \text{(slow)}$$

$$\mathbf{1} + Fe(CN)_6^{3-} \rightarrow \underset{\mathbf{2}}{RC(=NH)COOH} \rightarrow \underset{\mathbf{3}}{RC(=O)COOH} + NH_3 \qquad \text{(fast)}$$

This mechanistic pathway for the oxidation of glycine to the keto acid has been well established in the synthesis of α-keto esters[14].

CONCLUSIONS

The oxidation of glycine by alkaline hexacyanoferrate(III) yielded a radical intermediate, in the slow step. The radical underwent a rapid reaction with the oxidant giving

the α-imino acid, which was rapidly hydrolysed to the α-keto acid. The present investigation suggested that hexacyanoferrate(III), as a chemical oxidant, was capable of simulating enzymatic behaviour, and might prove useful in establishing model systems for the enzymatic oxidation of amino acids.

ACKNOWLEDGEMENT

Financial support from the University Grants Commission, New Delhi, as part of the Special Assistance Programme, is gratefully acknowledged.

REFERENCES

1. R. G. R. BACON, W. J. HANNA, D. STEWART Oxidation by Persulfate. Part V. Silver Catalyzed Oxidation of Secondary Aliphatic Amines and α-amino Acids. J. Chem. Soc.(C), 1388 (1966).
2. D. G. LAMBERT, M. M. JONES: Oxidation of Some Chelating Agents and Complexes with Alkaline Ferricyanide. J. Amer. Chem. Soc., **88**, 4615 (1966).
3. R. A. SHEIKH, W. A. WATERS: Oxidation of Organic Compounds by Cobaltic Salts. Part XIV. Oxidations of Some Aliphatic Amines and α-amino Acids. J. Chem. Soc.(B), 988 (1970).
4. G. CHANDRA, S. N. SRIVASTAVA: Kinetics and Mechanism of the Silver (I) Ion Catalyzed Oxidation of α-alanine by Peroxydisulfate. J. Inorg. Nucl. Chem., **34**, 197 (1972).
5. A. K. BOSE, R. M. MEHROTRA, S. P. MUSHRAN: Kinetics and Mechanism of the Oxidation of Amino Acids by Chloramines-T. Indian J. Chem., **11**, 896 (1973).
6. D. S. MAHADEVAPPA, K. S. RANGAPPA, N. M. M. GOWDA, B. T. GOWDA: Kinetics and Mechanistic Studies of Oxidation of Arginine, Histidine and Threonine in Alkaline Medium by N-chloro-N-sodio-*p*-toluenesulfonamide. Int. J. Chem. Kinet., **14**, 1183 (1982).
7. D. S. MAHADEVAPPA, S. ANANDA, A. S. A. MURTHY, K. S. RANGAPPA: Kinetics of Oxidation of L-isoleucine and L-leucine by Sodium N-bromobenzene-benzenesulfonamide in Perchloric Acid Medium. Indian J. Chem., **23**, 17 (1984).
8. D. LALOO, M. K. MAHANTI: Kinetics of Oxidation of Lysine by Alkaline Hexacyanoferrate(III). Oxid. Commun., **30**, 686 (2007).
9. A. I. VOGEL: Quantitative Inorganic Analysis. Longman and Green, London, 1961, p. 254.
10. F. FEIGL: Spot Tests in Organic Analysis. Elsevier, London, 1966, p. 485.
11. C. WALLING: Free Radicals in Solution. Wiley, New York, 1957, p. 38.
12. LANGE: Handbook of Chemistry. McGraw Hill, New York, 1973, Section 5.
13. T. NAKAMURA: Purification and Physicochemical Properties of Laccase. Biochem. Biophys. Acta, **30**, 44 (1958).
14. H. POISEL: α-Ketoesters from α-amino Acids. Chem. Ber., **111**, 3136 (1978).

Received 13 February 2009
Revised 20 March 2009

FIRST REPORT ON THE SYNTHETIC, SPECTRAL AND ANTIMICROBIAL STUDIES OF 4-(DIMETHYLAMINO)-1,4,4a,5,5a,6,11,12a-OCTAHYDRO-3,6,10,12,12a-PENTAHYDROXYNAPHTHACENE CARBOXAMIDO-METHYLAMINES

A. D. MANIKPURI

Department of Engineering Chemistry, Sanghvi Innovative Academy, Gram Kanadia, Old Sehore Road, Pragati vihar-II, 452 016 Indore, India
E-mail: *anju.dm@rediffmail.com*

ABSTRACT

The synthesis of 4-(dimethylamino)-1,4,4a,5,5a,6,11,12a-octahydro-3,6,10,12,12a-pentahydroxynaphthacene carboxamido-methylamines via aminomethylation approaches involving the Mannich reaction is described. The newly synthised Mannich bases are structurally elucidated on the basis of elemental and spectral (UV, IR, ^{1}H NMR) studies. All the newly synthesised Mannich bases exhibited significant and promising antimicrobial activity against various pathogenic gram-positive and gram-negative bacteria and are found to have low toxicity.

Keywords: 4-(dimethylamino)-1,4,4a,5,5a,6,11,12a-octahydro-3,6,10,12,12a-pentahydroxynaphthacene carboxamide, the Mannich base, antimicrobial activity, toxicity.

AIMS AND BACKGROUND

In organic chemistry carboxamides (or amino carbonyls) are functional groups with the general structure R–CO–NH_2 with R as an organic substituent. Carboxamides are outstanding class of natural products having notable antibacterial activity towards a broad range of pathogenic microorganisms and are characterised for very low toxicity to the mammalian hosts of these pathogens[1–5]. Recently, we showed that carboxamide is convenient class of compounds used for the synthesis of the Mannich bases of ultimate antibacterial property[6].

Some secondary amines like morpholine and piperazine are well known antibacterial and medicinal agents[7–9]. The Mannich reaction is a known pathway, which generates pharmacologically important drugs by incorporation of amino methyl group having versatile utility in the field of medicinal chemistry[10] as well as has diverse reactivity in industrial chemistry[11].

In view of the above stated, we thought it worthy to select the Mannich reaction to produce the Mannich bases of biologically active derivatives of carboxamide. Consequently and in continuation of our earlier studies on the Mannich condensation of various active hydrogen compounds[12] the present work was undertaken. The presented paper deals with the antibacterial screening of the newly synthesised Mannich, aminomethylation of carboxamide and comparison of the biological activity of newly synthesised with the parent sulphonamides. The results were critically analysed using statistical analyses[13].

EXPERIMENTAL

All the melting points were determined in open capillary tubes and are uncorrected. Thin layer chromatography was used for monitoring the reaction and to check purity. The silica gel of chromatographic grade was used for preparing plates.

UV spectra were recorded on a Schimadzu UV-160A, UV-vis. spectrophotometer; IR spectra in KBr matrix were recorded on a Schimadzu 820 IPC FTIR spectrometer. The ^{1}H NMR spectra on a Bruker DRX-300 FT NMR spectrometer and chemical shifts were expressed as (ppm) unit against tetramethylsilane (TMS) as internal reference. The chemical reagents used in the synthesis were E. Merck and Aldrich grade. Agar media used for antimicrobial studies were of Hi media make.

Scheme 1

Synthesis of the Mannich bases from sulphonamides (**4a**–**4e**)

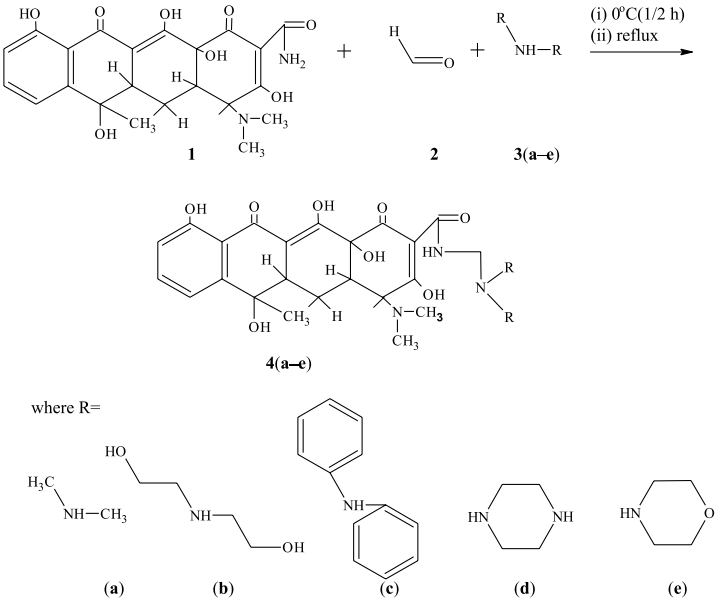

General procedure for the synthesis of compounds **4a**–**4e:** Synthetic pathway is shown in Scheme 1 and characterisation data for the synthesised compounds are given in Table 1. Carboxamide (0.01 mol) was dissolved in 20 ml methanol. This was followed by equimolar addition of secondary amines (0.01 mol) in small installments with constant stirring at efficient ice cooling. The reaction mixture was cooled well. Then 2.5 ml of formaldehyde solution (37%) were added slowly with continuous stirring. The mixture was kept as such for half an hour after adjusting the pH of reacting mixture to 3.5–4. After half an hour, the resulting reaction was placed on a water bath for refluxing. The reflux time varied with different secondary amines used. The mixture was then kept at 273°K for 4 days, when desired product was being formed. The Mannich base so formed was recrystallised with dry distilled ethanol**.**

Table 1. Study of antibacterial screening of the Mannich bases (zone of inhibition in mm)

S. No CN	*Salmonella enteritidis* concentration (mg/ml)				*Pasturella multocida* concentration (mg/ml)			
	20	30	40	average	20	30	40	average
4a	20.00	20.86	21.20	20.68	20.40	20.80	21.86	21.02
4b	21.06	21.22	22.06	21.44	21.26	22.00	23.20	22.15
4c	14.68	15.02	16.00	15.23	28.36	28.60	29.08	28.68
4d	20.00	25.00	25.00	23.33	15.20	15.24	15.60	15.34
4e	15.00	15.20	15.46	15.22	22.15	23.30	24.40	21.26
	Staphylococcus aureus concentration (mg/ml)				*Bacillus anthracis* concentration (mg/ml)			
	20	30	40	average	20	30	40	average
4a	20.40	20.80	21.86	21.02	8.42	9.20	10.46	9.36
4b	21.06	21.22	22.06	21.44	21.26	22.00	23.20	22.15
4c	21.26	22.00	23.20	22.15	13.46	13.60	13.86	13.64
4d	20.00	25.00	25.00	23.33	15.20	15.24	15.60	15.34
4e	28.00	28.24	29.20	28.48	18.06	18.20	18.06	18.38

RESULTS AND DISCUSSION

Compound (**4a**) – 4-(dimethylamino)-1,4,4a,5,5a,6,11,12a-octahydro-3,6,10,12,12a-pentahydroxynaphthacene carboxamido-methyl dimethylamine, m.p. 189–190°C, C(%) – 54.82 (54.84), H (%) – 4.60 (4.70), N (%) – 11.60 (11.63), UV 254 (Ar ring), 361 (diketone-moiety), IR (KBr)3441ν_{as} (NH) in sec amide, 3054 ν (=C–H) of aromatic ring, 2940 ν_{as} C–H in CH_2, 2731 ν >CH_2N<, 1836 ν (C=O), 1330, ν_{as} S=O, 1148, ν (C–H) in disubstituted benzene, 836 out of plane C–H in disubstituted aromatic ring, ^{1}H NMR 2.92 (d, 2H, *J* = 7.5, CH_2); 5.62 (s, 1H, NH); 6.50–7.90 (m, ArH); 7.22 (s, 1H,CONH); 1.80 (s, 1H, C_6Me_2); 2.67 (s, 1H, Nme_2); 2.20 (s, 1H, C_{4a}); 2.40 (s, 1H, C_{5a}); 2.30 (s,1H, C_5); 3.09 (s, 1H, C_4).

Compound (**4b**) – 4-(dimethylamino)-1,4,4a,5,5a,6,11,12a-octahydro-3,6,10,12,12a-pentahydroxynaphthacene carboxamido-methyl diethanolamine, m.p. – 135–137°C, C (%) – 54.45 (54.62), H (%) – 4.28 (4.62), N (%) – 9.16 (9.65), UV 253 (Ar ring), 362 (diketone-moiety), IR (KBr)3442ν_{as} (NH) in sec amide, 3052 ν (=C–H) of aromatic ring, 2940 ν_{as} C–H in CH_2, 2732 ν >CH_2N<, 1834 ν (C=O), 1332 ν_{as} S=O, 1148 ν (C–H) in disubstituted benzene, 838 out of plane C–H in disubstituted aromatic ring, ^{1}H NMR 2.90 (d, 2H, *J* = 7.5, CH_2); 5.60 (s, 1H, NH); 6.50–7.90 (m, ArH); 7.22 (s, 1H,CONH); 1.80 (s, 1H, C_6Me_2); 2.67 (s, 1H, Nme_2); 2.22 (s, 1H, C_{4a}); 2.42 (s, 1H, C_{5a}); 2.32 (s,1H, C_5); 3.09 (s, 1H, C_4).

Compound (**4c**) – 4-(dimethylamino)-1,4,4a,5,5a,6,11,12a-octahydro-3,6,10,12,12a-pentahydroxynaphthacene carboxamido-methyl diphenylamine, m.p. – 212–213°C, C (%) – 53.93(54.03), H (%) – 4.30 (4.96), N (%) – 8.19 (8.69), UV 254 (Ar ring), 361 (diketone-moiety), IR (KBr)3441ν_{as} (NH) in sec amide, 3327 ν_{NH} of SO_2NH, 3054 ν (=C–H) of aromatic ring, 2940 ν_{as} C–H in CH_2, 2731 ν >CH_2N<, 1836 ν (C=O), 1330, ν (C–H) in disubstituted benzene, 836 out of plane C–H in disubstituted aromatic ring, ^{1}H NMR 2.92 (d, 2H, *J* = 7.5, CH_2); 5.62 (s, 1H, NH); 6.50–7.90 (m, ArH); 7.22 (s, 1H,CONH); 1.80 (s, 1H, C_6Me_2); 2.67 (s, 1H, Nme_2); 2.20 (s, 1H, C_{4a}); 2.40 (s, 1H, C_{5a}); 2.30 (s,1H, C_5); 3.09 (s, 1H, C_4).

Compound (**4d**) – 4-(dimethylamino)-1,4,4a,5,5a,6,11,12a-octahydro-3,6,10,12,12a-pentahydroxynaphthacene carboxamido-methyl piperazine, m.p. – 203–204°C, C (%) – 52.23 (52.47), H (%) – 4.68 (4.45), N (%) – 12.18 (12.24), UV 256 (Ar ring), 362 (diketone-moiety), IR (KBr)3442ν_{as} (NH) in sec amide, 3056 ν (=C–H) of aromatic ring, 2942 ν_{as} C–H in CH_2, 2732 ν >CH_2N<, 1832 ν (C=O), 1146, ν (C–H) in disubstituted benzene, 836 out of plane C–H in disubstituted aromatic ring, ^{1}H NMR 2.90 (d, 2H, *J* = 7.5, CH_2); 5.60 (s, 1H, NH); 6.50–7.90 (m, ArH); 7.20 (s, 1H,CONH); 1.82 (s, 1H, C_6Me_2); 2.66 (s, 1H, Nme_2); 2.22 (s, 1H, C_{4a}); 2.42 (s, 1H, C_{5a}); 2.32 (s,1H, C_5); 3.08 (s, 1H, C_4).

Compound (**4e**) – 4-(dimethylamino)-1,4,4a,5,5a,6,11,12a-octahydro-3,6,10,12,12a-pentahydroxynaphthacene carboxamido-methyl morpholine, m.p. – 198–199°C, C (%) – 53.94 (53.70), H (%) – 4.22 (4.85), N (%) – 10.64 (10.74), UV 256 (Ar ring), 364 (diketone-moiety), IR (KBr) 3441 ν_{as} (NH) in sec amide, 3054 ν (=C–H) of aromatic ring, 2940 ν_{as} C–H in CH_2, 2731 ν >CH_2N<, 1836 ν (C=O), 1142, ν (C–H) in disubstituted benzene, 836 out of plane C–H in disubstituted aromatic ring, ^{1}H NMR 2.92 (d, 2H, *J* = 7.5, CH_2); 5.62 (s, 1H, NH); 6.50–7.90 (m, ArH); 7.22 (s, 1H,CONH); 1.80 (s, 1H, C_6Me_2); 2.67 (s, 1H, Nme_2); 2.20 (s, 1H, C_{4a}); 2.40 (s, 1H, C_{5a}); 2.30 (s,1H, C_5); 3.09 (s, 1H, C_4).

ANTIMICROBIAL ACTIVITY

The novel compounds (**4a**–**4e**) synthesised from secondary amines as reported in this paper are potent and demonstrate a specific antimicrobial activity against *S.aureus*, *S.enteritidis*, *P.multocida* and *B.anthracis.* Table 1 presents antibacterial activity as a measure of zone of inhibition against the bacterium under study. The Mannich bases

4e, **4d**, **4c** and **4b** are found to be potent active against the bacterium *S. aureus*, *S. enteritidis*, *P. multocida* and *B. anthracis*, respectively.

CONCLUSIONS

For the aforementioned results as discussion we conclude that the synthesised novel Mannich bases displayed a promising role in inhibiting the growth of pathogens under study. We believe that many future drugs and other useful products of industrial importance would be discovered and perhaps surprising medicinal molecules of the structural diversity of the Mannich bases could be synthesised might be envisioned by future chemists. Finally, it seems that the Mannich bases still constitute an important class of the medicines used today.

ACKNOWLEDGEMENT

The authors are indebted to Dr. K.P. Madhusudanan, R.S.I.C., CDRI, Lucknow for recording ^{1}H NMR spectra.

REFERENCES

1. L. S. GOODMAN, A. G. GILMAN: The Pharmacological Basis of Therapeutics. McGraw Hill Co., 9th ed., 1998.
2. T. J. FRANKALIN, G. A. SNOW: Biochemistry of Antimicrobial Action. 2nd ed. 1975.
3. D. LENDNICER: The Organic Chemistry of Drug Synthesis. 2nd ed. 1980.
4. J. C. DAVID, V. ISWARIAN, M. N. GARASWAMI: Pharmacology and Pharmacotherapeutic. 7th ed. 1975.
5. W. FOYE, L. THOMAS, D. A. WILLIAMS: Principle of Medicinal Chemistry. 4th ed. 1981.
6. S. JOSHI, A. D. MANIKPURI, P. TIWARI: Synthesis, Characterization and Biological Study of Medicinally Important Mannich Bases Derived from 4-(dimethylamino)-1,4,4a,5,5a,6,11,12a-octahydro-3,6,10,12,12a-pentahydroxynaphthacene carboxamide. Bioorg. Med. Chem. Lett., **17**, 645 (2007).
7. J. IMAI, M. I. JOHNSTON, P. F. TORRENCE: Chemical Modification Potentiates the Biological Activities of 2–5A and Its Congeners. J. Biol. Chem., **257** (21), 12739 (1982).
8. J. R. TAGAT, S. W. McCOMBIE, R. W. STEENSMA et al.: Piperazine-based CCR5 Antagonists as HIV-1 Inhibitors. I: 2(*S*)-methyl Piperazine as a Key Pharmacophore Element. Bioorg. Med. Chem. Lett., **11** (16), 2143 (2001).
9. A. H. El-MASRY, H. H. FAHMY, S. H. ALI ABDELWAHED: Synthesis and Antimicrobial Activity of Some New Benzimidazole Derivatives. Molecules, **5**, 1429 (2000).
10. S. JOSHI, A. D. MANIKPURI, D. KHARE: Synthetic, Spectroscopic and Antimicrobial Studies of Mannich Bases through Active Hydrogen Compounds. Intern. J. of Chem. Sci., **6**, 4 (2008).
11. S. JOSHI, A. D. MANIKPURI, P. V. KHADIKAR, D. KHARE: Synthesis and Structural Characterization of Mannich Bases of 5-uriedohydantoin. Oxid. Commun. (in press).
12. S. JOSHI, A. D. MANIKPURI, D. KHARE: Synthetic, Spectroscopic and Antibacterial Studies of Mannich Bases of 2-Chloro 4-nitro Benzamide. J. of Indian Chemical Society, **85**, 1 (2008).
13. W. B. TAYLOR: Incomplete Block Designs with Row Balance and Recovery of Interblock Information. Biometrics, **13**,1 (1957).

Received 2 February 2009
Revised 2 March 2009

PREPARATION AND CHARACTERISATION OF ULTRA-HIGH MOLECULAR WEIGHT POLYETHYLENE/RICE HUSKS ASH COMPOSITES

A. ATANASSOV[a]*, D. KIRYAKOVA[a], S. GENIEVA[b]

[a]*Department of Materials Science, Assen Zlatarov University, 1 Y. Yakimov Street, 8010 Bourgas, Bulgaria*
E-mail: *aatanassov@btu.bg*
[b]*Department of Physical Chemistry, Assen Zlatarov University, 1 Y. Yakimov Street, 8010 Bourgas, Bulgaria*

ABSTRACT

Composite materials were synthesised from ultra-high molecular weight polyethylene and white rice husks ash or black rice husks ash. The properties of the composites were studied as a function of the filler content (up to 6 mass. %). The apparent activation energy of thermal destruction of the materials obtained was found to decrease with the increase in the rice husks content. Slight reinforcing effect was observed (so far as tensile strength and elongation are concerned) at 1.5 mass. % content of white rice husk ash, while these characteristics remained almost the same as these of the initial polymer when black rice husks ash was used. Ultra-high molecular weight polyethylene (UHMWPE) composites containing 6 mass. % white rice husk ash showed higher thermostability, universal and plastic hardness as well as true elasticity modulus. The composite materials were characterised also by their Vicat softening point, shrinkage and the Shore hardness.

Keywords: rice husks ash, ultra-high molecular weight polyethylene, composite materials.

AIMS AND BACKGROUND

According to the statistical data of Food and Agriculture Organisation (FAO), the world annual paddy production of rice is approximately 582 million t. *Oryza sativa* L. husks (rice husk) comprise 25% of the rice grain and, therefore, 145 million t of rice husks residue are produced[1]. A number of reviews[2–7] have been dedicated to rice husks and the products obtained from its thermal degradation at different conditions. Large quantities of rice husks are available as waste from rice milling industry. These husks

* For correspondence.

are not of commercial interest and cause serious pollution problems, because they can not be used as food, fertiliser or fuel. It is necessary, then, to consider the use of this residue in polymer formulations with a clear positive effect to the environment.

Recently, the interest towards the use of rice husks as filler increased since it is harmless to environment and has low cost of production[8]. Various methods of rice husks utilisation have been developed involving biologic or thermochemical transformation. The thermal decomposition of raw rice husks in air atmosphere is known to occur in three main stages – drying (313–523 K), removal of organic volatile matters (488–623 K) and combustion of carbon (623–963 K)[9–11]. As a result, the so-called white rice husks ash (WRHA) containing ≥ 95 mass. % amorphous SiO_2 are obtained. If the thermal decomposition is carried out in nitrogen medium, the end product contains about 55 mass. % amorphous SiO_2 and 45 mass. % amorphous carbon, named as black rice husks ash (BRHA)[2–6].

There are a number of publications[8,12,13] devoted to the preparation and characterisation of composite materials (CM) on the basis of polypropylene (PP) filled with rice husks ash. It was found that the addition of BRHA filler to PP matrix increases the thermal degradation temperature while keeping the oxidative stability at the same level. The thermal degradation temperature of composites filled with WRHA does not depend on their content but the oxidative stability deteriorates with the increase of filler content[12]. The filling of PP with rice husks increases their flexural modulus and density, especially the composites filled with BRHA. The increase of the modulus is compensated for by the decrease of the tensile strength, elongation at break and impact strength with the increase of filler content[13].

Some data on the use of WRHA as filler for preparation of polypropylene/ethylene-propylene-diene terpolymer thermoplastic elastomer composites[14,15] were published. The utilisation of BRHA as filler in epoxy resins for preparation of different materials for use in electronic and electric appliances industries was also studied[16]. However, studies on the preparation of CM based on UHMWPE filled with WRHA or BRHA were not found in the available literature, although there are some investigations on the effect of the coupling agent and processing aid on the performance properties of high density polyethylene rice husk filled composite profiles[17].

The aim of the present work is to prepare and characterise composite materials on the basis of UHMWPE with these disperse fillers and determine their thermal, tensile, elasto-plastic and other properties.

EXPERIMENTAL

Materials. UHMWPE with melt index of 0.001 g/10 min (temperature 463 K; load of 21 kg) and molecular mass of 1.8×10^6, product of Lukoil-Neftochim Co., Bourgas, Bulgaria, was used.

Rice husks were obtained from suburb areas of Thrace (Pazardjik, Bulgaria). Before use, the raw rice husks (RRH) were thoroughly washed – two times with tap

water followed by three times with deionised water to remove adhering soil, clay and dust and finally, dried at 375±2 K overnight. The dried husks were ground in rotary cutting mill and sieved manually with 0.63–0.12 mm sieves. This starting material was thermally decomposed in nitrogen or air atmosphere. The thermal treatment of the rice husk fraction was carried out in quartz vertical tube, equipped with perforated quartz diaphragm at its lower end. The electrical heater used was wound around the quartz tube and insulated by asbestos sleeve. During the thermal treatment, nitrogen (or air) was flown below the quartz diaphragm into the lower end of the tube (100 $cm^3\ min^{-1}$) through the treated material. The controlled increase of temperature was performed using electronic thermal regulator Zeitplansolwertgeber (Germany) at a heating rate of 5 K min^{-1} up to 973 K, maintained for 2 h, after which the ash was quenched in nitrogen or air medium and used for further experiments. All the samples were stored in plastic sealer containers.

BRHA obtained by thermal decomposition of raw rice husks in nitrogen medium and WRHA obtained at thermal decomposition of raw rice husks in air atmosphere were used as fillers of UHMWPE. The mean particle size of the used fillers was 30–50 μm. According to the data from X-ray analysis, all the fillers were amorphous. The compositions were prepared by adding from 0 to 6 mass. % filler.

Preparation of UHMWPE composites. UHMWPE and BRHA or WRHA were mixed at room temperature in a laboratory mixer MPW-802 (Poland) at a stirring speed of 480 rpm for 4 min. The compositions were preformed into pellets (because of their low loose weight) and then pressed on a laboratory press PHI (England) between two aluminium foils under the following conditions: thickness of the sample ca. 1 mm, temperature 463 K, maintained for 11 min (the time of 11 min was chosen on experimental basis: 10 min were found to be insufficient to obtain UHMWE melt with suitable viscosity and, therefore, CM of proper quality). After 12 min at 463 K, partial destruction begins in virgin UHMWPE), pressing for 1 min at the same temperature and at a pressure of 9 MPa, followed by cooling at 40 K min^{-1} under the same pressure.

Materials characterisation. The morphology of the used fillers was examined by a scanning electron microscope (SEM) Tesla BS 340 (Czech Republic) under regime of secondary electrons at acceleration of 20 kV. The samples were metallised with aluminium in an Edwards 306 vacuum camera. The average thickness of the coating was measured to be 20 nm.

The thermal properties of UHMWPE samples were performed on an OD-102 derivatograph (MOM, Hungary) in air flow (25 $cm^3\ min^{-1}$). For determination of the apparent activation energy of thermal decomposition E_A of the studied composites the calculation procedure of Reich was used[18]. The tensile strength σ, elongation ε and the other characteristics of CM were measured on a dynamometer INSTRON 4203 (England) at a speed of 500 mm min^{-1} and room temperature. The elasto-plastic characteristics were determined using a nanotester FISCHERSCOPE H-100 (Germany)

at a load of 1000 mN. The thermostability of CM was calculated by weight loss (%) after 5 h at 406 K. The Vicat softening points were determined under the following conditions: cross-section of the finished rod 1 mm^2, load 1 kg and temperature increase rate 50 K h^{-1} (Fritz Heckert, Germany). The shrinkage (%) of CM was determined by the reduction of the linear dimensions of the samples after heat treatment at 373 K for 5 h compared to the dimensions before the treatment. The hardness by Shore was measured on an apparatus Stendal (Germany) by scale A.

RESULTS AND DISCUSSION

The morphologies of RRH, WRHA and BRHA were examined by scanning electron microscopy. The SEM micrographs of the samples are presented in Fig. 1. The main components of rice husks (cellulose, chemicellulose and lignin) are in lemma and palea form, which tightly interlock with each other[19]. Figure 1 shows the outer epidermis of raw rice husk, which is well organised and has a corrugate structure. The outer surface of lemma is highly ridged and the ridged structures have a linear profile. The epidermal cells of lemma are arranged in linear ridges and furrows and the ridges are punctuated with prominent globular protrusions[3,19–22]. The outer surface of lemma also contains papillae and hairs of varying sizes but they were often broken at their bases in the material examined and, therefore, are not illustrated. As can be seen in Fig. 1A, the structure of raw rice husk was globular. The relatively stable Si–O carcass and biomass assembled around it formed the structure of rice hull. The silicon atoms are presented all over but they are concentrated in the protuberances and hairs (trichomes) on the outer and inner epidermis, adjacent to the rice kernel. After combustion of rice husk in air (Fig. 1B), the morphology tended to maintain its original shape although the product is brittle and loose when carefully pinched with the fingers. The only difference that can be observed was that the globules were shrinked and compacted due to the release of the volatile products. The hard residue was formed of almost pure amorphous SiO_2 (96.8%). As it has been pointed out[21,23], the rate of combustion process depends strongly on the vapour diffusion rate from the bulk of the spherical globules. The structure of the pyrolysis product obtained in nitrogen medium was also globular (Fig. 1C), but due to the lower percentage of volatile products released, the solid residue contained significantly more carbon (42.6 mass. %). In this case, therefore, the initial globular structure of rice husk was also preserved due to the high thermal stability of SiO_2. The last two SEM micrographs showed that many residual pores are distributed within the ash samples, indicating that WRHA and BRHA are highly porous materials with large internal specific surface area.

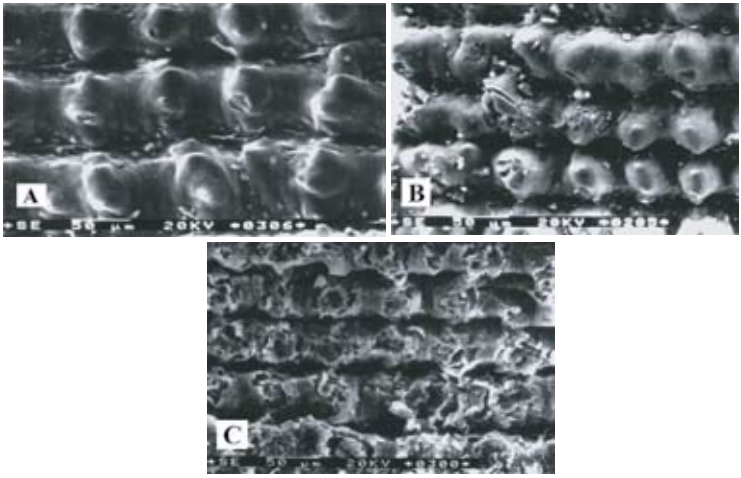

Fig. 1. Scanning electron micrographs of RRH (A), WRHA (B) and BRHA (C) at 973 K

The thermal characteristics of the studied composites are presented in Table 1. The activation energies E_A of thermal degradation of virgin UHMWPE was 160.9 kJ mol^{-1}, while for composite materials based on BRHA and WRHA it decreased to 143.8 and 121.2 kJ mol^{-1}, respectively, with the increase of filler content to 6 mass.%. It means that the composites studied are more susceptible to thermal destruction at higher content of WRHA and BRHA. This can be explained with disturbance of the initial polymer uniform structure when filler is introduced in it. Probably, the filler creates sites where the thermal destruction of the polymer is easier to start. The more substantial decrease of the activation energy for the sample filled with WRHA was attributed to its higher acidity determined by the presence of surface silanol (Si–OH) and siloxan (Si–O–Si) groups. This observation can be used in the recycling of waste polymers by thermal destruction in the presence of some hard acid catalyst (zeolites, amorphous silica-alumina and clays) to the corresponding monomers[24,25]. Besides, the coefficient of correlation was quite high – from 0.9542 to 0.9877. This was confirmed also by the temperature at 10 mass. % weight loss T_{10}. The melting temperature T_m was found to decrease by ca. 10 K for the material based on UHMWPE and BRHA while the melting temperature of the same polymer filled with WRHA remained the same. The temperature of thermal degradation T_d^i of the composite materials obtained on the basis of UHMWPE is the same as the initial polymer. The composites studied can be processed in the temperature interval 508–518 K. The ending temperature of destruction T_d^f of CM based on UHMWPE and WRHA decreased by 12–22 K while for these with BRHA – by 32 K.

Table 1. Thermal properties of UHMWPE composites with WRHA or BRHA

Property	Virgin UHMWPE	Filler content (mass. %)			
		WRHA		BRHA	
		1.5	6	1.5	6
Activation energy of decomposition E_A (kJ mol^{-1})	160.9	117.0	121.2	121.2	143.8
Melting temperature T_m (K)	419	418	413	408	408
Temperature of beginning of destruction T_d^i (K)	653	658	658	648	648
T_{10} % weight loss T_{10} (K)	713	678	673	663	658
Temperature interval of processing $T_d^i - T_m$ (K)	507	513	518	508	513
Temperature of end of destruction T_d^f (K)	785	763	773	753	753

The dependencies of the tensile strength σ and elongation ε of CM filled with WRHA or BRHA as a function of the filler content (*C*, mass.%) are shown in Figs 2 and 3. The high tensile strength of the initial UHMWPE is determined by the fact that during its crystallisation from melt all the elements of its supramolecular structure are interconnected to some extent by transverse molecules. Besides, this polymer always has certain amount of physical nodes, which remain intact for a long time. The contents of transverse macromolecules and physical nodes increase with the increase of macromolecules length and the content of fractions with higher molecular weight which leads to increase in the number of interconnected elements in the supramolecular structure[26].

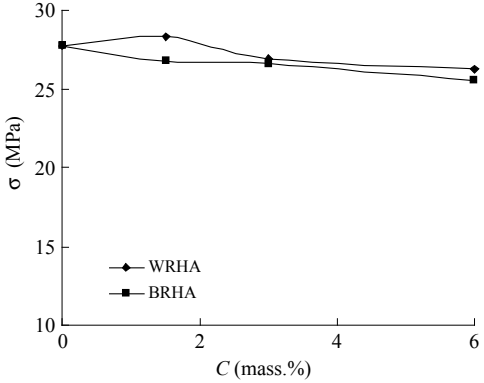

Fig. 2. Dependence of the tensile strength σ of CM based on UHMWPE on the nature and content of filler

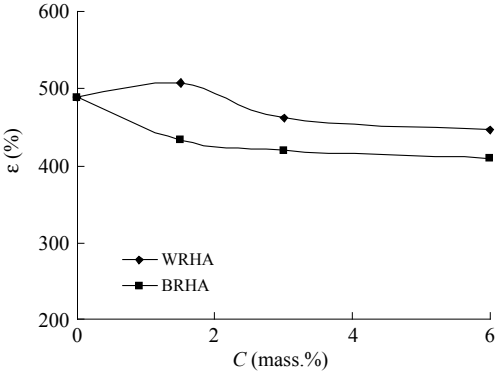

Fig. 3. Dependence of elongation ε of CM based on UHMWPE on the nature and content of filler

It can be seen from Figs 2 and 3 that the tensile strength σ and elongation ε had small maxima at 1.5 mass. % content of WRHA – 28.3 MPa and 510%, respectively. Besides, the percentage of uncertainty and confidence interval were 1.1% and 0.3 MPa for the determination of σ, and 2.3 and 12% for ε determined on an Instron instrument. Even at 6 mass. % filler content, the parameters studied were close to that of the initial UHMWPE. The tensile strength and the elongation depended insignificantly on the content of BRHA and their values were close to these of the initial UHMWPE. Probably, this was due to the more polar character of WRHA surface than that of BRHA. The results obtained for the tensile strength of CM obtained on the basis of UHMWPE with filler fiber monocrystals were relatively better than these observed with filler carbon fibers[27]. The better results observed with fiber monocrystals were due to their advantages over the other fillers – namely, an almost defect-free monocrystalline structure; high tensile strength close to the theoretical value, high aspect ratio at low diameter, etc.[28]

The results obtained for the dependence of energy at break *E* and the Young modulus *M* of the sample on the content of WRHA or BRHA correlated well with these for the tensile strength and elongation – Figs 4 and 5. The values of these properties did not change significantly and were close to these of virgin UHMWPE.

Table 2 shows the elasto-plastic properties of the composites based on UHMWPE filled with WRHA or BRHA. When WRHA was used as filler, the universal *HU* and the plastic H_{plast} hardnesses remained almost the same while the values of these parameters measured for CM with BRHA increased significantly to reach 56.0 and 76.3 MPa, respectively. The energy consumed for plastic deformation, W_r, was calculated to be in the range 6100–6650 nJ and the true elasticity modulus *E* increased with the increase of rice husks content up to 1.43 and 1.41 GPa at 6 mass. % content of WRHA or BRHA.

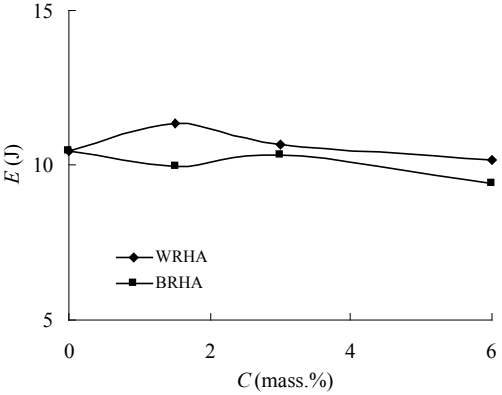

Fig. 4. Dependence of energy at break *E* of CM based on UHMWPE on the nature and content of filler

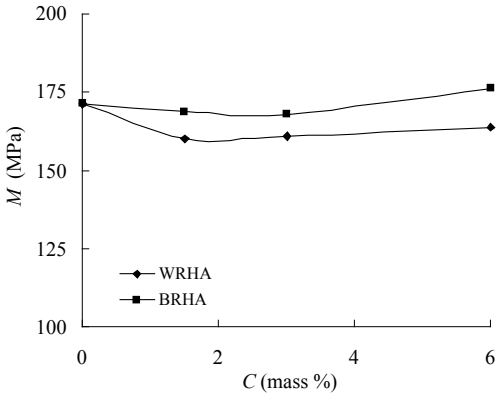

Fig. 5. Dependence of the Young modulus *M* of CM based on UHMWPE on the nature and content of filler

Table 2. Elasto-plastic characteristics of UHMWPE composites filled with WRHA or BRHA

Property	Virgin UHMWPE	Filler content (mass. %)			
		WRHA		BRHA	
		3	6	3	6
Universal hardness *HU* (MPa)	48.0	50.0	51.0	53.0	56.0
Plastic hardness H_{plast} (MPa)	64.5	65.5	66.1	70.5	76.3
True elasticity modulus *E* (GPa)	1.05	1.17	1.43	1.36	1.41
Energy for plastic deformation W_r (nJ)	6643	6124	6526	6518	6122

* The true elasticity modulus *E* was calculated by the formula $E^* = E/(1 - \nu^2)$, where E^* is the normalised elasticity modulus determined using nanotester FISCHERSCOPE H100, and *v* – the Poisson coefficient. For UHMWPE $v = 0.46$ (Ref. 29).

Some other properties of CM studied are also presented in Table 3 – thermal stability, the Vicat softening point, shrinkage and hardness by Shore. The thermal stability

of CM containing BRHA, determined by the weight loss, changed only slightly in the range 0.10–0.17%, while for the materials based on WRHA the weight loss was lower and reached 0.05% at 6 mass.% content of filler.

Table 3. Properties of CM based on UHMWPE filled with WRHA or BRHA

Property	Virgin UHMWPE	Filler content (mass.%)					
		WRHA			BRHA		
		1.5	3	6	1.5	3	6
Thermal stability (%)	0.17	0.13	0.11	0.05	0.10	0.10	0.11
The Vicat softening point (K)	415.3	415.8	418.6	418.4	415.8	418.0	418.7
Shrinkage (%)	1.45	1.43	1.30	1.28	1.46	1.45	1.30
The Shore hardness	94.3	97.0	96.8	97.3	94.3	95.5	95.8

The Vicat softening point of CM based on UHMWPE filled with WRHA or BRHA increased slightly compared to that of the initial polymer. The lowest shrinkage was observed for the composites based on WRHA – from 1.28 to 1.30% at 3–6 mass.% filler content. The Shore hardness was found to increase by about 3 units compared to that of the initial UHMWPE. It was in the range 94–97.

CONCLUSIONS

Composite materials were prepared on the basis of ultra-high molecular weight polyethylene and white or black rice husks ashes. The activation energies of thermal destruction of these materials decreased with the increase of rice husks ash content to 6 mass. % which makes them more unstable thermally. It can be used in the catalytic destruction of waste polymers to their monomers. By the use of white rice husks ash, the tensile strength and elongation had small maximum at 1.5 mass.% filler content while for the materials based on black rice husks ash these parameters did not change much and remained close to the values for the initial polymer. The universal and plastic hardnesses of the composites based on black rice husks ash increased by 17–18% at 6 mass. % filler content. The true elasticity modulus of both types of composites increased by 35–40% compared to the initial polymer. The composites containing white rice husks ash showed the highest thermal stability. The results obtained show that the fillers used improve to some extent or at least did not significantly worsen the physicomechanical properties of the initial polymer. Taking into account the low cost of the fillers, there are good reasons to reduce the cost of the final products manufactured from these composite materials. Besides, it opens opportunities for utilisation of waste rice husks which are major ecological problem for the countries of high rice production and widens the applicability of the products obtained using rice husks and as fillers for polymers.

ACKNOWLEDGEMENT

The financial support of the Bulgarian Ministry of Education and Sciences (National Science Fund), contract DO-02-61/2008, is gratefully acknowledged.

REFERENCES

1. P. M. STEFANY, D. GARCIA, J. LOPEZ, A. JIMENEZ: Thermogravimetric Analysis of Composites Obtained from Sintering of Rice Husk-scrap Tire Mixtures. J. Therm. Anal. Calorim., **81**, 315 (2005).
2. S. E. BAILEY, T. J. OLIN, R. M. BRIKA, D. D. ADRIAN: A Review of Potentially Low-cost Sorbents for Heavy Metals. Water. Res., **33**, 2469 (1999).
3. S. CHANDRASEKHAR, K. G. SATYANARAYANA, P. N. PRAMADA, P. RAGHAVAN, T. N. GUPTA: Processing, Properties and Applications of Reactive Silica from Rice Husk – An Overview. Review. J. Mater. Sci., **38**, 3159 (2003).
4. S. BABEL, T. A. KURNIAWAN: Low Cost Adsorbents for Heavy Metals Uptake from Contaminated Water: A Review. J. Hazard. Mater., **B 97**, 219 (2003).
5. T. H. LIOU: Evolution of Chemistry and Morphology during the Carbonisation and Combustion of Rice Husk. Carbon, **42**, 785 (2004).
6. T. G. CHUAH, A. JUMASIAH, I. AZNU, S. KATAYON, S. Y. CHOONG: Rice Husks as a Potentially Low-cost Biosorbent for Heavy Metal and Dye Removal: An Overview. Desalination, **175**, 305 (2005).
7. G. CRINI: Non-conventional Low-cost Adsorbents for Dye Removal: A Review. Bioresource Technol., **97**, 1061 (2006).
8. M. Y. AHMAD FUAD, Z. ISMAIL, M. S. MANSOR, Z. A. MOHD ISHAK, A. K. MOHD OMAR: Mechanical Properties of Rice Husk Ash/Polypropylene Composites. Polym. J., **27** (10), 1002 (1995).
9. A. CHAKRAVETY, P. MISHRA, K. BANERJEE: Investigation of Thermal Decomposition of Rice Husk. Thermochim. Acta, **94** (2), 267 (1985).
10. H. D. BANERJEE, S. SEN, H. N. ACHARYA: Investigations on the Production of Silicon from Rice Husks by the Magnesium Method. Mater. Sci. Eng., **52** (2), 173 (1982).
11. M. A. HAMAD: Thermal Characteristics of Rice Hulls. J. Chem. Technol. Biot., **31** (10), 624 (1981).
12. M. Y. AHMAD FUAD, J. MUSTAFAH, M. S. MANSOR, Z. A. MOHD ISHAK, A. K. MOHD OMAR: Thermal Properties of Polypropylene/Rice Husk Ash Composites. Polym. Int., **38** (1), 33 (1995).
13. M. Y. AHMAD FUAD, J. MUSTAFAH, M. S. MANSOR, Z. A. MOHD ISHAK, A. K. MOHD OMAR: Rice Husk Ash as Fillers in Polypropylene: A Preliminary Study. Int. J. Polym. Mater., **19** (1–2), 75 (1993).
14. S. SIRIWARDENA, H. ISMAIL, U. S. ISHIAKU: Mechanical Properties and Recyclability of Thermoplastic Elastomer Composites of White Rice Husk Ash-Ethylene/Propylene/Diene Terpolymer-Polypropylene. Plast. Rubber Compos., **31** (4), 167 (2002).
15. S. SIRIWARDENA, H. ISMAIL, U. S. ISHIAKU, M. C. S. PERERA: Mechanical and Morphological Properties of White Rice Husk Ash Filled Polypropylene/Ethylene-Propylene-Diene Terpolymer Thermoplastic Elastomer Composites. J. Appl. Polym. Sci., **85** (2), 438 (2002).
16. J. SUWANPRATEEB, K. HATTHAPANIT: Rice-husk-ash-based Silica as a Filler for Embedding Composites in Electronic Devices. J. Appl. Polym. Sci., **86** (12), 3013 (2002).
17. S. PANTHAPULAKKAL, S. LAW, M. SAIN: Enhancement of Processability of Rice Husk Filled High-density Polyethylene Composite Profiles. J. Thermoplast. Compos. Mater., **18** (5), 445 (2005).

18. L. REICH, H. T. LEE, D. W. LEVI: Note on the Thermal Degradation of Teflon. J. Polym. Sci., Part B: Pol. Lett., **1**, 535 (1963).
19. B. D. PARK, S. G. WI, K. H. LEE, A. P. SINGH, T. H. YOON, Y. S. KIM: Characterization of Anatomical Features and Silica Distribution in Rice Husk Using Microscopic and Micro-analytical Techniques. Biomass Bioenerg., **25**, 319 (2003).
20. A. A. M. DAIFULLAH, B. S. GIRGIS, H. M. H. GAD: Utilization of Agro-residues (Rice Husk) in Small Waste Water Treatment Plants. Mater. Lett., **57**, 1723 (2003).
21. M. PATEL, A. KARERA, P. PRASANNA: Effect of Thermal and Chemical Treatments on Carbon and Silica Contents in Rice Husk. J. Mater. Sci., **22**, 2457 (1987).
22. C. REAL, M. D. ALCALA, J. M. CRIADO: Preparation of Silica from Rice Husk. J. Am. Ceram. Soc., **79**, 2012 (1996).
23. K. G. MANSARAY, A. E. GHALY: Determination of Kinetic Parameters of Rice Husk in Oxygen Using Thermogravimetric Analysis. Biomass Bioenerg., **17**, 19 (1999).
24. W. KAMINSKY, I. J. N. ZORRIQUETA: Catalytical and Thermal Pyrolysis of Polyolefins. J. Anal. Appl. Pyrol., **79**, 368 (2007).
25. D. S. ACHILIAS, C. ROUPAKIAS, P. MEGALOKONOMOS, A. A. LAPPAS, E. V. ANTONAKOU: Chemical Recycling of Plastic Wastes Made from Polyethylene (LDPE and HDPE) and Polypropylene (PP). J. Hazard. Mater., **149** (3), 536 (2007).
26. A. N. KARASEV, I. I. ANDREEVA, N. M. DOMAREVA: Svyaz mehanicheskih svoistv polietilena visokoi plotnosti s molekulyarno-vesovim raspredelenie. Vysokomol. Soedin., **12** (5), 1127 (1970) (in Russian).
27. A. ATANASOV, D. KOLEVA: Synthesis and Properties of Composites of Ultra-high Molecular Weight Polyethylene with Carbon Fibers or Fiber Monocrystals. Polym. Polym. Compos., **14** (4), 413 (2006).
28. J. V. MILEWSKI, H. S. KATZ: Handbook of Reinforcements for Plastics. Van Nostrand Reinhold Co, New York, 1987.
29. A. A. EDIDIN, S. M. KURTZ: Influence of Mechanical Behavior on the Wear of 4 Clinically Relevant Polymeric Biomaterials in a Hip Simulator. J. Arthroplasty, **15** (3), 321 (2000).

Received 17 April 2009
Revised 18 May 2009

OXIDATION OF BENZOINS TO BENZILS WITH THE JONES REAGENT SUPPORTED ON GRAPHITE

JI-DONG LOU[a]*, YI-CHUN MA[a], N. VATANIAN[b], Q. WANG[b], CH. ZHANG[c]

[a]*College of Life Sciences, China Jiliang University, Hangzhou, 310 018 Zhejiang, China*
[b]*Sirnaomics Inc., 401 Professional Drive, Gaithersburg, MD 20879, USA*
[c]*Instituto de Biologia Experimental e Tecnologia, Universidade Nova de Lisboa, Oeiras, Portugal*
E-mail: *lou@cjlu.edu.cn*

ABSTRACT

The preparation of benzils by oxidation of corresponding benzoins using the Jones reagent supported on graphite reagent under heterogeneous conditions and reflux at room temperature is described. All the reactions are completed within 1 h in yields between 82–92% and this procedure is an extension of application for the Jones reagent supported on graphite reagent as well.

Keywords: benzoins, benzils, graphite, the Jones reagent, oxidation.

AIMS AND BACKGROUND

The oxidation of benzoins into corresponding benzils is one of the important reactions in organic chemistry, which reaction has received a great deal of attention due to the practical applications of benzils such as photosensitive agents and synthetic agents in organic and pharmaceutical chemistry[1–6]. For the above transformation, many oxidising reagents have been employed, for example, chromium oxide[7], nitric acid[8], the Fehling solution[8], ammonium nitrate–copper acetate[9], thallium nitrate[10], nickel acetate[11], lanthanum nitrate[12], ferric nitrate–clay[13], ammonium chlorochromate–alumina[14], ferric(III) chloride[15], bismuth(III) nitrate–copper(II) acetate[16], zeolite[17], $H_{3+n}PMo_{12-n}V_nO_{40}$ (Ref. 18), ferric oxide–aluminum oxide[19], manganese dioxide–silica[20], ferric nitrate–silica[21], bismuth(III) nitrate–silica[22], potassium iodide[23], triarylstibanes[24], ferric(III) nitrate-graphite[25], manganese dioxide under viscous conditions[26], chromium trioxide-kieselguhr[27], ferric(III) nitrate-kieselguhr[28], chromium trioxide-kieselguhr under viscous conditions[29], and chromium trioxide in dimethyl sulphoxide[30], etc. Although a diversity of methods is available for this oxidation,

* For correspondence.

development of convenient, selective, and mild procedures is important objective of current relevance. Consequently, introduction of new methods or reagents is still fraught with experiment challenges, especially in search of versatile and selective reagents.

RESULTS AND DISCUSSION

The Jones reagent is one of the best known chromium(VI) reagents for the oxidation of secondary alcohols to ketones. But it fails to produce satisfactory results for oxidation of primary alcohols, including benzyl alcohols, to the corresponding aldehydes[7]. The problem in this oxidation reaction is due to the fact that aldehydes react with water and alcohols under acidic aqueous media employed in the Jones oxidation procedure, producing hydrates and hemiacetals, which are then oxidised to carboxylic acids and esters, respectively. Therefore, new experimental procedures for conducting selective oxidation with chromium reagents are still of interest.

Recently, we have reported that the Jones reagent supported on graphite was successfully used to oxidise benzyl alcohols to the corresponding aldehydes as well as secondary alcohols to the corresponding ketones[31], and it seems that the above problem can be overcome by using this supported Jones reagent. Since in most reactions, solid supported reagents have been found superior to the non-supported reagents, especially in efficiency and selectivity, employment of solid supported reagents in organic synthesis has generated great interest. Based on our previous study[31], we now report here an efficient and selective oxidation of benzoins (**1**) to the corresponding benzils (**2**) with the Jones reagent supported on graphite (Scheme 1), which is an extension of application for this reagent as well.

Scheme 1

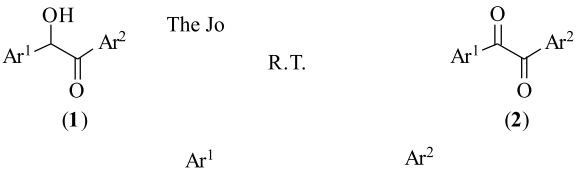

modification by copper leads to the formation of copper oxide species, not strongly shared to the support. The obtained copper oxide particles are prone to the process of agglomeration and the formation of large copper oxide particles occurs even in the case of the mesoporous support (see XRD data). Simultaneously with the formation of large metal oxide particles, a part of copper is disposed in the channels of the mesoporous support as finely dispersed oxide species, resulting in BET surface area and pore volume decrease. Tsoncheva et al.[23] found that the presence of micropores in the SBA-15 support facilitates the formation of copper oxide species in them. The hydrophobicity index has significantly changed only in the case of Cr/SBA-15. The formed chromium oxide species in this case possess different adsorption properties than that formed on SiO_2 support (Fig. 4, Table 1). The differences in the FTIR spectrum of Cr/SBA-15 in comparison to that of the initial SBA-15 material are also indicative for the formation of chromium oxide species, which are strongly shared to the support (Fig. 3). The presence of high amounts of silanols favours their interaction with the chromium precursor as well as the formation of finely dispersed chromium oxide species, which are responsible for the significant changes of the hydrophobicity index.

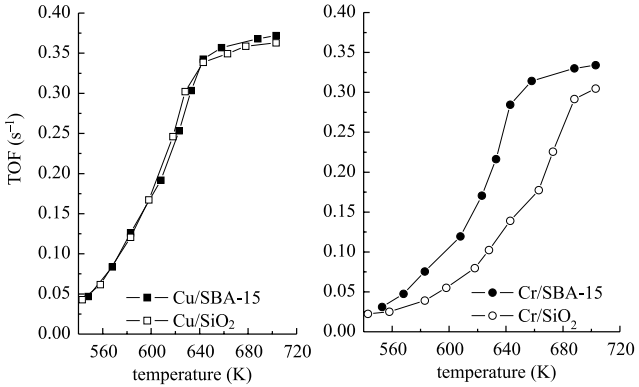

Fig. 5. Catalytic activity versus temperature on the modified SiO_2 and SBA-15 materials

Toluene oxidation is investigated in the temperature interval of 550–700 K. All samples show catalytic activity above 550 K and CO_2 is the main registered carbon-containing product. Data on the changes of catalytic activity (calculated as TOF per metal site) versus temperature are presented in Fig. 5. The copper-containing samples show close catalytic activity, whereas in the case of chromium containing samples Cr/SBA-15 possesses higher catalytic activity than its SiO_2 supported analog. It is obvious that in the case of copper modifications, the silica support does not have any significant effect on the state of the formed copper oxide species and, therefore, on their catalytic activity. The process of agglomeration leads to the formation of large CuO particles (about 20 nm) on both supports, which possess close catalytic activity (Fig. 5). The slight changes in the hydrophobicity index after the modification by copper are observed for both supported modifications, which are in a good accord-

ance with the catalytic result. The formed chromium oxide species on Cr/SBA-15 possess a higher catalytic activity in toluene oxidation in comparison to these formed in its SiO_2 supported analog (Fig. 5). The significant difference in the hydrophobicity index for the Cr/SBA-15 and Cu/SBA-15 materials is in a good accordance with their different catalytic behaviour.

CONCLUSIONS

The effect of post-synthesis modification with chromium and copper via wet impregnation of SiO_2 and SBA-15 materials was studied. The process of modification of the bulk SiO_2 leads to the formation of metal oxide species, which slightly decrease their hydrophobicity indices and are not influenced by the nature of the loaded metal oxide species. The modification of the mesoporous SBA-15 silica leads to the formation of different types of metal oxide species in dependence on the nature of the loaded metal. The formation of crystalline copper oxide particles was observed for the copper-modified SBA-15 material. The hydrophobicity index was significantly decreased only for the chromium-modified SBA-15, where finely dispersed chromium oxide species, strongly shared to the silica support, were formed. The catalytic activity of the samples in total toluene oxidation is in a good accordance with the adsorption results. In the case of the copper modifications, the activity was not influenced by the used silica support, whereas in the case of the chromium modifications the SBA-15 support has favourable effect on the formation of highly active chromium oxide species. Summarising the observations above, we could conclude that the hydrophobicity index (HI) can be used as a fast test for evaluation of the changes in the support hydrophobicity, due to its interaction with the formed metal oxide species.

ACKNOWLEDGEMENT

Financial support by BY-X-305/07 is greatly acknowledged. The author thanks to S. Popova and L. Ivanova for FT-IR, XRD and N_2 physicosorption measurements and to Assoc. prof. T. Tsoncheva for the helpful discussion on the manuscript.

REFERENCES

1. T. GARCIA, B. SOLSONA, D.CAZORLA-AMOROS, A. LINARES-SOLANO, S. H. TAYLOR: Total Oxidation of Volatile Organic Compounds by Vanadium Promoted Palladium-Titania Catalysts: Comparison of Aromatic and Polyaromatic Compounds. Appl. Catal., B, **62**, 66 (2006).
2. F. BERTINCHAMPS, C. GREGOIRE, E. M. GAINEAUX: Systematic Investigation of Supported Transition Metal Oxide Based Formulations for the Catalytic Oxidative Elimination of (Chloro)-aromatics: Part II: Influence of the Nature and Addition Protocol of Secondary Phases to VO_x/TiO_2. Appl. Catal., B, **66**, 10 (2006).
3. A. A. DOS SANTOS, K. M. LIMA, R. T. FIGUEIREDO, S. M. Da S. EGUES, A. L. D. RAMOS: Toluene Deep Oxidation over Noble Metals, Copper and Vanadium Oxides. Catal. Lett., **114**, 59 (2007).
4. A. CORMA: From Microporous to Mesoporous Molecular Sieve Materials and Their Use in Catalysis. Chem. Rev., **97**, 2373 (1997).

5. J. GEORGE, S. SHYLESH, A. P. SINGH: Vanadium-containing Ordered Mesoporous Silicas: Synthesis, Characterization and Catalytic Activity in the Hydroxylation of Biphenyl. Appl. Catal., **290**, 148 (2005).
6. M. S. HAMDY, G. MUL, J. C. JANSEN, A. EBAID, Z. SHAN, A. R. OVERWEG, Th. MASCHMEYER: Synthesis, Characterization, and Unique Catalytic Performance of the Mesoporous Material Fe-TUD-1 in Friedel–Crafts Benzylation of Benzene. Catal. Today, **100**, 255 (2005).
7. T. KAWABATA, Y. OHISHI, S. ITSUKI, N. FUJISAKI, T. SHISHIDO, K. TAKAKI, Q. ZHANG, Y. WANG, K. TAKEHIRA: Iron-containing MCM-41 Catalysts for Baeyer–Villiger Oxidation of Ketones Using Molecular Oxygen and Benzaldehyde. J. Mol. Catal., **236**, 99 (2005).
8. CH.-H. WANG, Sh.-Sh. LIN, Ch.-L. CHEN, H.-Sh. WENG: Performance of the Supported Copper Oxide Catalysts for the Catalytic Incineration of Aromatic Hydrocarbons. Chemosphere, **64**, 503 (2006).
9. R. S. ARAUJO, D. C. S. AZEVEDO, E. RODRIGUEZ-CASTELLON, A. JIMENEZ-LOPEZ, C. L. CAVALCANTE, Jr.: Al and Ti-containing Mesoporous Molecular Sieves: Synthesis, Characterization and Redox Activity in the Anthracene Oxidation. J. Mol. Catal., **281**, 154 (2008).
10. A. C. C. RODRIGUES: Metallic Mixed Oxides (Pt, Mn or Cr) as Catalysts for the Gas-phase Toluene Oxidation. Catal. Comm., **8**, 1227 (2007).
11. Y. WANG, X. YUAN, X. LIU, J. REN, W. TONG, Y. WANG, G. LU: Mesoporous Single-crystal Cr_2O_3: Synthesis, Characterization, and Its Activity in Toluene Removal. Solid State Science, **10** (9), 1117 (2007).
12. V. GAUR, A. SHARMA, N. VERMA: Catalytic Oxidation of Toluene and *m*-xylene by Activated Carbon Fiber Impregnated with Transition Metals. Carbon, **43**, 3041 (2005).
13. V. PARVULESCU, C. ANASTASESCU, B. L. SU: Bimetallic Ru-(Cr, Ni, or Cu) and La-(Co or Mn) Incorporated MCM-41 Molecular Sieves as Catalysts for Oxidation of Aromatic Hydrocarbons. J. Mol. Catal. A, **211**, 143 (2004).
14. M. M. L. R. CARROTT, C. GALACHO, F. L. CONCEICAO, P. J. M. CARROT: Influence of the Synthesis Conditions on the Pore Structure and Stability of MCM-41 Materials Containing Aluminium or Titanium. Stud. Surf. Sci. Catal., **160**, 567 (2007).
15. S. ORDONEZ, L. BELLO, H. SASTRE, R. ROSAL, F. V. DIEZ: Kinetics of the Deep Oxidation of Benzene, Toluene, *n*-hexane and Their Binary Mixtures over a Platinum on γ-alumina Catalyst. Appl. Catal., B, **38**, 139 (2002).
16. V. GAUR, A. SHARMA, N. VERMA: Catalytic Oxidation of Toluene and *m*-xylene by Activated Carbon Fiber Impregnated with Transition Metals. Carbon, **43**, 3041 (2005).
17. M. A. CENTENO, M. PAULIS, M. MONTES, J. A. ODRIOZOLA: Catalytic Combustion of Volatile Organic Compounds on $Au/CeO_2/Al_2O_3$ and Au/Al_2O_3 Catalysts. Appl. Catal. A, **234**, 65 (2002).
18. A. SZEGEDI, Z. KONYA, D. MEHN, E. SOLYMAR, G. PAL-BORBELY, Z. E. HORVATH, L. P. BIRO, I. KIRICSI: Spherical Mesoporous MCM-41 Materials Containing Transition Metals: Synthesis and Characterization. Appl. Catal. A, **272**, 257 (2004).
19. A. SZEGEDI, M. HEGEDUS, J. L. MARGITFALVI, I. KIRICSI: Low Temperature CO Oxidation over Iron-containing MCM-41 Catalysts**.** Chem. Commun., **11**, 1441 (2005).
20. J. WEITCAMP, P. KLEINSCHMIT, A. KISS, C. H. BERKE: The Hydrophobicity Index – A Valuable Test for Probing the Surface Properties of Zeolitic Adsorbents or Catalysts. In: Proc. of the 9th International Zeolite Conference (Eds R. von Ballmoos et al.). Monreal, 1992, p.79.
21. R. GLASER, R. ROESKY, T. BOGER, G. EIGENBERGER, S. ERNST, J. WEITCAMP: Probing the Hydrophobic Properties of MCM-41-type Materials by the Hydrophobicity Index. Stud. Surf. Sci. Catal., **105**, 695 (1997).
22. D. ZHAO, J. FENG, Q. HUO, N. MELOSH, G. H. FREDRICKSON, B. F. CHMELKA, G. D. STUCKY: Triblock Copolymer Syntheses of Mesoporous Silica with Periodic 50 to 300 Angstrom Pores. Science, **279**, 548 (1998).
23. T. TSONCHEVA, J. ROSENHOLM, M. LINDEN, L. IVANOVA, Ch. MINCHEV: Iron and Copper Oxide Modified SBA-15 Materials as Catalysts in Methanol Decomposition: Effect of Copolymer Template Removal. Appl. Catal., **318**, 234 (2007).

Received 27 May 2009
Revised 29 June 2009

DECOMPOSITION OF NO ON DIFFERENT SOL–GEL Pd/SiO_2 CATALYSTS

L. RADEV[a], M. KHRISTOVA[b], D. MECHANDJIEV[b]*

[a]*University of Chemical Technology and Metallurgy, 8 'Kliment Ohridski' Blvd., 1756 Sofia, Bulgaria*
E-mail: *metkomeh@svr.igic.bas.bg*
[b]*Insitute of General and Inorganic Chemistry, Bulgarian Academy of Sciences, Acad. G. Bontchev Street, Bl. 11, 1113 Sofia, Bulgaria*

ABSTRACT

$Ag+Pd/SiO_2$ and Pd/SiO_2 catalysts have been prepared via sol–gel method from tetra-ethoxysilane (TEOS) and the salts of corresponding metals. Their activity in reduction of nitric oxide (NO) with carbon monoxide (CO) has been investigated. It has been established that the increasing of the concentration of Pd has led to activity increase, but goes through a maximum about 0.7% Pd/SiO_2 and decreased at 2.5% Pd/SiO_2. On the synthesised Pd/SiO_2 catalysts over 180°C together with the catalytic reduction process begins direct decomposition of NO to N_2 and O_2. Therefore, two types of catalytically-active complex (CAC) were formed on the surface of Pd, which catalyse different reactions. This effect is observed in palladium catalysts enriched with Ag. The obtained results indicate that the synthesised Pd catalysts are perspective for deactivation of NO by direct decomposition to N_2 and O_2.

Keywords: sol–gel, Pd/SiO_2 catalysts, decomposition of NO.

AIMS AND BACKGROUND

One of the major ecological problems, which are not yet solved optimally, is decomposition of NO in the exhaust gases from motors and industry. The basic method for neutralisation is the catalytic reduction with different catalysts[1–5]. Catalysts based on Pd and Pt (Refs 6–9) are of great importance for solving of these problems. The oxides of transition metals as well as Ag and Au over different oxides have also been used[10–27]. The fundamental problem is now connected with the need to use expensive reductor agents such as NH_3 or to work with the stoichiometric mixture of excess of the reducer – hydrocarbon or CO (Refs 28–35). Therefore, the task which is staying to resolve, is to create a catalyst that may reduce NO in excess of oxygen or to decompose NO to N_2 and O_2.

* For correspondence.

In our preliminary paper we showed that in the reduction of NO with CO over carbon catalysts, promoted with Ni, the decomposition of NO to N_2 and O_2 was observed[36]. The same result was obtained for the Pd/SiO_2 catalysts prepared via sol–gel method[37]. Therefore, the aim of the present paper is to examine how the process of reduction of NO with CO and decomposition of NO to N_2 and O_2 influenced the concentration of Pd^{2+} in Pd/SiO_2 catalysts prepared via sol–gel technique. The influence of Ag as an additive was also examined. The obtained results could serve as a basis for establishing of catalysts for NO decomposition in waste gases.

EXPERIMENTAL

Preparation of catalysts. The studied catalytic samples were prepared via sol–gel method. TEOS (Merck) was hydrolysed in the presence of C_2H_5OH, H_2O and HCl as a catalyst. The molar ratio of the obtained silica sol was $TEOS:C_2H_5OH:H_2O:HCl$ = 1:1:3:0.01. Monometallic (Pd/SiO_2) and bimetallic ($Ag+Pd/SiO_2$) catalysts were prepared by adding the salts of corresponding metals ($AgNO_3$ and/or $PdCl_2$, purchased by Merck) dissolved in distillated water to the hydrolysed TEOS. The obtained mixed sol was readjusted to pH=9 in the presence of 25% NH_4OH for preparing the samples with high specific surface area. The prepared sols were gelated at 50°C, dried at 100°C overnight and thermally treated at 600°C for 3 h. The specific surface area of samples was carried out by adsorption of nitrogen (77.4 K) using a convention volumetric apparatus and was determined by BET method. Table 1 presents the composition and characteristics of the obtained catalysts.

Table 1. Composition of the prepared gels and BET specific surface area of the samples after thermal treatment at 600°C for 3 h

Samples	Composition of the prepared samples (wt. %)			Specific surface area (m^2/g)
	Ag	Pd	SiO_2	
$0.5\%Pd/SiO_2$	–	0.50	2.72	338
$0.7\%Pd/SiO_2$	–	0.70	2.72	434
$2.5\%Pd/SiO_2$	–	2.50	2.72	73
$0.025\%\ Ag0.02\%Pd/SiO_2$	0.025	0.02	2.72	338

XRD measurements. The amorphous and crystallographic state of the thermally treated at 600°C/3 h samples was established by X-ray phase analysis within the range from 10° to 80° (2θ) with a constant step 0.04° (2θ) and coating time 1 s/step on a Bruker D8 Advance diffractometer with CuKα radiation and SolX detector. The spectra were evaluated with the Diffrac*plus* EVA package.

XPS measurements. XPS measurements were performed in a VC Escalab II spectrometer using monochromatic MgKα radiation ($h\nu$ =1253.6 eV). The base pressure of the instrument was 1×10^{-10} Torr. Electrostatic surface charging was observed in all

investigated samples due to their poor electric conductivity. Therefore, C 1s, with a binding energy (BE) of 285.0 eV from carbon contaminants was used as a reference level. The binding energies reported here accurate to ± 0.2 eV. XPS surface compositions were calculated from photoelectron peak areas of each element after correcting for instrument parameters.

Catalytic activity measurements. Catalytic activity experiments in NO reduction with CO were carried out in the flow apparatus, described in Ref. 38 in the temperature range 25–400°C. Temperature-programmed desorption (TPD) experiments were carried out on the same catalytic apparatus at a heating rate of 13°C/min in an Ar flow. Argon (purity 99.99 vol. %) was used as a carrier gas at a total gas-flow rate of 433 $cm^3\,min^{-1}$ (GHSV = 20 000 h^{-1}). A catalyst amount of l cm^3 (particle size 0.3–0.6 mm) was used in all experiments and placed into the reactor with a quartz tube (d = 10 mm). The catalytic activity tests were performed using gas mixture NO+CO+Ar (1200 ppm NO and 1200 ppm CO), i.e. conditions close to the stoichiometric ones. Before a catalytic test, the catalysts were treated in an Ar flow at 400°C for 1 h and cooled to room temperature. After a catalytic test at room temperature in a NO+CO+Ar mixture and isothermal desorption in Ar flow, temperature programmed desorption (TPD) was carried out in the temperature range 50–400°C and the TPD spectra of NO, CO and CO_2 were registered. The chronology of this set of experiments involved a reaction stage (NO+CO+Ar) and an isothermal desorption stage (Ar flow) carried out at the desired temperatures in the range from 50 to 400°C. The concentrations of NO, CO and CO_2 were continuously measured by gas analysers and the data were collected by a CSY-10 microprocessor computer system. The inlet concentration of CO was controlled by an Infralyt 2106 NDIR gas analyser. The outlet concentrations of NO and CO were controlled by UNOR 5 (Maihak) and that of CO_2, by Infralyt 2106. The N_2 concentration in the outlet gas was determined on the basis of the material balance with respect to NO consumption. The transient response method[17] was used to study the interaction of the gas phase with the catalyst surface.

RESULTS AND DISCUSSION

XRD of the obtained samples, thermally treated at 600°C/3 h, are given in Fig. 1.

From the obtained results it can be seen that in all prepared catalysts, PdO phase (PDF 43-1024) can be detected (XRD data for 0.5% Pd/SiO_2 are not shown in Fig. 1, because they are the same as for 0.7% Pd/SiO_2). In Fig. 1, the presence of SiO_2, determined by the amorphous halo, centered at ~22° (2θ), can also been depicted.

These results are confirmed by XPS analysis. XPS spectra are presented in Fig. 2.

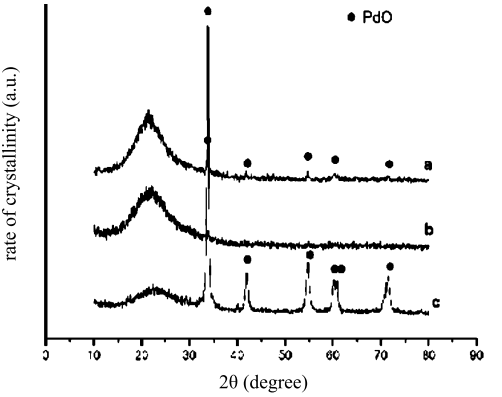

Fig. 1. XRD for prepared and thermal treated at 600°C for 3 h catalysts – 0.7% Pd/SiO_2 (a), 0.2%Pd+0.025% Ag/SiO_2 (b) and 2.5% Pd/SiO_2 (c)

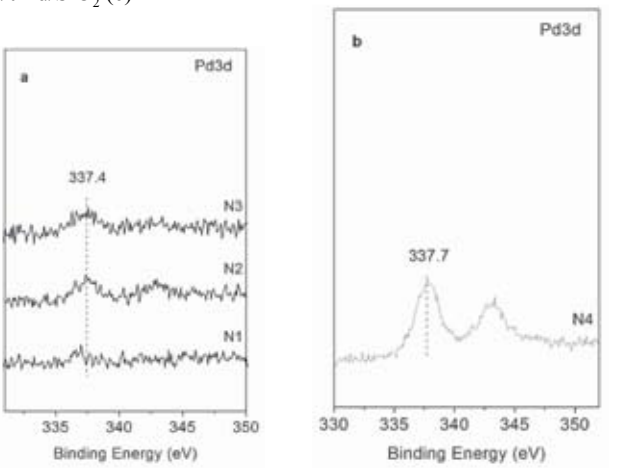

Fig. 2. XPS for the synthesised and thermal treated at 600°C for 3 h samples with different quantity of Pd^{2+}: *a* – N_1 (0.5%Pd/SiO_2), N_2 (2.5%Pd/SiO_2) and N_3 (0.02%Pd+0.0025%Ag/SiO_2), *b* – N_4 (0.7%Pd/SiO_2)

The main forms in which palladium is presented in the samples are Pd^{2+}.

The concentrations of the elements on the surface of the prepared samples are presented in Table 2.

Table 2. Relative concentration of the elements (at. %) in the prepared catalysts, observed from XPS analysis

Samples	Relative concentration of the elements (at. %)			
	O	Si	Pd	Ag
0.5%Pd/SiO_2	61.1	38.9	<0.1	–
0.7%Pd/SiO_2	52.0	33.3	0.5	–
2.5%Pd/SiO_2	59.8	40.1	0.1	–
0.02%Pd+0.025%Ag/SiO_2	60.9	38.9	0.1	0.1

As it can be seen the concentration of Pd^{2+} on the surface of the catalysts is lower than their concentration, whereas in the presence of Ag is higher.

The results from the investigations on the catalytic activity of the samples with different quantity of Pd (0.5, 0.7 and 2.5 wt. %) are shown in Figs 3, 4 and 5. In the presented figures is shown the dependence of the degree of reduction of NO (in %) with CO and the decreasing of CO (in %) η_{NO} and η_{CO}, respectively, on temperature.

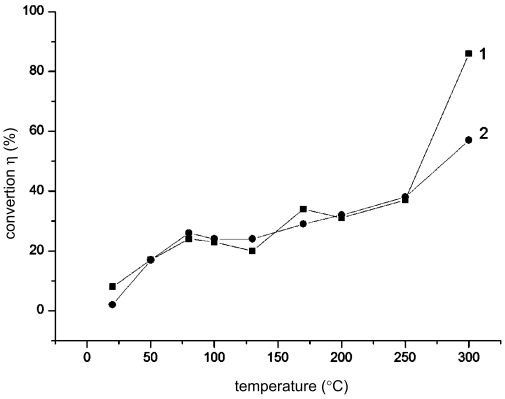

Fig. 3. Dependence of the degree of NO and CO conversions on temperature for 0.5% Pd/SiO_2: NO (1), CO (2) in a NO+CO+Ar mixture

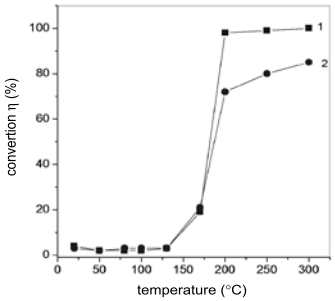

Fig. 4. Dependence of the degree of NO and CO conversions on temperature for 0.7% Pd/SiO_2: NO (1), CO (2) in a NO+CO+Ar mixture

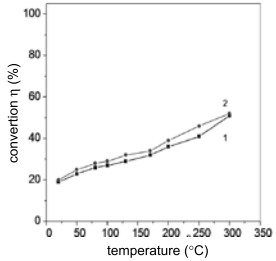

Fig. 5. Dependence of the degree of NO and CO conversions on temperature for 2.5% Pd/SiO_2: NO (1), CO (2) in a NO+CO+Ar mixture

As could be seen from the figures, the sample with 0.7% Pd/SiO_2 is most active. According to the presented data, the prepared sample shows the 90% degree of decomposition of NO at 200°C. An interesting moment in the visualised data is that over a certain temperature, for 0.5% Pd/SiO_2 at 200°C, but for the sample 0.7% Pd/SiO_2 at 175°C, the degree of NO conversion (η_{NO}) is higher than that of CO. Taking into account that we work with stoichiometric gas mixture (NO:CO=1:1) these levels should be the same. A very low activity has the sample with 2.5% Pd/SiO_2. Most likely this due to the fact that the most of Pd^{2+} is unavailable for conversion of NO with CO. Also, as it is seen from the presented in Table 1 data, the specific surface area for this sample is too low.

Figure 6 presents η_{NO} and η_{CO} for the 0.025%Ag+0.02%Pd/SiO_2 catalyst in which the concentrations of Ag and Pd are below 0.1 wt. % with respect to Pd:Ag =1:1.

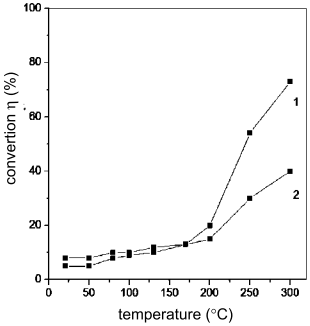

Fig. 6. Dependence of the degree of NO and CO conversions on temperature for 0.02%Pd +0.025%Ag/SiO_2: NO (1), CO (2) in a NO+CO+Ar mixture

This catalyst has high activity regardless of the low content of the active components – Ag and Pd. This result could be explained by the data of XPS analysis. From the presented XPS data (Table 2) we can see that the concentration of Ag^+ and Pd^{2+} on the surface is high. On the same sample we observe higher η_{NO} to that of η_{CO} for temperatures above 180°C. Apparently, Ag^+ and Pd^{2+} form a very active catalytic active complex (CAC).

From the presented results we can conclude that with increasing the Pd^{2+} content, the catalytic activity of the prepared samples increases and goes through a maximum. The adding of the sample with Ag^+, regardless of low concentrations of the active components, leads to higher activity in NO conversion with CO. The obtained results are in a good confirmation with those reported in Ref. 37.

As in our other studies over Pd-containing catalysts[37] and *x*% Pd/SiO_2 (*x*=0.5, 0.7 and 2.5% Pd) catalysts obtained via sol–gel technique it can be seen that from certain temperature has been observed high rate of reduction of NO although working with stoichiometric gas mixture (NO:CO =1:1).

In the catalytic deactivation of NO with CO the following processes are possible:

$$2NO + 2CO \rightarrow N_2 + 2CO_2 \quad (1)$$

$$2NO + CO \rightarrow N_2O + CO_2 \quad (2)$$

$$2NO \rightarrow N_2 + O_2 \quad (3)$$

$$NO \rightarrow NO_{ads.cat} \quad (4)$$

in which the acronym $NO_{ads.cat}$ is adsorbed on the catalyst NO.

If only reaction (1) took place, then $\eta_{NO} = \eta_{CO}$. For the other cases (reactions (2), (3) and 4)) $\eta_{NO} > \eta_{CO}$.

In order to make clear if the higher observed η_{NO} was due to adsorption, in a series of experiments a stoichiometric gas mixture NO:CO = 1:1 previously omitted through the catalyst, followed by a thermo-programmed desorption (TPD) in temperature range 50–400°C (described in the experimental part in details).

The obtained results for the samples 0.7% Pd/SiO_2, 2.5% Pd/SiO_2 and 0.025% Ag +0.02% Pd/SiO_2 are given in Figs 7, 8, and 9. In the same figures are presented transient response curves during absorption process.

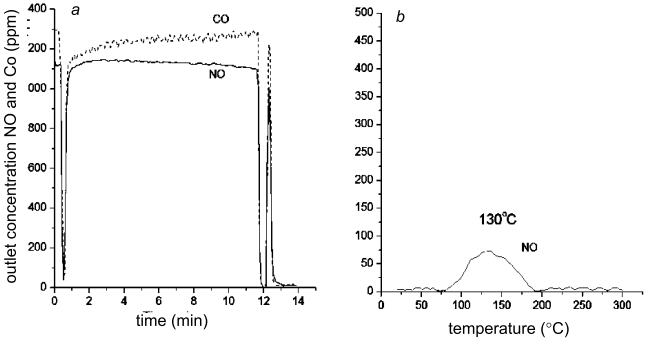

Fig. 7. Transient response curves obtained during the reaction stages with a NO+CO+Ar flow (*a*) and desorption stages with an Ar flow performed at 20°C and the temperature programmed desorption (TPD) spectra of NO desorbed by Ar flow on catalyst 0.7%Pd/SiO_2 (*b*)

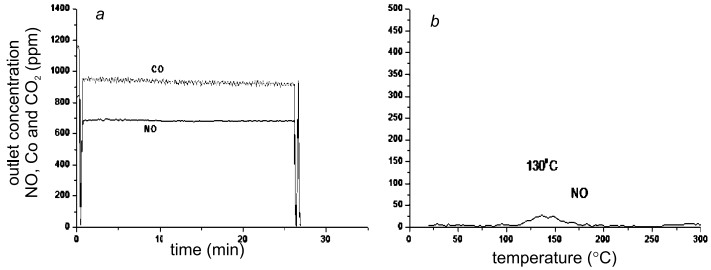

Fig. 8. Transient response curves obtained during the reaction stages with a NO+CO+Ar flow (*a*) and desorption stages with an Ar flow performed at 20°C and the temperature programmed desorption (TPD) spectra of NO desorbed by Ar flow on catalyst 2.5%Pd/SiO_2 (*b*)

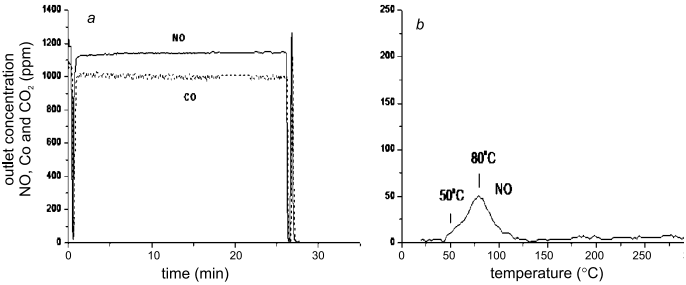

Fig. 9. Transient response curves obtained during the reaction stages with a NO+CO+Ar flow (*a*) and desorption stages with an Ar flow performed at 20°C and the temperature programmed desorption (TPD) spectra of NO desorbed by Ar flow on catalyst 0.02%Pd+0.025Ag%/SiO_2 (*b*)

From the presented figures could be seen that only adsorption of NO actually goes. The results show that in the temperature range 120–150°C NO was desorbed. From the character of TPD curves it can be concluded that there is a difference between the adsorption forms for the investigated samples, but hence the maximum of desorption is coming at the same temperature. It can be concluded from the figures that whether the adsorption runs or not, at temperature above 180°C, the desorption process was completed. This shows that the observed effect of η_{NO} was not due to reaction (4). It is confirmed by the lack of the decreasing of η_{NO} over time, which is typical for an adsorption process due to saturation of the surface of adsorbents and adsorption balance.

Another possible reason is (the course of reaction (2)) the obtaining of N_2O. It is, however, known that this reaction runs at low temperatures and goes through a maximum at 150°C (Ref. 38). Furthermore, the material balance for NO, CO and CO_2 showed that above this temperature N_2O could not be obtained. Therefore, it is assumed that on the catalyst over 180°C had run reactions (1) and (3), which explains the higher value of η_{NO}. To prove this possibility, further studies were carried out using the transient response method (the Kobayashi method). It is known that depending on the nature of the response curves it can be judged for the limiting stage and mechanism of the reaction[39]. If above a certain temperature, an intensive reaction (3) begins to run – direct decomposition of NO, it should be expected a change in the response curves.

Figure 10 shows the presented response curves for the investigated samples at different temperatures.

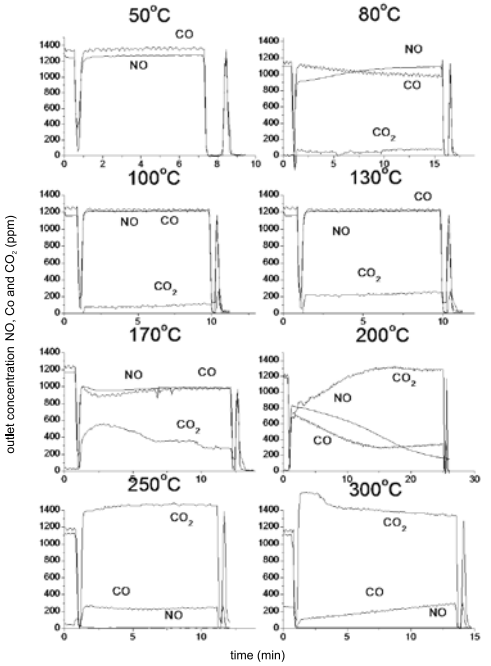

Fig. 10*a*. Transient response curves obtained during the reaction stages with a NO+CO+Ar flow and desorption stages with an Ar flow performed at different temperatures on catalyst 0.5%Pd/SiO_2

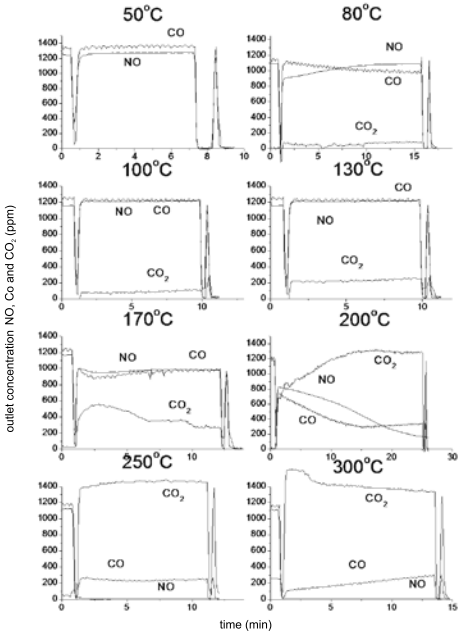

Fig. 10*b*. Transient response curves obtained during the reaction stages with a NO+CO+Ar flow and desorption stages with an Ar flow performed at different temperatures on catalyst 0.7%Pd/SiO_2

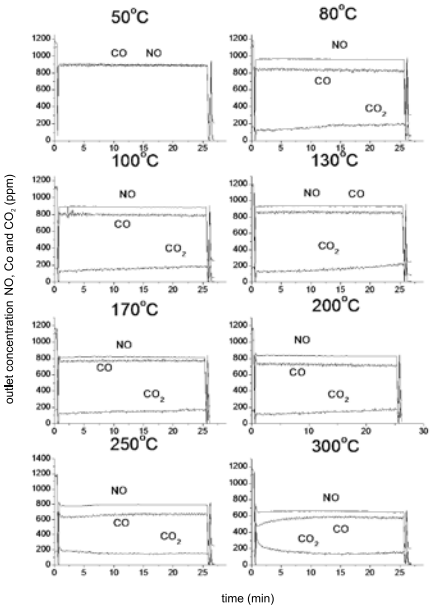

Fig. 10*c*. Transient response curves obtained during the reaction stages with a NO+CO+Ar flow and desorption stages with an Ar flow performed at different temperatures on catalyst 2.5%Pd/SiO_2

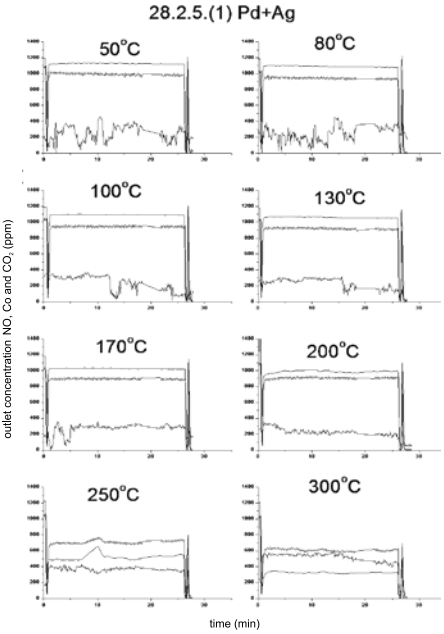

Fig. 10*d*. Transient response curves obtained during the reaction stages with a NO+CO+Ar flow and desorption stages with an Ar flow performed at different temperatures on catalyst 0.02%Pd+0.025%Ag/SiO_2

As can be seen in Fig. 10*a–d*, the response curves of the reactants NO and CO at temperatures below 200°C are of instantaneous type. According to this conclusion, the surface reaction of adsorption of reactants is the rate-determining step. At higher temperature this is also overshot response for NO, which satisfies the limiting stage of regeneration of catalytic active centers. Hence, the conclusion that those over 180°C on the samples begin to run two reactions – reduction of NO with CO (equation (1)) and direct decomposition of NO to N_2 and O_2 (equation (3)).

CONCLUSIONS

The investigations carried out on the silica catalyst obtained by sol–gel method showed that they exhibit high activity at comparatively low temperatures on reduction of NO with CO. It has been established that increasing the concentration of Pd has led to activity increase, but goes through a maximum about 0.7% Pd/SiO_2 and decreased at 2.5% Pd/SiO_2. The most important result is that over 180°C together with the catalytic reduction process begins direct decomposition of NO to N_2 and O_2. Therefore, two types of catalytically-active complex (CAC) were formed on the surface of Pd, which catalyse different reactions. This effect is observed in palladium catalysts enriched with Ag. Despite the low content both of Pd^{2+} (0.02%) and Ag^{+} (0.025%), this catalyst exhibits high activity especially on the catalytic reduction of NO with CO. Probably Ag has been included in the CAC for this reaction, compensating the lack of Pd. It is known[37] that catalysts of this type with a weight of 0.2 wt. % Pd/SiO_2 do not have such activity. The obtained results indicate that the synthesised Pd catalysts are perspective for deactivation of NO by direct decomposition to N_2 and O_2.

REFERENCES

1. F. NAKAJIMA: Air Pollution Control with Catalysis – Past, Present and Future. Catal. Today, **10**, 1 (1991).
2. L. GLEBOV, A. ZAKIROVA, V. TRETKOV, T. BURDEINAYA, G. AGOPOVA: Sostoianie issledovanii v oblasti kataliticheskih prevrastenii NO v N_2. Neftechimia, **3** (42), 163 (2002) (in Russian).
3. R. J. FARRAUTO, R. M. HECK: Catalytic Converters: State of the Art and Perspectives. Catal. Today, **51**, 351 (1999).
4. P. W. PARK, C. S. RAGLE, C. L. BAYER, M. L. BALMER: In_2O_3/Al_2O_3 Catalysts for NO_x Reduction in Lean Condition. J. Catal., **210**, 97 (2002).
5. R. BURCH, J. P. BREEN, F. C. MEUNIER: A Review of the Selective Reduction of NO_x with Hydrocarbons under Lean-burn Conditions with Non-zeolitic Oxide and Platinum Group Metal Catalysts. Appl. Catal. B: Environ., **39** (4), 283 (2002).
6. D. LORIMER, A. T. BELL: Reduction of NO by CO over a Silica-supported Platinum Catalyst: Infrared and Kinetic Studies. J. Catal., **59**, 223 (1979).
7. B. K. CHO: Mechanistic Importance of Intermediate N_2O + CO Reaction in Overall NO + CO Reaction System: II. Further Analysis and Experimental Observations. J. Catal., **148**, 697 (1994).
8. Y. NISHIHATA, J. MIZUKI, T. AKAO, H. TANAKA, M. UENISHI, M. KIMURA, T. OKAMOTO, N. NAMADA: Self-regeneration of a Pd-Perovskite Catalyst for Automotive Emissions Control. Nature, **418**, 164 (2002).

9. K. ZHOU, H. CHEN, Q. TIAN, Zh. HAO, D. SHEN, X. XU: Pd-containing Perovskite-type Oxides Used for Three-way Catalysts. J. Mol. Catal. A: Chemical, **189** (2), 225 (2002).
10. R. NICKOLOV, N. STANKOVA, M. KHRISTOVA, D. MEHANDJIEV: Copper Oxide Supported on Carbon Modified Alumina as Catalyst for Reduction of NO with CO. J. Colloid and Interface Science, **265** (1), 121 (2003).
11. R. A. BAKER, R. C. DOERR: Catalyzed Nitric Oxide Reduction with Carbon Monoxide. Ind. Eng. Chem. Progress Des. Develop., **4**, 188 (1965).
12. M. SHELEV, K. OTTO, H. GALALHI: The Oxidation of CO by O_2 and by NO on Supported Chromium Oxide and Other Metal Oxide Catalysts. J. Catal., **12**, 361 (1968).
13. J. W. LONDON, A. T. BELL: A Simultaneous Infrared and Kinetic Study of the Reduction of Nitric Oxide by Carbon Monoxide over Copper Oxide. J. Catal., **31**, 96 (1973).
14. R. T. RIWICK, H. WISE: Reduction of Nitric Oxide by Carbon Monoxide on Copper Catalysts. J. Catal., **40**, 301 (1975).
15. G. ALHASOV, G. Z. GASSAN-ZADE, N. OSMANOV, N. Y. SULTANOV: Mechanism of the Interactions of NO with CO on Oxide Catalysts. Kinet. Katal., **16**, 1230 (1975).
16. A. E. GIANNAKAS, A. K. LAVADOS, P. J. POMONIS: Preparation, Characterization and Investigation of Catalytic Activity for NO+CO Reaction of $LaMnO_3$ and $LaFeO_3$ Perovskites Prepared via Microemulsion Method. Appl.Catal. B: Environ. l, **49** (3), 147 (2004).
17. A. A. LEONTIOU, A. K. LADAKOS, P. J. POMONIS: Catalytic NO Reduction with CO on $La_{1-x}Sr_x(Fe^{3+}/Fe^{4+})O_{3\pm\delta}$ Perovskite-type Mixed Oxides (x = 0.00, 0.15, 0.30, 0.40, 0.60, 0.70, 0.80, and 0.90). Appl.Catal. A: General, **241**, 133 (2003).
18. V. C. BELESSI, C. N. COSTA, T. V. BAKAS, T. ANASATANASIDOU, P. J. POMONIS, A. M. EFSAHIOU: Catalytic Behavior of La–Sr–Ce–Fe–O Mixed Oxidic/Perovskitic Systems for the NO+CO and NO+CH_4+O_2 (Lean-NO_x) Reactions. Catal. Today, **59**, 347 (2000).
19. M. IWAMOTO, H.YAHIRO, T. KAYSUNO, S. BUNYU, S. KAGAVA: Enhancement of Catalytic Activity of Copper Ion-exchanged Y Type Zeolites for the Decomposition of Nitrogen Monoxide. Bull. Chem. Soc. Jpn., **62** (2), 583 (1989).
20. R. D. ZHANG, A. VILLANUEVA, W. ALAMADARI, S. KALIAGUINE: Cu- and Pd-substituted Nanoscale Fe-based Perovskites for Selective Catalytic Reduction of NO by Propene. J. Catal., **237** (2), 368 (2006).
21. R. D. ZHANG, A. VILLANUEVA, W. ALAMADARI, S. KALIAGUINE: Catalytic Reduction of NO by Propene over $LaCo_{1-x}Cu_xO_3$ Perovskites Synthesized by Reactive Grinding. Appl. Catal. B.: Environ., **64** (3–4), 220 (2006).
22. R. D. ZHANG, A. VILLANUEVA, S. KALIAGUINE: SCR of NO by Propene over Nanoscale $LaMn_{1-x}Cu_xO_3$ Perovskites. Appl. Catal. A: General., **307** (1), 85 (2006).
23. D. PETER, E. GARBOWSKI, V. PERRICHON, B. POMIER, M. PRIMET: Activity Enhancement of Mixed Lanthanum-copper-iron-Perovskites in the CO+NO Reaction. Appl. Catal. A: General, **205** (1–2), 147 (2001).
24. M. HARUTA, T. TSUBOTA, T. KABAYASHI, H. KAGEYAMA, M. JENET, B. DELMON: Low-temperature Oxidation of CO over Gold Supported on TiO_2, α-Fe_2O_3, and Co_3O_4. J. Catal., **144**, 175 (1993).
25. G. BAMWENDA, S. TSUBOTA, T. NAKAMURA, M. HARUTA: The Influence of the Preparation Methods on the Catalytic Activity of Platinum and Gold Supported on TiO_2 for CO Oxidation. Catal. Lett., **44**, 1 (1997).
26. M. MACIAJEWSKI, P. FABRIZOLI, J. GRUNWALDT, O. BECKER, A. BAIKER: Supported Gold Catalysts for CO Oxidation: Effect of Calcination on Structure, Adsorption and Catalytic Behavior. Phys. Chem. Chem. Phys., **3**, 3846 (2001).
27. P. KONOVA, A. NAYDENOV, C. VENKOV, D. MEHANDJIEV, D. ADREEVA, T. TABAKOVA: Activity and Deactivation of Au/TiO_2 Catalyst in CO Oxidation. J. Mol. Catal. A: Chemical, **213**, 235 (2004).

28. M. IWAMOTO, H. HAMADA: Removal of Nitrogen Monoxide from Exhaust Gases through Novel Catalytic Processes. Catal. Today, **10**, 57 (1991).
29. K.-I. AIKA, T. KAKEGAWA: On-site Ammonia Synthesis in De-NO_x Process. Catal. Today, **10**, 73 (1991).
30. M. IWAMOTO, S. YOKOO, K. SAKAI, S. KAWADA: Catalytic Decomposition of Nitric Oxide over Copper (II)-exchanged, Y-type Zeolites. J. Chem. Soc. Faraday Trans., **77**, 1629 (1981).
31. M. IWAMOTO, H. FURUKAWA, Y. MINE, F. UEMURA, S. MIKURIYA: Copper(II) Ion-exchanged ZSM-5 Zeolites as Highly Active Catalysts for Direct and Continuous Decomposition of Nitrogen Monoxide. J. Chem. Soc. Chem. Commun., **16**, 1272 (1986).
32. M. IWAMOTO, H. YAHIRO, Y. MINE, S. KAGAWA: Excessively Copper Ion-exchanged ZSM-5 Zeolites as Highly Active Catalysts for Direct Decomposition of Nitrogen Monoxide. Chem. Lett., **2**, 213 (1989).
33. M. IWAMOTO, H. YAHIRO, K. TANDA, N. MIZUNO, Y. MINE, S. KAGAWA: Removal of Nitrogen Monoxide through a Novel Catalytic Process. 1. Decomposition on Excessively Copper-ion-exchanged ZSM-5 Zeolites. J. Phys. Chem., **95**, 3727 (1991).
34. M. IWAMOTO, H. YAHIRO, N. MIZUMO, W. ZHANG, Y. MINE, H. FURUKAWA, S. KAGAWA: Removal of Nitrogen Monoxide through a Novel Catalytic Process. 2. Infrared Study on Surface Reaction of Nitrogen Monoxide Adsorbed on Copper Ion-exchanged ZSM-5 Zeolites. J. Phys. Chem., **96**, 9360 (1992).
35. S. SATO, Y. YU-U, H. YAHIRO, N. MIZUMO, I. IWAMOTO: Cu-ZSM-5 Zeolite as Highly Active Catalyst for Removal of Nitrogen Monoxide from Emission of Diesel Engines. Appl. Catal., **70**, L1 (1991).
36. M. KHRISTOVA, D. MEHANDJIEV: Conversion of NO on a Ni Impregnated-active Carbon Catalyst in the Presence of Oxygen. Carbon, **36** (9), 1379 (1989).
37. L. RADEV, M. KHRISTOVA, D. MEHANDJIEV: Sol-gel Ag + Pd/SiO_2 as a Catalyst for Reduction of NO with CO. Catal. Lett., **112** (3–4), 181 (2006).
38. D. PANAYOTOV, M. KHRISTOVA, D. MEHANDJIEV: Study of the Interaction between Nitric Oxide and Carbon Monoxide over Co_3O_4 and $Cu_xCo_{3-x}O_4$ Catalysts Using the Transient Response Method. Appl. Catal., **34** (1–2), 49 (1987).
39. M. KOBAYASHI: Characterization of Transient Response Curves in Heterogeneous Catalysis-I. Chem. Eng. Sci., **37** (3), 393 (1982).

Received 24 September 2009
Revised 23 December 2009

ENHANCED REMEDIATION OF CADMIUM AND COPPER FROM CLAYEY SOIL

A. ALOK*, R. P. TIWARI, R. P. SINGH

Department of Civil Engineering, Motilal Nehru National Institute of Technology, Allahabad, U.P., India
E-mail: *artialok123@yahoo.com*

ABSTRACT

The adsorption/desorption behaviour of copper and cadmium on soils was investigated in this study. The adsorption isotherm of copper and cadmium conformed to the Langmuir equation. The effect of pH, ammonium citrate on the desorption of copper and cadmium was studied. The desorption of copper and cadmium enhanced by ammonium citrate was influenced by pH. Ammonium citrate showed excellent enhancement on the desorption both of copper and cadmium. This study provides a guidance for the selection of purging solutions to enhance the electrokinetic (EK) remediation of copper and cadmium from contaminated soils.

Keywords: heavy metals, desorption, chelating agent, soil.

AIMS AND BACKGROUND

Copper (Cu)- and cadmium (Cd)-contaminated soils can be considered as the most extensive pollution. They are toxic trace metals, which can be introduced into and accumulate in soil through agricultural application of sewage sludge and fertilisers, and/or through land disposal of metal-contaminated municipal and industrial wastes[1]. They have been included on the US Environmental Protection Agency (EPA) list of priority pollutants[2]. Conventional soil remediation processes are mostly suitable to clean permeable soils. Phytoremediation is considered as a promising process[3–5], but it needs special plants and complicated post-treatment. Electrokinetic (EK) remediation was developed particularly for fine-grained clayey soils. It has shown great potential to the remediation of heavy metal contaminated soils[6–9]. However, the slow desorption of heavy metals from soils has been a major impediment to the successful remediation of contaminated sites[10,11]. It is, therefore, important to investigate the desorption behaviour of heavy metals from soils and to deploy appropriate ways to enhance the desorption efficiency so as to elevate EK remediation efficiency. The adsorption be-

* For correspondence.

haviour of copper and cadmium on soils has been widely investigated[12–17]. However, the desorption behaviour was studied relatively less. Most desorption processes were conducted immediately after the completion of adsorption process[16,18,19]. It has been well published that ionic strength have heavy effect on the adsorption/desorption behaviour of heavy metals on soils[17,18,20–22].

The present study was conducted to investigate the desorption behaviour of copper and cadmium from soils. Copper- or cadmium-contaminated soils were prepared artificially. Soil pH was controlled with acid or base. The objectives are: (1) to explore the effect of pH on the desorption of copper and cadmium from contaminated soils; (2) to compare the desorption efficiency of copper and cadmium from soils enhanced by tri-ammonium citrate to provide guidance for the selection of facilitating agents to enhance the EK remediation efficiency; (3) to investigate the desorption mechanism in the presence of tri-ammonium citrate.

Desorbing agents. While choosing desorbing agents in remediation process, the following factors should be considered: (i) the metal to be extracted; (ii) the chemical suiting the metals; (iii) the physicochemical nature of the material undergoing remediation (pH, chemical composition, etc.).

Complexing or chelating agents may be the best choice in remediation process because formation of stable complexes/chelates may bring heavy metals in solution at pH values where they are otherwise insoluble (neutral to high pH) and it may be possible to find selective complexing/chelating agents, favouring the metal.

Therefore, it is necessary to use such enhancement solutions which are beneficial or even necessary for removal of heavy metals from soil or for some combination of pollutants within a reasonable remediation time as well as with negligible damage to original soil structure.

Ammonium citrate. Ammonium citrate dissolves in water, forming citrate and ammonium ions. In Table 1, the dissociation constant for citric acid and ammonia are shown[23]. It is expected that cadmium will form both positively and negatively charged complexes, while copper will form some uncharged complexes that will most likely to be dissolved in the soil solution.

Table 1. Dissociation constant for citric acid and ammonia at 25°C

Chemicals	Dissociation constant
Citric acid	$pK_1 = 3.1$
	$pK_2 = 4.7$
	$pK_3 = -5.4$
Ammonia	$pK_b = 4.7$

Benjamin and Leckie[24] studied the competitive adsorption of Cd, Cu, Pb, and Zn. The adsorption of cadmium decreased by approximately 18% in the presence of copper. They concluded that competitive interactions between metals were minimal,

because each metal adsorbed to a different set of sites on the oxide surface. However, when metals exceed their saturation, both precipitation and adsorption may occur, therefore, adsorption effects can not be distinguished from surface precipitation.

Irah et al.[25] have reported the results on heavy metal sorption by different Estonian soil types at low equilibrium solution concentrations. Batch sorption experiments were conducted with heavy metal solutions in 0.01 M $CaCl_2$ at low equilibrium concentrations of Cu, Pb, Cd, and Cr in 10 different intact soil samples. Metal solid/liquid distribution coefficients K_d were determined from the adsorption isotherms obtained. Their values varied over a range from 57 to 53 000 ml/g. The soils used in the experiment were chosen according to their organic matter content and origin to represent differential behaviour with regard to heavy metal sorption. Correlations of K_d (distribution coefficient) with soil parameters were observed together with varying sorption behaviour of metal cations to different soil types. Desorption of metals from soil phase to solution was found to be very small, suggesting that at least during the initial period after the metal pollutants have reached the soil surface they accumulate in the top humus layer. Heavy metal desorption into the water phase also depends on the character of the metal and on soil type. The association of the studied heavy metal cations with soils depends on many soil parameters, most significantly on its organic matter and clay content, but also other parameters such as concentrations of Fe and Mn oxides are important. Pb and Cr are adsorbed to a greater extent to soils with high organic matter content. Cu and Cd sorption tends to be significantly affected by the mineral part of the soils, especially the calcite-dolomite content. For this reason their K_d-organic matter content relations are different from those obtained for Pb and Cr. The observed desorption of metals from soil to the solution phase was very small. This suggests that at least in the first stage after the heavy metals are emitted to the soil environment they remain mainly in the upper A horizons of the soils. Heavy metal desorption (or leaching of adsorbed compounds) into the water phase also depends on the character of the metal and on the soil type.

Sun et al.[26] found that Zn, Cd, Cu, and Pb could be extracted from the soils contaminated with these four heavy metals with similar efficiency in batch experiments with 0.01 M EDTA, while elution patterns were different in column leaching experiments. Cu was the most mobile, followed by Zn, Cd, and Pb was the least mobile, suggesting that the liability of metals in soils, the kinetics of metal desorption/dissolution and the mode of EDTA addition were the main factors controlling the behaviour of metals leached with EDTA.

Arias et al.[15] reported the competitive adsorption equilibrium isotherms of Cu^{2+} and Cd^{2+} on kaolin in the presence and the absence of humic acids (HAs). HAs were found to enhance the metal adsorption capacity of mineral surfaces, in particular kaolin. This enhancement was also observed in the competitive adsorption of copper and cadmium on kaolin and kaolin–HA complex. This competitive adsorption shows that the presence of Cd^{2+} has not an important effect on Cu^{2+} adsorption, whereas a dramatic decrease is observed on the adsorption of Cd^{2+} in the presence of Cu^{2+}. The

Freundlich isotherm equation was found to provide an excellent fit to the experimental data. These results were compared with the independent adsorption of both heavy metals. This study provided guidance for the selection of organic acids[27] to enhance the electrokinetic (EK) remediation of copper and cadmium from contaminated soils.

EXPERIMENTAL

CHEMICALS AND MATERIAL

$CuSO_4.5H_2O$ (Qualigens fine chemicals, Mumbai, 99% pure) and Cd $(NO_3)_2.4H_2O$ (Otto Kemi, Mumbai, 99% pure) were used as the source of copper and cadmium, respectively. Triammonium citrate $(NM_4)_3C_6H_5O_7$ (Otto Kemi, Mumbai, 98% pure) was used as purging solution. Solutions with different pH were prepared by the addition of glacial acetic acid and ammonia solution. Deionised water was used in all the experiments. All the other reagents used were above analytical grade. As EK process is most suitable to remediate clayed contaminated soils, kaolin, a typical clayed soils that was often used in EK tests[28] was used in the present study. The main properties of clay (Agricultural soil of Meja village of Allahabad district, Uttar Pradesh, India) are shown in Table 2. It is highly alkaline, negatively charged and contains low content of cationic exchangeable capacity and organic matters.

Table 2. Main characteristics of soil

Characteristic	Values
Percentage of different particles in soil aggregation[a]	
Gravel	6.60%
Sand	18.4%
Silt	60.0%
Clay	15.0%
Organic matter[b]	6.25%
Cation exchange capacity (CEC)[c]	22 meq/100 g
pH[d]	9.66
$CaCO_3$	2.5%

[a] Particle size measured by method IS 2720 Part 4 – 1985; [b] Organic matter measured by heating the dried sample at 600°C for 5 h; [c] CEC determined by EPA SW-846 method 9081 (USEPA, 1986); [d] pH measured by the mixture of soil and water (1:2, w/w) with pH-meter (Orion Model, 920 A^+).

PROCEDURES AND EQUIPMENTS

Sorption of copper and cadmium on clay soil. Soil samples (4 g) were equilibrated in borosil bottles of 300-ml capacity (120 rpm) at room temperature (25 ± 1°C) in 200 ml of different concentration of copper and cadmium solutions with concentrations 5, 50, 100, 200, 400, 800 and 1000 mg/l, respectively, for 10 days. The equilibrated suspensions were centrifuged at 4000 rpm for 10 min. The supernatant was drawn and diluted, and its copper or cadmium content was measured by atomic absorption

spectro-photometry (Perkin–Elmer). Adsorbed copper and cadmium were calculated as the difference between the amount initially present in solution and the amount remaining in solution after equilibration.

Desorption of copper and cadmium on clay soil. Copper-contaminated soil of 10.52 g/kg dry soils close to the maximum adsorption capacity obtained from the above study, was prepared by spiking $CuSO_4.5H_2O$ solution in soils The soil and solution were stirred thoroughly to obtain an uniform distribution of copper in the contaminated soil. After equilibration for 7 days at room temperature, the soil was dried at 105°C for 8 h, then ground and sieved by 425 μ sieve. It was stored in dark for the following desorption experiments. The content of copper in the contaminated soils was analysed by digesting the contaminated soils with concentrated HNO_3 at 170°C for 24 h. The real content of copper was determined to be 10.52 g/kg dry soils. The similar procedure was performed to prepare the cadmium-contaminated soils of 9.07 g/kg dry soils.

Simulated copper- or cadmium-contaminated soil samples (4 g) were equilibrated (120 rpm) at room temperature (28 ± 1°C) in 200 ml of 1 M ammonium citrate solution as background electrolyte. Known quantity of HNO_3 or NaOH was added to the solutions and the final pH 2, 7.15, and 10.15 of the soil-solution system was measured. The equilibrated suspensions were centrifuged at 4000 rpm for 10 min. A certain amount of the supernatant was drawn and diluted, and its copper and cadmium content were measured by atomic absorption spectrophotometer. The desorption of copper and cadmium was calculated as the percentage of the amount remaining in solution after equilibration. All the desorption experiments were conducted in triplicate. The final pH of the soil-solution mixture in the vial was determined with a pH-meter (Orion Model, 920 A^+)

RESULTS AND DISCUSSION

Sorption of copper and cadmium. The adsorption behaviour of copper and cadmium on soils is crucial to understand their partition and mobility in soil solution. The adsorption isotherms are plotted in Fig. 1, in which Ce and Cs are the equilibrated content in solution and adsorbed contents in soils, respectively. Figure 1 shows that the adsorbed amount of copper and cadmium increased with the increase in the aqueous equilibrium concentration. It is noteworthy that the adsorbed amount of copper was larger than that of cadmium in the studied concentration range. Generally, the adsorption of heavy metals on clayed minerals includes specific adsorption and exchangeable adsorption[29]. Specific adsorption stems from the existence of surface charges and exchangeable adsorption is due to the interlayer charges[29]. In addition, the organic matters contained in soils may contribute to the adsorption[16]. Copper has a smaller ionic diameter than cadmium (0.146 nm versus 0.194 nm)[29], so it may enter into the interlayer more easily, suggesting the greater exchangeable adsorption. It has been reported that organic

matters may adsorbed copper much more than cadmium. Therefore, the soils adsorbed more copper than cadmium in the studied concentration range.

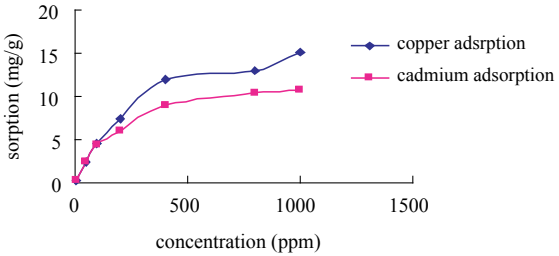

Fig. 1. Adsorption isotherm of copper and cadmium on soil

The adsorption isotherms were analysed by using Langmuir and Freundlich equations[30]. The results are shown in Table 3. The copper and cadmium adsorption data were fitted satisfactorily by Langmuir equation. According to the regression equations obtained in Table 3, the maximum adsorption capacity of copper and cadmium on soils was calculated as 10.52 and 9.07 g/kg, respectively; the coefficients of determination (R^2) were obtained as 0.9995 and 0.9993 for copper and cadmium, respectively. A higher value of adsorption coefficient for copper than for cadmium suggested a stronger affinity of soils to copper than to cadmium[30]. Therefore, high content of copper and cadmium in soils was prepared with respect to the maximum adsorption capacity.

Table 3. Langmuir equation fitted to the copper and cadmium adsorption data

Equation (Langmuir)	Regression equation
Copper	$y = 0.4803x + 0.095$
Cadmium	$y = 0.5022x + 0.1102$

Effect of initial metal concentration on sorption. In case of Cu^{2+} and Cd^{2+} it is seen that on increasing initial concentration, the amount of metal sorbed at the experimental equilibrium period increased, or on increasing the initial concentration of metal solution, an increase of sorption was registered by the soil.

The ascending effect of raising the initial concentration of the Cu^{2+} and Cd^{2+} in sorption experiments on the corresponding uptake of the Cu^{2+} and Cd^{2+} by the soil is obvious. However, the increase in metal uptake by the soil is not proportional to the increase in corresponding initial concentrations of the Cu^{2+} and Cd^{2+} instead a negative or decreasing trend is observed. With increasing metal concentration in solution, a decreasing percent of increase has been observed.

Several investigators have found the same results as regards the effect on sorption with increasing concentration of the heavy metal sorbates. Carriere et al.[31], through their studies on sorption experiments, observed that lead sorption was fast at low initial

concentrations, but at higher concentrations the reaction became slower. They suggested that precipitation reactions, as they are more noticeable at higher concentrations, were responsible for the slow sorption reactions. Wanzuhairi[32] conducted experiments on removal of Pb, Cu, and Zn on clays from South Wales, U.K. and concluded that the amount of metals including zinc increased with increasing equilibrium concentrations in solution. However, the percentage increase falls as the initial concentration is increased. Srivastava et al.[33] have also reported the similar sorption behaviour for Zn and Cd on phosphatic clay.

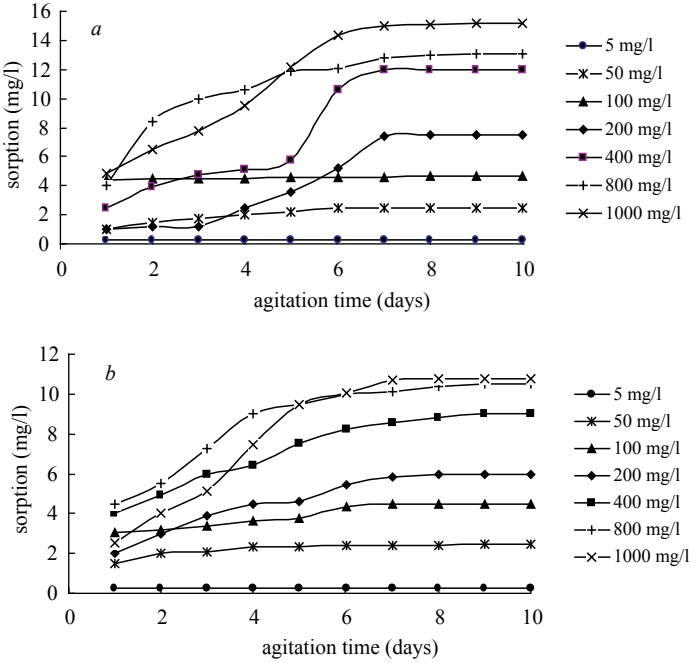

Fig. 2. Effect of initial concentration on sorption of Cu (*a*) and Cd (*b*)

Effect of pH on the desorption of copper and cadmium. It has been widely reported that pH highly affects the adsorption/desorption behaviour of heavy metals on soils[13,17–19,21,22]. Figure 3 *a*, *b* presents the effect of pH on the desorption of copper and cadmium from soils. When pH was below 4.0 the desorption of copper and cadmium decreased linearly with the rise of pH. Effect of pH on the desorption of copper and cadmium had no significant difference. Generally, the zeta potential of soils became more negative with the rise of soil pH. The specific adsorption, which stemmed from the existence of surface charge, was enhanced with the rise of pH (Ref. 28). Thus, the desorption became difficult at high pH. This result was in agreement with the data in literature, where the rise of pH led to more adsorption of heavy metals on soils[17,18,22]. In addition, the preferential adsorption of hydroxy-metal species by soil organic matter and/or hydrous iron and aluminium oxide may be enhanced[17]. Higher pH values

resulted in the precipitation of insoluble metal hydroxide, thus making adsorption studies impossible. As a consequence, low pH was preferred in the EK remediation of copper and cadmium contaminated soils.

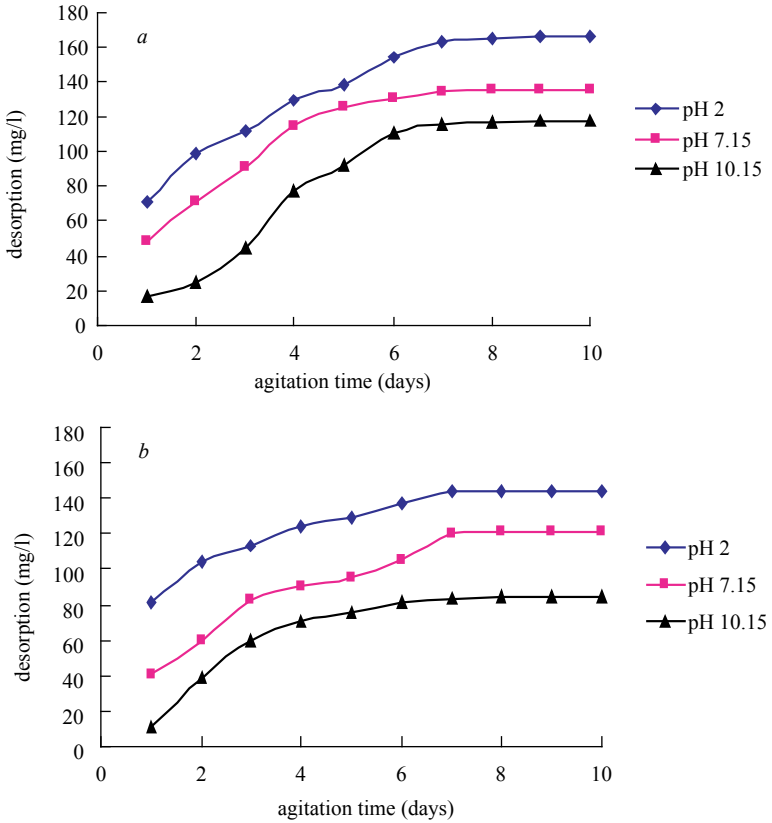

Fig. 3. Effect of pH on desorption of Cu (*a*) and Cd (*b*) at different contact times

Effect of agitation/contact period. From Fig. 3 *a*, *b* it can be easily understood that the desorption at pH 2 was maximum. At pH 2 fast desorption is followed by slow reaction rate. In the first 4–5 days of the desorption process, about 83% of total copper desorbed and 87–90% of cadmium also desorbed by within this time with 1 M ammonium citrate solution. The rate of sorption for Cu^{2+}/Cd^{2+} was much faster in the first 4–5 days. After that metal released by soil slows down considerably and equilibrium condition reached in about 9 days. Similar is in case of pH 7.15 and 10.15.

CONCLUSIONS

This study investigated the adsorption/desorption behaviour of copper and cadmium on soils. The effect of ionic strength, agitation or contact time, pH and chelating

agent ammonium citrate on the desorption of copper and cadmium was studied. The important conclusions were drawn as follows.

The adsorption isotherm of copper and cadmium corresponds to Langmuir equation. The maximum adsorption capacity of copper and cadmium on soils was calculated as 10.52 and 9.07 g/kg, respectively. Soils showed a stronger affinity to copper than to cadmium.

Both ionic strength and pH had greater influence on the desorption of copper and cadmium from soils. The desorption of copper and cadmium increased with increase in ionic strength, while the desorption decreased with the rise of pH. At pH below 4.0 the desorption of copper and cadmium declined linearly with increase in pH.

The desorption mechanism of copper and cadmium in the presence of chelating agent ammonium citrate was explained as the competition of complex, adsorption and precipitation. The effect of complex contributed to the desorption, while the effect of adsorption and precipitation related the desorption. These effects were highly influenced by pH. High pH led to a high ratio of L^{n-}, which generally were effective species to form complex with copper and cadmium. But the ratio of L^{n-} changed negligibly when pH rose to a certain value. However, higher pH results in more adsorption and precipitation. The net effect determines the desorption efficiency.

This study provided guidance for the selection of purging solution to enhance the EK remediation of copper and cadmium from contaminated soils. Ammonium citrate can be used to enhance the EK removal of copper and cadmium from contaminated soil.

REFERENCES

1. K. J. WANG, B. S. XING: Adsorption and Desorption of Cadmium by Goethite Pretreated with Phosphate. Chemosphere, **48**, 665 (2002).
2. C. N. MULLIGAN, R. N. YONG, B. F. GIBBS: Remediation Technologies for Metal-contaminated Soils and Groundwater: An Evaluation. Eng. Geol., **60**, 193 (2001).
3. P. B. A. N. KUMAR, V. DUSHENKOV, H. MOTTO, L. RASKIN: Phytoremediation: The Use of Plants to Remove Heavy Metal from Soils. Environ. Sci. Technol., **29**, 1232 (1995).
4. J. W. HUANG, J. J. CHEN, W. R. BERTI, S. CUNNINGHAM: Phytoremediation of Lead-contaminated Soils – Role of Synthetic Chelates in Lead Phytoextraction. Environ. Sci. Technol., **31**, 800 (1997).
5. S. D. EBBS, L. V. KOCHIAN: Phytoremedaiton of Zinc by Oar (*Avina sativa*), Barley (*Hordeum vulgare*) and Indian Mustard (*Brassica juncea*). Environ. Sci. Technol., **32**, 802 (1998).
6. R. LAGEMAN: Electroreclamation: Applications in the Netherlands. Environ. Sci. Technol., **27**, 2648 (1993).
7. R. F. PROBSTEIN, R. E. HICK: Removal of Contaminants from Soils by Electric Field. Science, **260**, 498 (1993).
8. D. M. ZHOU, C. F. DENG, L. CANG, A. N. ALSHAWABKEH: Electrokinetic Remediation of a Cu–Zn Contaminated Red Soil by Controlling the Voltage and Conditioning Catholyte pH. Chemosphere, **61**, 19 (2005A).
9. D. M. ZHOU, L. CANG, A. N. ALSHAWABKEH, Y. J. WANG, X. Z. HAO: Pilot-scale Electrokinetic Treatment of a Cu Contaminated Red Soil. Chemosphere, **63**, 964 (2006).

10. C. D. COX, M. A. SHOESMITH, M. M. GHOSH: Electrokinetic Remediation of Mercury-contaminated Soils Using Iodine/Iodide Lixiviant. Environ. Sci. Technol., **30**, 1933 (1996).
11. D. M. ZHOU, C. F. DENG, L. CANG: Electrokinetic Remediation of a Cu Contaminated Red Soil by Conditioning Catholyte pH with Different Enhancing Chemical Reagents. Chemosphere, **56**, 265 (2004).
12. C. N. HAAS, N. D. HOROWITZ: Adsorption of Cadmium to Kaolinite in the Presence of Organic Material. Water Air Soil Pollut., **27**, 131 (1986).
13. R. W. PULS, R. M. POWELL, C. DONALD, C. J. ELDRED: Effect of pH, Solid/Solution Rate, Ionic Strength, and Organic Acids on Pb and Cd Sorption on Kaolinite. Water Air Soil Pollut., **57**–**58**, 423 (1991).
14. V. RAMACHANDRAN, T. J. D. SOUZA: Adsorption of Cadmium by Indian Soils. Water Air Soil Pollut., **111**, 225 (1999).
15. M. ARIAS, M. T. BARRAL, J. C. MEJUTO: Enhancement of Copper and Cadmium Adsorption on Kaolin by the Presence of Humic Acids. Chemosphere, **48**, 1081 (2002).
16. M. ARIAS, C. P. NOVO, F. OSORIO, E. LOPEZ, B. SOTO: Adsorption and Desorption of Copper and Zinc in the Surface Layer of Acid Soils. J. Colloid Int. Sci., **228**, 21 (2005).
17. I. R. PHILLIPS, D. T. LAMB, D. W. WARKER, E. D. BURTON: Effect of pH and Salinity on Copper, Lead, and Zinc Sorption Rates in Sediments from Moreton Bay, Australia. Bull. Environ. Contam. Toxicol., **73**, 1041 (2004).
18. T. UNDABEYTIA, S. NIR, G. TYTWO, C. SERBAN, E. MORILLO, C. MAQUEDA: Modeling Adsorption–Desorption Processes of Cu on Edge and Planar Sites of Montmorillonite. Environ. Sci. Technol., **36**, 2677 (2002).
19. Y. Z. GAO, J. Z. HE, W. T. LING, H. Q. HU, F. LIU: Effects of Organic Acids on Copper and Cadmium Desorption from Contaminated Soils. Environ. Int., **29**, 613 (2003b).
20. H. M. CHEN: Heavy Metal Pollution in Soil–Plant System. Science Press, Beijing, 1996.
21. Y. H. XU, D. Y. ZHAO: Removal of Copper from Contaminated Soil by Use of Poly(amidoamine) Dendrimers. Environ. Sci. Technol., **39**, 2369 (2005).
22. A. H. OREN, A. KAYA: Factors Affecting Adsorption Characteristics of Zn^{2+} on Two Natural Zeolites. J. Hazard. Mater., **B131**, 59 (2006).
23. G. M. NYSTROM: Investigation of Soil Solution during Enhanced Electrodialytic Soil Remediation. Master Thesis, The Technical University of Denmark, DTU, 2001.
24. M. M. BENJAMIN, J. O. LECKIE: Multiple-site Adsorption of Cd, Cu, Zn, the Amorphous Iron Oxyhydroxide. J. of Colloid and Interface Science, **79**, 29 (1981a).
25. N. IRAH, E. STEINNES, U. KIRSO, V. PETERSELL: Mobility of Cd, Pb, Cu and Cr in Some Estonian Soil Types. Estonian J. of Earth Science, **58** (3), 209 (2009).
26. B. SUN, F. J. ZHAO, E. LOMBI, S. P. McGRATH: Leaching of Heavy Metals from Contaminated Soil Using EDTA. Environmental Pollution, **133** (2), 111 (2001).
27. S. YUAN, Xi. ZHIIN, Y. JING, J. WAN, W. CHAN, Z. ZHENG, Ku. XIAOHUA: Desorption of Copper and Cadmium from Soils Enhanced by Organic Acids. Chemosphere, **68**, 1289 (2007).
28. A. T. YEUNG, C. N. HSU: Electrokinetic Remediation of Cadmium Contaminated Clay. J. Environ. Eng., **131**, 298 (2005).
29. H. P. HE: Studies on the Interaction of Clayed Mineral and Metallic Ions. Petrolic Industrial Press, Beijing, 2001.
30. X. C. FU, W. X. SHEN, T. Y. YAO: Physical Chemistry. High Education Press, Beijing, 2000.
31. P. P. E. CARRIERE, B. E. REED, S. R. CLINE: Retention and Release of Lead by a Silty Loam and a Fine Sandy Loam. II. Kinetics. Sep. Sci. Tech., **30** (18), 3471 (1995).
32. W. Y. WANZUHAIRI: Sorption Capacity on Lead, Copper and Zinc by Clay Soils from South Wales, United Kingdom. Environmental Geology, **45** (2), 236 (**2003).**
33. P. SRIVASTAVA, B. SINGH, M. ANGOVE: Competitive Adsorption Behavior of Heavy Metals on Kaolinite. J. Colloid Int. Sci., **290**, 28 (2005).

Received 27 May 2009
Revised 29 June 2009

DETERMINATION OF HERBICIDE BROMACIL IN WATER AND SOIL SAMPLES BY KINETIC-SPECTROPHOTOMETRIC METHOD AND HPLC METHOD

E. T. PECEV[a]*, Z. M. GRAHOVAC[a], S. S. MITIC[a], R. M. SIMONOVIC[b], A. N. PAVLOVIC[a]

[a]*Faculty of Natural Sciences and Mathematics, Department of Chemistry, 33 Visegradska Street, P. O. Box 224, 18 000 Nis, Serbia*
[b]*Faculty of Natural Sciences and Mathematics, University of Pristina, 38 220 Kosovska Mitrovica, Kosovo*
E-mail: *emapecev@medianis.net*

ABSTRACT

The aim of this work was to develop a new kinetic method for determination of herbicide bromacil. The method is based on reaction of sulphanilic acid oxidation by hydrogen-peroxide in phosphate buffer in the presence of Cu(II) ion as catalyst. The herbicide bromacil shows an inhibited effect in this reaction. Bromacil was determined with linear calibration graph in the interval from 2.70 to 16.10 μg/cm^3. The optimised conditions yielded a theoretical detection limit of 0.55 μg/cm^3 based on the $3S_b$ criterion. The RSD is 3.26–0.32% for the concentration interval of bromacil 2.70–16.10 μg/cm^3. The reaction was followed spectrophotometrically at 370 nm. The kinetic parameters of the reaction are reported, and the rate equations are suggested. The developed procedure was successfully applied to the rapid determination of bromacil in soil and water samples. Solid-phase extraction (SPE) was used for extraction of bromacil from soil and water samples with Chromabond® (Macherey-Nagel) C18 cartridges. The HPLC method was used like a comparative method to verify the results. The results obtained by two different methods showed good agreement.

Keywords: bromacil, kinetic method, solid-phase extraction, HPLC method, water and soil samples.

AIMS AND BACKGROUND

Several hundred compounds are available for use as pesticides. The pesticides include insecticides, herbicides, germicides, fungicides, rodenticides, nematocides and acaricides. On a worldwide basis, intoxications attributed to these pesticides have been

* For correspondence.

estimated to be as high as 3 million cases of acute and severe poisoning annually, with as many or more unreported cases and with some 220 000 deaths[1].

Bromacil [5-bromo-6-methyl-3-(1-methylpropyl)-2,4-(1H, 3H)-pyrimidinedione] (Fig. 1) is one of a group compounds called substituted uracils. This herbicide is the most frequently applied for weed control in citrus orchards. This herbicide can be applied alone or, in mixtures, to control a broad spectrum of weeds. This is herbicide used for weed and brush control on road shoulders and non-cropland, as well as for selective weed control on a limited number of crops, such as citrus fruit and pineapple[2]. It is especially useful against perennial grasses. Bromacil stops photosynthesis, which is turn causes plants to stop growing.

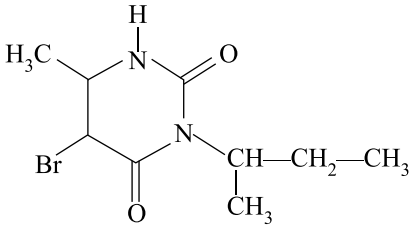

Fig. 1. Chemical structure of bromacil

Bromacil binds, or absorbs, only lightly to soil particles, is soluble in water, and has a relatively lengthy soil half-life (60 days). For these reasons, bromacil is expected to move (leach) quite readily through the soil and it can contaminate groundwater.

A number of analytical methods have previously been reported for the determination of bromacil in various matrices. However, as far as we know, there is no kinetic-spectrophotometric method for the bromacil determination in literature.

Many papers reported determination of pesticide residues by gas chromatography (GC) with different detectors, like flame ionisation detection (FID)[3], nitrogen-phosphourous detector (NPD)[4], electron capture detection[5–7], flame photometric detection (FPD)[8], mass selective detection (MSD)[9–16], and mass spectrophotometric detection by selected ion monitoring GC/MS-SIM[17,18]. Determination of bromacil in water was reported by different authors using a gas chromatography with MSD, NPD and FID detection[19–21].

Some authors developed a new method for pesticide determination using a solid-phase microextraction followed by GC and HPLC (Ref. 22).

Bromacil determination in soil[23–26] and water[27,28] was reported by different authors using a HPLC and GC method.

Solid-phase extraction (SPE) is an innovative method for efficiently and quantitatively extracting pesticides from large numbers of soil samples. Baranowska and Pieszko used SPE and derivative spectrophotometry to determine bromacil in environmental materials. Calibration graph was linear from 1 to 50 mg/dm^3 of bromacil. Recoveries were 98–120% for water and 90–130% for soil[29].

The primary objective of this study was to develop a sensitive kinetic-spectrophotometric method for the bromacil determination based on reaction of sulphanilic acid oxidation by hydrogen-peroxide in phosphate buffer in the presence of Cu(II) ion as catalyst[30], and to apply this method for bromacil determination in water and soil samples. However, SPE is used for isolation, concentration and purification of analytes from matrices, and HPLC method is used like comparative method to verify results.

EXPERIMENTAL

Apparatus. The reaction rate was monitored spectrophotometrically by measuring the rate of change of absorbance at 370 nm. The readings were performed on a Perkin–Elmer Lambda 15 UV-vis. spectrophotometer, connected to a thermo-circulating bath.

The pH measurements were carried out using a Hanna Instruments pH-meter.

HPLC was performed using an Agilent technologies 1200 model. The analytical column was C18 (Zorbax 5 μm, 250 mm x 4.6 mm).

A J. T. Baker Model SPE-12 with vacuum pump was used for solid phase extraction of samples.

A BÜCHI R-200/205 rotary vacuum evaporator including bath B-490 with an vacuum pump was used to evaporate the extracts.

In addition, high precision volume micropipettes (Lab Mate$^+$) of 50, 500 and 1000 μl were used for handling or pipetting the solutions.

The solutions were thermostated at 25.0 ± 0.1ºC before the beginning of the reaction in a Julabo MP-SA model thermostatic bath.

Reagents. All materials were of highest purity available. Bromacil standard, with a certified purity of 99.80%, was obtained from Dr Ehrenstorfer (Germany). A sulfanilic acid (SA) (Merck) solution was prepared by dissolving a 0.3463 g of a SA in water (50 ml) standard flask. The initial 2 mol/dm^3 solution of hydrogen peroxide was prepared from 30% H_2O_2 (Merck), and its exact concentration was standardised permanganometrically. Because of their limited stability, it was prepared just before use. A solution of Cu(II) 1×10^{-3} mol/dm^3 was prepared by dissolving $CuCl_2{\cdot}2H_2O$ (Merck) in water. The phosphate[31] buffer pH 7.8 was obtained by mixing solutions of KH_2PO_4 (0.067 mol/dm^3) and Na_2HPO_4 (0.067 mol/dm^3) in a volume ratio 4.5: 95.5 cm^3, respectively. HPLC grade methanol, acetone and acetonitrile were obtained from Baker (UK). Samples of tap water (town Nis, Serbia), ground water (village Grdelica, Serbia) and river water (river Morava, Serbia) were collected in May 2008.

Soil samples were collected in period April–May (2008) from different locations (Knez Selo – village, Grdelica village, Nis town).

Analytical grade chemicals and deionised water (MicroMed high purity water system TKA Wasseraufbereitungssysteme GmbH) were used for the preparation of all solutions.

Procedure. In order to obtain good mechanical and thermal stability, the instruments were run for 10 min before the first measurement. The reaction was carried out in the following way. In reaction-mixture vessel with 4 compartments, the solution of SA was placed in the first compartment, H_2O_2 in the second, phosphate buffer in the third, Cu(II) and bromacil in fourth compartment and water was added to total volume of 10 cm^3. The vessel was thermostated at 25.0±0.1ºC. The content was mixed well and then immediately transferred to the spectrophotometric cell with a path length of 10 cm. The change in absorbance was recorded at 370 nm as a function of time every 30 s over a period of 6 min. The rate of the reaction at different concentrations of each of the reactants was obtained by measuring the slope of the linear part of the kinetic curves to the absorbance-time plot (from the Beer law $A = \varepsilon lc$, $dA/dt = \varepsilon l(dc/dt)$, slope = dA/dt, rate=dc/dt =$(dA/dt)/\varepsilon l$). The calibration graph was constructed by plotting the slope of the linear part of the kinetic curve, versus concentration of the bromacil (c_{bromacil}, μg/cm^3).

Water sample preparation. Spiked water samples for recovery determination were prepared by addition of appropriate amount of standard stock solution (2.7 mg/cm^3) and stay for 1 day.

SPE with Chromabond® HR-P cartridge was used for extraction of bromacil. Each sample solution was poured into a chromabond HR-P C18 cartridge (sorbent mass 200 mg Macherey-Nagel, Germany) which had been conditioned with 1 column volume methanol, then 1 column volume deionised water, then water sample was filtered through the column, and column was dried for 30 min. The sample was eluted with 3×1 cm^3 (methanol–aceton 3:2, v/v) and then extract was collected and evaporated at 35°C in a rotary vacuum evaporator till dryness.

The residue was dissolved with methanol and transferred into volumetric flask (25 cm^3), and made up with methanol. For HPLC determination aliquots of this solution were transferred into vessels. For kinetic determination 10 cm^3 of this solution was taken and evaporated at temperature of 35°C till dryness. The residue was dissolved in 10 cm^3 volumetric flask and used for kinetic determination.

Soil sample preparation. Spiked soil samples for recovery determination were prepared by addition of appropriate amount of standard stock solution (2.7 mg/cm^3) and stay for few hours. The soil sample is shaken with methanol/water mixture (80:20, v/v), then it was centrifuged 3 times for 10 min at 3000 rpm. The separated supernatant is then diluted with a concentrated NaCl solution and filtered through a 0.45 μm membrane filter (Millipore). Then that solution was drawn through an SPE column (Chromabond® HR-P cartridge, sorbent mass 200 mg Macherey-Nagel, Germany), which had been first conditioned. The further preparation was the same as in the case of the water.

Comparative method. HPLC method was performed with an Agilent Technologies Model 1200 instrument with UV detector, fitted with C18 (Zorbax 5 μm, 250 mm × 4.6 mm) analytical column, operating at 25°C. The mobile phase was acetonitrile–water

(40:60, v/v), the eluate was monitored at wavelength of 280 nm. Injected volume was 20 μl, and the flow rate of the mobile phase was 1 ml/min.

RESULTS AND DISCUSSION

Kinetic studies. The tangent method was used for processing of the kinetic data. The rate of the reaction was obtained by measuring the slope of the linear part of the kinetic curves of the absorbance-time plot (slope=dA/dt). In order to determine the lowest possible determinable concentration of bromacil, the working conditions required optimisation. Therefore, the dependence of the rate of reactions on the concentration of each of the reactants was determined.

The effect of the pH on the rate of both reactions, catalytic and inhibited, was studied in the interval pH from 7.2 to 8.0. It can be seen that reaction rate increased with increasing of pH. For further work a pH of 7.9 was used (Fig. 2).

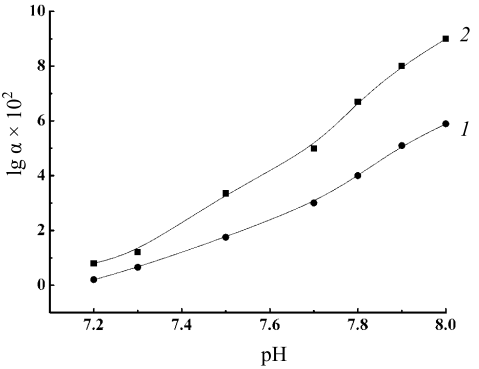

Fig. 2. Dependence of the reaction rate on the pH for the inhibited (*1*) and catalysed (*2*) reaction. Initial concentrations: $c_{SA} = 4\times10^{-3}$ mol/dm^3; $c_{H_2O_2} = 0.2$ mol/dm^3; $c_{Cu(II)} = 5\times10^{-6}$ mol/dm^3; $c_{bromacil} = 16.20$ μg/cm^3; $t = 25.0\pm0.1$°C

The effect of the concentration of H_2O_2 on the rates of reactions (Fig. 3) was studied in the range 0.04–0.28 mol/dm^3. It can be seen that the reaction rate of both reactions increased with increasing H_2O_2 concentration. A H_2O_2 concentration of 0.24 mol/dm^3 was selected for the further work.

The effect of the concentration of SA was studied (Fig. 4) in the interval of $(1.2–4.8)\times10^{-3}$ mol/dm^3. It can be seen that the rate of the catalysed and inhibited reaction increased with increasing SA concentration from 1.2 to 4.0×10^{-3} mol/dm^3, then reaction rate of both reactions decreased from 4 to 4.8×10^{-3} mol/dm^3. For further work a concentration of 4×10^{-3} mol/dm^3 was selected.

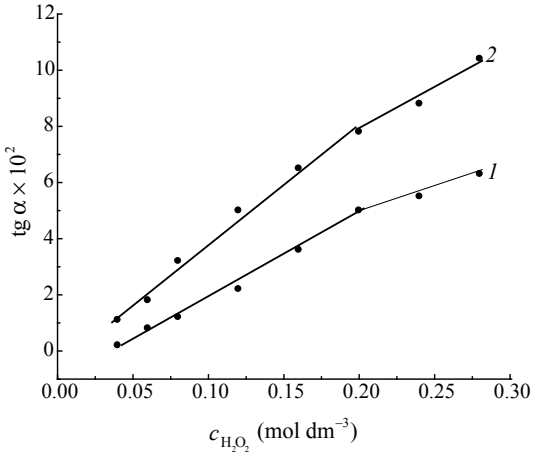

Fig. 3. Dependence of the reaction rate on the H_2O_2 concentration for the inhibited (*1*) and catalysed (*2*) reaction. Initial concentrations: pH = 7.9; $c_{SA} = 4\times10^{-3}$ mol/dm³; $c_{Cu(II)} = 5\times10^{-6}$ mol/dm³; $c_{bromacil}$ = 16.20 μg/cm³; t = 25.0±0.1°C

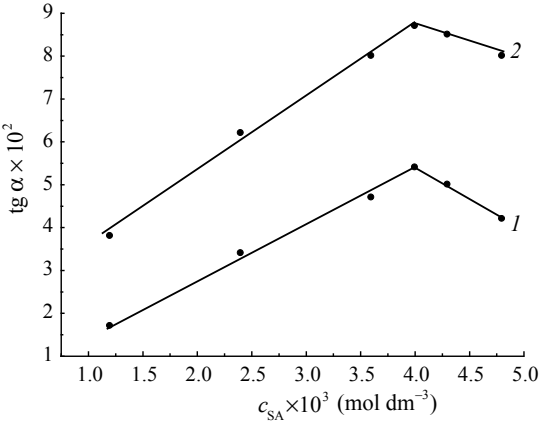

Fig. 4. Dependence of the reaction rate on the SA concentration for the inhibited (*1*) and catalysed (*2*) reaction. Initial concentrations: pH = 7.9 ; $c_{H_2O_2} = 0.24$ mol/dm³; $c_{Cu(II)} = 5\times10^{-6}$ mol/dm³; $c_{bromacil}$ = 16.20 μg/cm³ ; t = 25.0±0.1°C

The correlation between the slope and the Cu(II) concentration is given in Fig. 5. The influence of the concentration of Cu(II) ion on the reaction rates of catalysed and inhibited reactions was examined in the range $(2–7) \times 10^{-6}$ mol/dm³. A concentration of 6×10^{-6} mol/dm³ in the final solution was used throughout the experiments.

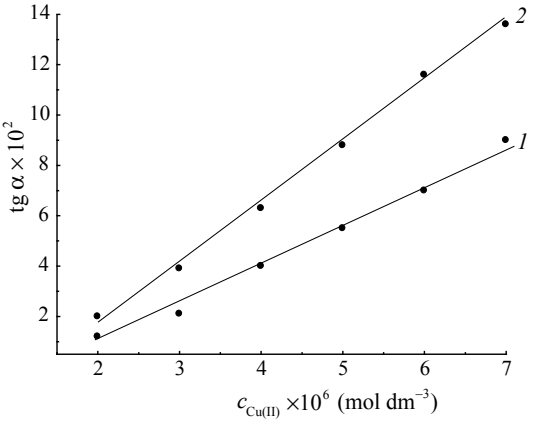

Fig. 5. Dependence of the reaction rate on the Cu(II) concentration for the inhibited (*1*) and catalysed (*2*) reaction. Initial concentrations: pH = 7.9; $c_{H_2O_2}$ = 0.24 mol/dm³; c_{SA} = 4×10⁻³ mol/dm³; $c_{bromacil}$ = 16.20 μg/cm³ ; t = 25.0±0.1°C

Under the optimum reaction conditions: pH=7.9; $c_{H_2O_2}$ = 0.24 mol/dm³; c_{SA}=4×10⁻³ mol/dm³; $c_{Cu(II)}$= 6×10⁻⁶ mol/dm³; t = 25.0±0.1°C, the bromacil concentration was varied from 2.70–16.20 μg/cm³.

Figure 6 shows the calibration curve at the temperature of 25.0°C, which can be used for the determination of the bromacil concentration in the interval 2.70–16.20 μg/cm³.

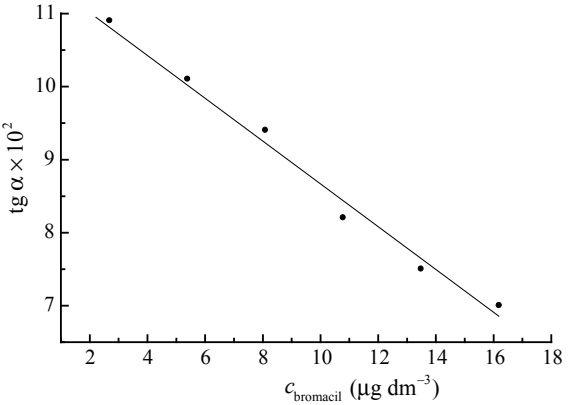

Fig. 6. Dependence of the reaction rate on the bromacil concentration in the interval 2.70–16.20 μg/cm³ for the inhibited reaction. Initial concentrations: pH = 7.9 ; $c_{H_2O_2}$ = 0.24 mol/dm³; c_{SA} = 4×10⁻³ mol/dm³; $c_{Cu(II)}$ = 6×10⁻⁶ mol/dm³; t = 25.0±0.1°C

The least square equation ($y = bx + a$, where b and a are the slope and intercept, respectively) for the calibration graph and correlation coefficient, r (Ref. 32) for the

determination of bromacil in the concentration range 2.70–16.20 μg/cm^3 under the optimum reaction conditions, mentioned above, were calculated:

$$\text{slope} \times 10^2 = -0.00316\, c_{\text{bromacil}} + 11.70\times10^2 \qquad r = -0.9943 \quad (1)$$

where slope is the slope of the linear part of the kinetic curve of the absorbance-time plot (slope = dA/dt = εl (dc/dt)) and c_{bromacil} is the bromacil concentration expressed in μg/cm^3.

The variance (S_0^2) of the calibration lines were evaluated to be 2.085×10^{-6} μg/cm^3. The low value of the variance indicates negligible scattering of the experimental data points around the line of regression. The quantitative parameters of the analysis are given in Table 1.

Table 1. Quantitative parameters of analysis

Calibration range, μg ml^{-1}	2.70–16.20, n= 6
Regression equation	slope ×10^2 = –0.00316c_{bromacil} + 11.70×10^2
Slope ± SD	(–0.30159 ± 0.01605) ×10^{-2}
Intercept ± SD	(11.70 ± 0.16875) ×10^{-2}
Correlation coefficient, r	–0.9943
Variance, S_0^2	2.08×10^{-6}
Detection limit (μg/cm^3)	0.55
Quantification limit (μg/cm^3)	1.86

The following kinetic equations for the catalysed and inhibited reaction were deduced based on the obtained graphic correlations:

$$\text{rate}_{\text{I}} = k\, c_{\text{H+}}^{-1}\, c_{\text{H}_2\text{O}_2}\, c_{\text{SA}}\, c_{\text{Cu(II)}} \quad (2)$$

$$\text{rate}_{\text{II}} = k_1\, c_{\text{H+}}^{-1}\, c_{\text{H}_2\text{O}_2}\, c_{\text{SA}}\, c_{\text{Cu(II)}}\, c_{\text{bromacil}}^{-1} \quad (3)$$

where k and k_1 are constants proportional to the rate constant of the catalysed and inhibited reaction, respectively.

The equations are valid for the following concentrations: phosphate buffer pH 7.2–8.0; $c_{\text{H}_2\text{O}_2}$ = 0.04–0.28 mol/dm^3; c_{SA} = 1.2 to 4.8×10^{-3} mol/dm^3; $c_{\text{Cu(II)}}$ = 2–7.0×10^{-6} mol/dm^3 and c_{bromacil}= 2.70–16.20 μg/cm^3.

The limit of detection (LOD) and quantification (LOQ) was evaluated using the following equations[33–36]:

$$\text{LOD} = 3.3S_0/b \text{ and } \text{LOQ} = 10S_0/b \quad (4)$$

where S_0 is the standard deviation of the calibration line and b – the slope. They were found to be 0.55 and 1.86 μg/cm^3, respectively.

The precision and accuracy of the system were studied by performing the experiment 5 times for different concentration of bromacil. The results of accuracy and precision of the recommended procedure are presented in Table 2.

Table 2. Accuracy and precision of the bromacil determination

Taken ($\mu g/cm^3$)	Found[a] $\bar{x} \pm SD$ ($\mu g/cm^3$)	n	RSD (%)[b]	G (%)	$((\bar{x} - \mu)/\mu) \times 100$ (%)[c]
2.70	2.85±0.02	5	3.26	4.06	5.55
8.10	8.22±0.01		3.00	3.74	1.51
16.20	3.23±0.01		0.32	0.40	0.18

[a] Mean and standard deviation of five determinations at 95% confidence level; [b] relative standard deviation; G – relative error; [c]accuracy of the method.

Interference studies. To assess the selectivity of the method, the interference of several foreign ions on the determination of bromacil was studied. Table 3 gives the tolerance limits (expressed as w/w ratios), for the species studied in the determination of 8.10 $\mu g/cm^3$ of bromacil. The maximum level tolerated was taken as that causing a difference in the rate of the inhibited reaction not larger than 5%. As can be seen that ions Mg^{2+}, Li^+, Na^+, K^+, CH_3COO^-, F^-, SO_4^{2-} do not interfere with the method. Ions like Co^{2+}, Mn^{2+} Fe^{3+}, Fe^{2+}, Zn^{2+} and Al^{3+} do not interfere when its concentration lower 10 times than concentration of bromacil. The other ions investigated have practically no influence on the determination of bromacil by this method. And we come to the conclusion that selectivity of the method is good.

Table 3. Effect of the foreign species on the determination of 8.10 $\mu g/cm^3$ of bromacil

Foreign species	Tolerance level ($c_{interferent}/c_{bromacil}$)
Li^+, Na^+, K^+, Mg^{2+}, Cl^-, CH_3COO^-, SO_3^{2-}, F^-, SO_4^{2-}	10^2
NH_4^+, $C_2O_4^{2-}$, J^-, Mo^{6+}, V^{5+}	10
Ca^{2+}, Ba^{2+}, Ni^{2+}, W^{6+}	1
Fe^{2+}, Fe^{3+}, Mn^{2+}, Zn^{2+}, Co^{2+}, Al^{3+}	0.1

Applicability of the proposed method. The proposed method was applied to the determination of bromacil in water and soil samples using the direct calibration curve. They were treated as described in the Experimental section. As can be seen in Table 4 the results obtained for this method are in accordance with the official HPLC method.

Table 4. Determination of bromacil in water and soil samples by kinetic and HPLC method

Sample	Taken (μg/cm³)	Found by proposed method[a] $\bar{x}$ ± SD (μg/cm³)	RSD [a] (%)	$((\bar{x}-\mu)/\mu)\times100$ (%)[a]	Recovery[a] (%)	HPLC[a] $\bar{x}$ ± SD (μg/cm³)	Recovery[a] (%)	F value[b]	*t* value[b]
Soil Knez Selo village	8.50	8.16±0.02	1.87	4.00	95.00	8.18±0.01	96.00	1.167	0.255
Soil Grdelica village	11.20	10.81±0.02	0.46	3.57	96.00	10.86±0.01	97.00	1.96	0.30
Soil Nis town	10.80	10.26±0.02	0.80	5.20	95.00	10.28±0.02	95.10	1.19	1.5
Tap water	11.20	11.65±0.02	0.46	4.91	95.00	10.87±0.01	97.00	1.08	1.19
Ground water	8.50	8.04±0.01	0.72	5.41	94.00	8.28±0.01	97.40	1.81	1.12
River water	10.40	9.83±0.01	1.21	5.44	94.55	9.82±0.02	94.00	3.24	0.11

[a] Data are based on the average obtained from 5 determinations; [b] theoretical *F*-value (ν_1=4, ν_2=4) and *t*-value (ν=8) at 95% confidence level are 6.39 and 2.306, respectively.

Figure 7 shows the chromatogram for a bromacil determination in spiked water (A) and soil sample (B) for its concentration of 11.2 μg/cm^3 under the optimum conditions (acetonitrile–water, 40:60, v/v at a flow rate of 1 ml/min, and wavelength of 280 nm). Detection at constant wavelength of 280 nm gave satisfactory results for the sensitivity of all spiked samples. The results of the proposed method were statistically compared with those of the parallel methods using a point hypothesis test[37,38]. Therefore, the proposed method could be used for determination of bromacil in water and soil samples after extraction. Table 4 show that the *F* and *t* values at 95% confidence level are less than the theoretical ones, confirming no significant differences between the performance of the proposed and parallel method. Both recovery percentages and relative standard deviations (RSD) were satisfactory and indicated good performance of the proposed method for the analysis of bromacil in water and soil samples.

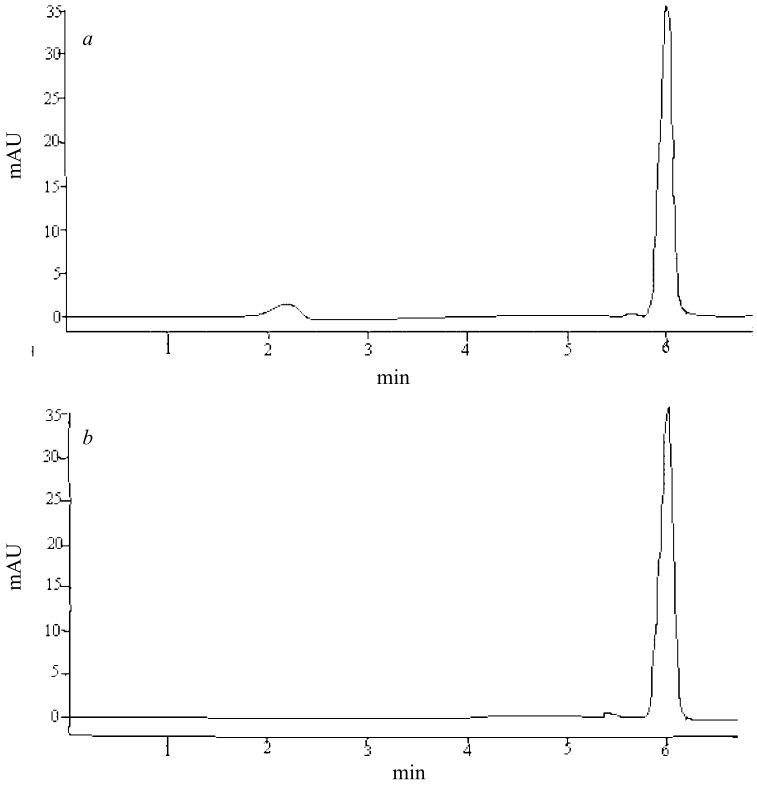

Fig. 7. HPLC chromatograms of spiked water sample with 11.20 μg ml^{-1} bromacil (*a*) and spiked soil sample with 11.20 μg/cm^3 bromacil (*b*). Column C18 (Zorbax, 5 μm, 250 mm × 4.6 mm); mobile phase: acetonitrile-water, 40:60 (v/v); detection: spectrophotometer at 280 nm

CONCLUSIONS

The proposed kinetic-spectrophotometric method for determination of bromacil in water and soil samples reported in this paper is simple, rapid, inexpensive and thus is very appropriate for routine quality control analysis of herbicide bromacil in the real samples. The procedure is easier to execute and requires less sample handling than methods currently described in the literature. Statistical comparison of the results with HPLC method showed good agreement and indicates no significant difference in accuracy and precision. Reliable recovery data were found at various concentrations, after spiking water and soil, and good limits of quantification were attained.

ACKNOWLEDGEMENT

This research was supported by grant number 142015 from the Serbian Ministry of Science. The authors are grateful for the financial support provided by this Ministry.

REFERENCES

1. D. J. ECOBICHON, C. D. KLAASSEN: Casarett and Doull's Toxicology – The Basic Science of Poisons. Mc Graw-Hill, New York, 1996, p. 643.
2. G. D. CLAYTON, F. E. CLAYTON: Patty's Industrial Hygiene and Toxicology. John Wiley and Sons, New York, 1981.
3. T. KUMAZAWA, O. SUZUKI: Separation Methods for Amino Group-possessing Pesticides in Biological Samples. J. Chromatogr. B, **747**, 241 (2000).
4. D. GÓMEZ de BARREDA, Jr., M. GAMÓN VILA, E. LORENZO RUEDA, A. SAEZ OLMO, D. GÓMEZ de BARREDA, J. GARCIA de la CUADRA, A. TEN, C. PERIS: Dissipation of Some Citrus Selective Residual Herbicides in Irrigation Well. J. Chromatogr. A, **795**, 125 (1998).
5. A. SANNINO, M. BANDINI, L. BOLZONI: Determination of Pyrethroid Pesticide Residues in Processed Fruits and Vegetables by Gas Chromatography with Electron Capture and Mass Spectrometric Detection. J. AOAC Int., **86**, 101 (2003).
6. H. S. DOREA, L. L. SOBRINHO: Analysis of Pesticide Residues in Rice Using Matrix Silid-phase Dispersion (MSPD). J. Braz. Chem. Soc., **15**, 690 (2004).
7. S. CHEN, L. SHI, Z. SHAN, Q. HU: Determination of Organochlorine Pesticide Residues in Rice and Human and Fish Fat by Simplified Two-dimensional Gas Chromatography. Food Chem., **104**, 1315 (2007).
8. H. G. BOLLES, H. E. DIXON-WHITE, R. K. PETERSON, J. R. TOMERLIN, E. W. DAY, G. R. OLIVER: U. S. Market Basket Study to Determine Residues of the Insecticide Chlorpyrifos. J. Agric. Food Chem., **47**, 1817 (1999).
9. T. D. NGUYEN, B. S. LEE, B. R. LEE, D. M. LEE, G. H. LEE: A Multiresidue Method for the Determination of 109 Pesticides in Rice Using the Quick Easy Cheap Effective Rugged and Safe (QuEChERS) Sample Preparation Method and Gas Chromatography/Mass Spectrometry with Temperature Control and Vacuum Concentration. Rapid Commun. Mass Spectrom., **21**, 3115 (2007).
10. L. PENGYAN, L. QUINGXUE, M. YUSONG, L. JINWEI, J. XUAN: Analysis of Pesticide Multiresidues in Rice by Gas Chromatography-Mass Spectrometry Coupled with Solid Phase Extraction. Chin. J. Chromatogr., **24**, 228 (2006).
11. L. LIBIN, Y. HASHI, Q. YAPING, Z. HAIXIA, L. JINMING: Rapid Analysis of Multiresidual Pesticides in Agricultural Products by Gas Chromatography-Mass Spectrometry. Chin. J. Anal. Chem., **34**, 783 (2006).

12. L. B. LIU, Y. HASHI, Y. P. QIN, H. X. ZHOU, J. M. LIN: Development of Automated Online Gel Permeation Chromatography-Gas Chromatograph Mass Spectrometry for Measuring Multiresidual Pesticides in Agricultural Products. J. Chromatogr. B, **845**, 61 (2007).
13. C. FERRER, M. J. GÓMEZ, J. F. GARCÍA-REYES, I. FERRER, E. M. THURMAN, A. R. FERNÁNDEZ-ALBA: Determination of Pesticide Residues in Olives and Olive Oil by Matrix Solid-phase Dispersion Followed by Gas Chromatography/Mass Spectrometry and Liquid Chromatography/Tandem Mass Spectrometry. J. Chromatogr. A, **1069**, 183 (2005).
14. E. G. AMVRAZI, T. A. ALBANIS: Multiresidue Method for Determination of 35 Pesticides in Virgin Olive Oil by Using Liquid-Liquid Extraction Techniques Coupled with Solid-phase Extraction Clean up and Gas Chromatography with Nitrogen Phosphorus Detection and Electron Capture Detection. J. Agric. Food Chem., **54**, 9642 (2006).
15. J. HAJSLOVA, J. ZROSTLIKOVA: Matrix Effects in (Ultra)trace Analysis of Pesticide Residues in Food and Biotic Matrices. J. Chromatogr. A, **1000**, 181 (2003).
16. G. ALAVI, M. SANDA, B. LOO, R. E. GREEN, C. RAY: Movement of Bromacil in a Hawaii Soil under Pineapple Cultivation – A Field Study. Chemosphere, **72**, 45 (2008).
17. T. D. NGUYEN, E. M. HAN, M. S. SEO, S. R. KIM, M. Y. YUN, D. M. LEE, G. H. LEE: A Multiresidue Method for the Determination of 203 Pesticides in Rice Paddies Using Gas Chromatography/Mass Spectrometry. Anal. Chim. Acta, **619**, 67 (2008).
18. Y. LI, J. E. GEORGE, C. L. McCARTY: Online *in situ* Analysis of Selected Semi-volatile Organic Compounds in Water by Automated Microscale Solid-phase Extraction with Large-volume Injection/ Gas Chromatography/ Mass Spectrometry. J. Chromatogr. A, **1176**, 223, (2007).
19. A. A. BOYD-BOLAND, J. B. PAWLISZYN: Solid-phase Microextraction of Nitrogen-containing Herbicides. J. Chromatogr. A, **704**, 163 (1995).
20. A. A. BOYD-BOLAND, S. MAGDIC, J. B. PAWLISZYN: Simultaneous Determination of 60 Pesticides in Water Using Solid-phase Microextraction and Gas Chromatography-Mass Spectrometry. Analyst, **121**, 929 (1996).
21. F. HERNANDEZ, J. BELTRAN, F. J. LOPEZ, J. V. GASPAR: Use of Solid-phase Microextraction for the Quantitative Determination of Herbicides in Soil and Water Samples. Anal. Chem., **72**, 2313 (2000).
22. L. J. KRUTZ, S. A. SENSEMAN, A. S. SCIUMBATO: Solid-phase Microextraction for Herbicide Determination in Environmental Samples. J. Chromatogr. A, **999**, 103 (2003).
23. Y. ZHU, Q. X. LI: Movement of Bromacil and Hexazinone in Soils of Hawaiian Pineapple Fields. Chemosphere, **49**, 669 (2002).
24. A. K. ALVA, M. SINGH: Sorption of Bromacil, Diuron, Norflurazon and Simazine at Various Horizons in Two Soils. Bull. Environm. Contam. Toxicol., **45**, 365 (1990).
25. C. D. LINDE, S. J. GEE, K. S. GOH, J. C. HSU, B. D. HAMMOCK, T. A. BARRY, D. J. WEAVER: Regulatory Application of ELISA: Compliance Monitoring of Bromacil in Soil. Bull. Environm. Contam. Toxicol., **57**, 264 (1996).
26. P. H. BENNETT, P. R. de BEER: A Rapid Quantitative Bioassay for the Determination of Biologically Available Bromacil in Soils. Pest. Science, **15**, 425 (2006).
27. I. BARANOWSKA, C. PIESZKO: Determination of Selected Herbicides and Phenols in Water and Soils by Solid-phase Extraction and High-performance Liquid Chromatography. J. Chromatogr. Sci., **38**, 210 (2000).
28. S. B. KIM, H. S. ON, D. J. KIM, W. A. JURY, Z. WANG: Determination of Bromacil Transport as a Function of Water and Carbon Content in Soils. J. Environm. Sci. Health B, **42**, 529 (2007).
29. I. BARANOWSKA, C. PIESZKO: Derivative Spectrophotometry in the Analysis of Bromacil and Metoxuron in the Presence of Simazine or Propazine and Hexazinone. Anal. Letters, **35**, 473 (2002).
30. A. A. ALEXIEV, P. R. BONTCHEV, S. GANTCHEVA: New Catalytic Reaction for Determination of Nanogram Amounts of Copper. Microchimica Acta, **66**, 487 (1976).

31. Y. Y. LURUYE: Spravochnik po Analiticheskoi Khimii. Khimia, Moscow, 1989, p. 256 (in Russian).
32. J. N. MILLER: Basic Statistical Methods for Analytical Chemistry. Part 2. Calibration and Regresion Methods. A Review. Analyst, **116**, 3 (1991).
33. J. ERMER: Validation in Pharmaceutical Analysis. Part I: An Integrated Approach. J. Pharm. Biomed. Anal., **24**, 755 (2001).
34. D. PEREZ-BENDITO, M. SILVA: Kinetic Methods in Analytical Chemistry. Ellis Horwood, Chichester, 1988, p. 251.
35. H. A. MOTTOLA: Kinetic Aspects of Analytical Chemistry. Wiley, New York, 1988, p. 40.
36. V. THOMSEN, D. SCHATZLEIN, D. MERCURO: Limits of Detection in Spectroscopy. Spectroscopy, **18**, 112 (2003).
37. C. HARTMANN, J. SMEYERS-VERBEKE, W. PENNINCKX, Y. V. HEYDEN, P. VANKEERBERGHEN, D. L. MASSART: Reappraisal of Hypotesis Testing for Method Validation: Detection of Systematic Error by Comparing the Means of Two Methods or of Two Laboratories. Anal. Chem., **67**, 4491 (1995).
38. D. A. SKOOG, D. M. WEST, F. J. HOLLER: Fundamentals of Analytical Chemistry. Saunders College Publishing, Philadelphia, 1996, p. 51.

Received 17 April 2009
Revised 23 July 2009

POLYMERISATION OF VINYLACETATE TO DEEP CONVERSIONS. STUDY OF THE OBTAINED POLYMERIC PRODUCTS AND THEIR TRANSFORMATIONS

R. V. YEGHOYAN, N. M. BEYLERIAN*, A. G. KHOROZIAN

Yerevan State University, 1 A. Manoogian Street, 0049 Yerevan, Armenia
E-mail: *norbey@ysu.am*

ABSTRACT

To avoid technical complications polymerisation of vinylacetate (VAc) is being carried out either in methanol solutions or in aqueous dispersions. The medium choice depends on the aims for which polyvinylacetate (PVAc) is being synthesised. This approach is convenient especially in those cases when the obtained PVAc is an intermediate, e.g. to transform it in polyvinylalcohol (PVAl).

It is obvious that the quality of obtained products to a great extent depends on the reaction medium characteristics.

An attempt was done to carry out VAc polymerisation in methanol–water solutions maintaining the medium homogeneity. This approach allows to use water-soluble initiators as well as water soluble-redox initiating systems. The advantages of this approach are discussed

Keywords: vinylacetate polymerisation, polyvinylalcohol, water–methanol solutions.

AIMS AND BACKGROUND

Vinylacetate bulk polymerisation is not being used for industrial purposes because of some important technical complications, for example, heat removal, prevention of the Trommsdorf effect, branching of the formed polymer, etc.

Those undesirable phenomena may be removed carrying out the polymerisation in the presence of dilutants, e.g. in solutions or emulsions. In the case of VAc polymerisation methanol solutions and aqueous dispersions are being used[1].

In some cases the desired products are, for example, PVAl, polyvinylbutyral, which are results of the initial PVAc transformations. The methanol solutions are convenient to realise such transformations[1].

* For correspondence.

It is well known that changing definite characteristics of the medium it is possible to govern, on the one hand, the polymerisation rate (R_p), and on the other, the properties of the obtained polymer.

Our studies showed that carrying out the VAc polymerisation in methanol–water mixtures it is possible to enhance the R_p using water-soluble initiating systems at ambient temperatures and to obtain PVAc with very improved characteristics. It must be noted that the quantity of added water does not alter the medium homogeneity. Kinetic data are discussed in Refs 2–8.

EXPERIMENTAL

R_p was determined by dilatometry. The polymer yield was determined gravimetrically. Mean molecular masses $\bar{M}_\eta$ were determined using viscosimetry $[\eta] = 1.88 \times 10^{-4}\ M^{0.69}$ for PVAc in acetone at 218 K and $[\eta] = 6.66 \times 10^{-4}\ M^{0.64}$ for PVAl in water at 303 K. The mean number MM $\bar{M}_n$ was determined by osmometry and the mean mass MM $\bar{M}_w$ – by light-scattering method. $\bar{P}$ is the mean polymerisation degree.

The methanolysis of the obtained PVAc samples was carried out in the presence of added NaOH (Ref. 1).

The branching degree of polymers chains was determined by the following formulae:

$$\varphi = \frac{\bar{P}_{in}^{PVAc} - \bar{P}_{reac}^{PVAc}}{\bar{P}_{in}^{PVAc}} \qquad (1)$$

where φ shows the mean quantity of branchings per one macromolecule; $\bar{P}_{reac}^{PVAc}$ – the mean polymerisation degree concerning the PVAc molecule after re-acetylation of the PVAl molecule (PVAl → PVAc) – the product of PVAc hydrolysis.

RESULTS AND DISCUSSION

Different initiating systems are used to realise VAc polymerisation in the presence of water with different concentrations. As standard initiator AIBN is chosen. In Table 1 some data are shown.

Table 1. Polymer yield dependence on water content in water–methanol mixtures

$[H_2O]$ (mass.%)	Polymerisation time (h)	Polymer yield (%)	$\bar{M}_\eta \times 10^{-5}$
0	8	94.0	1.17
16.4	6	98.0	1.36
18.0	6	98.0	1.54
23.0	4	99.8	3.44

As it was mentioned the use of CH_3OH+H_2O mixture allowed to use water-soluble initiators. AIBN was substituted by potassium persulphate (PP), triethanolamine

(TEA). For comparison benzoylperoxide (BP) has been used as initiator. Some data are summarised in Table 2.

Table 2. Dependence of polymer yield and mean molecular mass on the initiator nature (PP and BP) in the presence of TEA

[VA] (M)	Concentration of initiators × 10^3 (M)		[CH_3OH] (M)	[H_2O] (M)	T (K)	Polymer yield (%)	$\bar{M}_\eta \times 10^{-5}$
	PP	TEA					
6.0	5.0	2.0	8.2	3.9	313	94	1.54
4.7	7.5	5	8.1	3.3	323	100	1.60
5.3	[BP]=7.5	5	9.2	3.0	323	83	1.40

From the data in Table 2 it follows that the system PP+TEA is more preferable.

It is shown[9] that the methanolysis of the obtained PVAc may be performed in the same reaction vessel. In this case the initiators remain in the reaction medium. To prevent their undesirable action adding of some inhibitors to the reaction mixture could be proposed. The positive action of TEMPO has been established.

Considering the above cited data for the water action on the obtained PVAc and P on the corresponding PVAl samples, some characteristics have been studied mainly their dependence on the conversion degree is determined[10].

Table 3. Dependence of mean molecular mass of PVAc and PVAl as well CH_3CHOO content in re-acetylated PVAl on the water content and on monomer conversion degree

[H_2O] (%)	Conversion degree (%)	PVAc				PVAl		CH_3COO groups (mass.%)
		[η] (dl/g)	10^{-5}			[η] (dl/g)	$\bar{M}_\eta \times 10^{-4}$	
			$\bar{M}_\eta$	$\bar{M}_n$	$\bar{M}_w$			
0	68.9	0.61	1.23	1.88	3.30	0.53	3.41	3.9
10	65.5	1.15	3.07	2.80	4.15	0.78	6.20	3.7
15	90.0	1.12	2.96	2.88	3.61	0.85	7.13	3.7
20	73.5	1.08	2.80	2.46	4.96	0.90	7.79	2.3

These PVAl samples have undergone acetylation to obtain the corresponding polyvinyl butyral (BuT). The properties of the synthesised BuT also depend on the [H_2O] in the reaction medium.

Table 4. Dependence of [η], φ and P_{sh} of the obtained BuT samples on the water content

[H_2O] (%)		0	10	15	20	Butvel
BuT	[η] (dl/g)	1.20	1.56	1.79	1.8	1.6
	φ	43.3	43.3	45.3	41.1	43.6
	P_{sh}	1.75	1.48	1.24	2.01	

Note: Butvel was a sample of butyral produced in Japan.

The water concentration acts, of course, on the obtained polymer characteristics. But when the added water results in formation of a heterogeneous system its action becomes considerable. For example, it acts on the Schulz parameters: $\bar{M}_w/\bar{M}_n \equiv P_{sh}$ on which depends MM distribution.

The water is a 'bad' solvent for PVAc. So it can act on the macroradicals conformation. The diffusion of monomers into macromolecules balls can be impeded. Apart the H-bond formation between growing macromolecules and HOH molecules can not be excluded which results in decrease of macroradical reactivity. It is interesting to note that even in the case when high-molecular PVAc is being formed at high degree of conversion there is no autoacceleration due to the Trommsdorf effect and MM get enhanced because the medium becomes very viscous.

Table 5. Dependence of [η] of PVAc on the monomer conversion degree and water content in methanol–water mixtures

Conversion (%)	2.2	18	24	38.5	47	55	63	87	In the presence of
[η] (dl/g)	0.71	0.69	0.73	0.76	0.74	0.67	0.73	0.67	CH_3OH
Conversion (%)	5.9	13	20	27	37	46	81	99	
[η] (dl/g)	1.01	1.02	1.07	0.97	1.06	1.03	0.93	1.01	CH_3OH+H_2O

It is interesting to discuss the dependence of some molecular characteristics of the formed polymer molecules on water contents in the reaction medium as well as on the degree of polymerisation conversion.

Table 6. PVAc branching degree dependence on the degree of monomer conversion in methanol and methanol–water mixtures

Polymerisation medium	CH_3OH				CH_3OH+H_2O	
Conversion (%)	38.5	47	63	87	46	99
$\bar{P}_{in}$ PVAc	1960	1895	1850	1460	3050	2960
$\bar{P}_{reac}$ PVAc	1135	1130	1140	885	1840	1770
φ	0.42	0.40	0.38	0.39	0.39	0.40

The MM distribution is an important characteristic of the obtained polymers. It depends on kinetic parameters and predetermines their practical significance.

The study of the MM distributions of the obtained PVAc and PVAl showed that they also depend on water content in the reaction medium. In water presence the obtained polymers are more monodispersed; the MM distribution curves are narrow.

CONCLUSIONS

It is shown that adding water to VAc methanol solution favours the use of water-soluble initiators, particularly the persulphate + triethanolamine system which allows to decrease the process temperature. On the other hand, the water acts on the kinetic

parameters on which the process rate depends, the mean molecular mass of the formed polymer. In the presence of water the formed PVAc as well as its hydrolysis product PVAl are more high-molecular and less branched. The quality of polyvinylbutyral, obtained on the basis of the corresponding PVAl, is better in comparison with the sample of polyvinylbutyral using PVAl obtained on the basis of PVAc synthesised in the absence of water. The polymers obtained in the presence of water are monodispersed. It is worthy to note that water is ecologically pure matter and quite accessible.

REFERENCES

1. M. E. ROZENBERG: Polymers on the Basis of Vinylacetate. Khimia, Leningrad, 1983
2. N. M. BEYLERIAN, R. V. YEGHOYAN, G. A. MARMARYAN: Vinylacetate Polymerization in Methanol and Water–Methanol Homogeneous Solutions. Arm. Chem. J., **26**, 442 (1973).
3. N. M. BEYLERIAN, R. V. YEGHOYAN, L. B. KNYAZIAN: Kinetics of Vinylacetate Polymerization in Methanol and Water–Methanol Solutions in Presence of Triethanol Amine. Arm. Chem. J., **26**, 985 (1973).
4. R. V. YEGHOYAN, N. M. BEYLERIAN, S. S. POSTOLAKIAN, G. A. MARMARIAN: Some Regularities of Vinylacetate Polymerization in Aqueous Methanol Homogenous Solutions. Arm. Chem. J., **27**, 369 (1974).
5. R. V. YEGHOYAN, N. M. BEYLERIAN, P. V. ARAMIAN, S. A. FARADIAN, V. H. DANIELIAN: On the Influence of Water on Kinetics and Rate Constants of the Elementary Steps of Vinylacetate Polymerization in Different Solutions. Arm. Chem. J., **28**, 88 (1975).
6. R. V. YEGHOYAN, N. M. BEYLERIAN, L. S. GEVORKIAN: The Influence of Medium Viscosity on the Radical Polymerization of Vinylacetate. Arm. Chem. J., 30, 555 (1977).
7. R. V. YEGHOYAN, V. V. GRIGORYAN, L. Kh. SIMONIAN: About the Mechanism of Water Influence on the Elementary Steps of Vinylacetate Radical Polymerization in Methanol. Vysokomol. Soed., **30B** (1), 8 (1988).
8. R. V. YEGHOYAN: The Water Action on Kinetics of Homo- and Copolymerization of Some Vinylic Monomers Carried out in Organic Solvents and on Physicochemical Properties of Obtained Polymers. Ph. D. Thesis, Yerevan, 1998.
9. R. V. YEGHOYAN, N. M. BEYLERIAN, G. A. MARMARIAN, L. S. GEVORKIAN: Saponification of Polyvinylacetate without Isolation of the Polymer at Vinylacetate Polymerization in Presence of Water. Arm. Chem. J., **30** (7), 559 (1977).
10. A. G. KHOROZIAN, R. V. YEGHOYAN, G. E. SAFARIAN, V. H. DANIELIAN, N. M. BEYLERIAN: Polymer Analogous Transformations of Polyvinylacetate Obtained in Water–Methanol Mixtures at High Degrees of Monomer Conversion. Arm. Chem. J., **44** (9–10), 570 (1991).

Received 17 June 2008
Revised 1 August 2008

TENDENCIES IN THE SCOPE AND STRUCTURE OF THE CONTROLLING PROCESSES RELATED TO THE USE OF MOTOR FUELS

ST. PETKOVA, Y. TASHEVA*, P. PETKOV

University 'Prof. Dr. Asen Zlatarov', Bourgas, Bulgaria
E-mail: *jtasheva_2006@abv.bg*

ABSTRACT

The development of world economy is closely related with the high rate of consumption of primary energy sources (PES). Under the present conditions of growth, the fuels produced from petroleum are of major importance. Statistic data show for the period from 1900 to 1980 that the total energy consumption has increased 10 times but for petroleum-based fuels the increase is 150 times. After that, the share of petroleum in the development of world energy industry was gradually increasing to reach 74% in 2007. This process was accompanied by new tendencies in the scope and structure of the controlling processes related to the use of motor fuels.

Keywords: controlling, motor fuels, energy sources.

AIMS AND BACKGROUND

The aim of the present paper is to show the current tendencies in the scope and structure of the controlling processes related to the use of motor fuels.

The market globalisation, search for solutions to minimise expenses, competition dynamics and other factors lead to higher requirements towards the management in the petroleum-based energy industry. They can be satisfied by regular use of operative controlling instrumentation. The intense growth of the role of petroleum for securing the energy and other needs of the world economy is affected by a number of factors. The most important one is the unique physicochemical properties of petroleum, compared to the other known sources, which allow complex utilisation of all the products obtained from its processing.

In this respect, the main share is held by the different kinds of motor fuels and fuel oils, 89% of which are produced from petroleum[1,2]. Another part of petroleum (about 6%) is used as raw material for chemical and petrochemical industries. About 5% of world production of petroleum derivatives are used for to produce lubricants, bitumen, electrode coke, etc.[3]

* For correspondence.

The increasing use of petroleum is stimulated by the enhanced capability of petroleum geology, exploration of fields, improved methods of drilling and technologies for extraction. This provided possibilities to reduce the costs for extraction and transportation of petroleum from many hardly accessible regions of the world. As a result, industrial exploitation has been started in large petroleum basins in the Middle East, Africa, Latin America, USA and Russia.

The high volume-mass concentration of heat energy in petroleum-based fuels and the combination with the scientific and technological progress in the pipeline, railroad, sea and river transportation provided possibilities to reduce the transportation costs compared to the other PES. Thus, petroleum can be transported comparatively easy at distances of thousands of kilometers from the remote regions of extraction. Calculations performed showed that the transfer of equivalent quantities of energy at certain distance, the transportation of petroleum through pipelines is 4 to 6 times cheaper than the transportation of natural gas. Under the same conditions but with sea transport, petroleum transportation is 7 times cheaper. The data published showed that the cost of transportation of petroleum from the Persian Gulf to Japan is 6.2 USD/t while for liquefied gas accompanying petroleum (propane-butane) it is 28.5 USD/t and for pressurised natural gas (using methane carriers) it is 44 USD/t (in petroleum equivalent)[3].

DISCUSSION

An important advantage for the reasonable utilisation of petroleum is the development of the technological processes and the schemes for deep refining of petroleum and the corresponding modern controlling. Proper implementation of the operative instrumentation controlling given in Table 1 presents excellent economic results[2,4].

Table 1. Operative instruments of controlling processes

1.	Activity-based costing (ABC)
2.	Analysis of the order fulfillment criteria
3.	Optimisation of orders
4.	Analysis of the profit limit
5.	Calculation of prime costs
6.	Analysis of problematic production units
7.	Intra-production rationalisation
8.	Calculation of investment profitability
9.	System for operation accounting
10.	Optimisation of the quantities of individual batches
11.	Motivating commission system for achieved productivity
12.	Effective total quality management (TQM)
13.	System for analysis of the prime costs reduction
14.	System for analysis of the return of investment (ROI)
15.	Marketing analysis of sales
16.	Function cost analysis
17.	XYZ-analysis

For successful implementation of controlling processes, the management of petroleum energy industry should know and master the individual controlling instruments. This allows for rapid reaction to the requirements of petroleum fuels market. Usually, these requirements involve changes in volume, range of products and their quality which lead to changes in transportation infrastructure for better servicing the consumers.

The main factor affecting the use of petroleum is its price. The low prices formed in the period 1950–1973 were based on petroleum produced in the Middle East. Statistical data shows that, in the beginning of this period, petroleum prices were 98% of coal prices do decrease to 55% at the end of the period[3]. In the following years until 1981, the increasing prices and some political factors caused certain decrease of the demand for petroleum on world markets. This tendency lasted till 1985 and affected mainly the former socialist and developing countries[5]. After that, the growth of petroleum consumption as main energy source was the main reason the incessantly increasing petroleum prices which exceeded 100 USD/barrel in 2008. The price of the black gold exceeded the psychological limit of 100 USD/barrel in February when the prices reached 100.1 USD/barrel. A record was reached on March 3, 2008 when the prices at the New York Merchantile Exchange (NYMEX) reached 103.51 USD/barrel while at London International Petroleum Exchange (IPE) it was 100.1 USD/barrel. The dynamics and structure of petroleum usage in basic economic segments like transportation, power generation, domestic services and retail trade vary in the different countries. They are determined basically by the state of their economic development, availability of their own energy sources, social-economic conditions, etc. The surveys carried out showed that the energy generated from petroleum in the developed countries was about 50% of the total energy production and covered 99% of the needs of transportation industry, 39 for domestic services and about 17% – for electric power generation[6]. The increased petroleum prices is the main reason urging the governments to implement policies for reduction of its use in all industries and mainly in the extraction, refining and application of the different petroleum derivatives. A general tendency in the structure of petroleum usage, which gradually covered the world energy network, is the decrease of the use of petroleum for production of fuel oils and redirection of higher amounts to secondary processes giving motor fuels. Increasing amounts are now used as raw material for petrochemical synthesis to obtain a number of valuable products of wide practical application[5].

The tendencies in the volume and structure of the controlling processes implemented in the production of motor fuels are related mainly to the expansion of transportation, industrial and agricultural activities where motor driven machines are widely used. The investigations showed that the total power of automobile engines in the world doubled at the beginning of the 21st century compared to the 90's. Thus, for just 10 years, it exceeded 10 times the power of the power of all the electricity generating stations in the world[7]. The statistical data show that the implementation of controlling processes in Russia only gave increase of motor power over electricity-

generating stations more than 7 times while for USA it is 12 times. As can be seen, the problems related to the provision of enough motor fuels for the economy are quite complex and involve many branches of industry. The structure and production of technical means using motor fuels is a complex function of the needs of country structures for versatile transportation vehicles. They can be classified as cargo and passenger ones, which are further divided into automobile, railroad, water and air transport or, according to the industrial branch, into agricultural, industrial, construction, etc. On the other hand, all this forms the corresponding structure of technical means according to their usage: transportation – automobiles, air, sea and river facilities, locomotives; agriculture and industry – tractors, harvesters, elevating machines and mechanisms, generators, road construction machines, etc. Depending on construction and the fuel used, the engines mounted in the different machines need benzenes, diesel and fuel oils. For this reason, a calculation of the amounts of the necessary fuels should be approached by taking into account their quality, type, etc. The quality characteristics of these fuels depend mainly on the conditions under which the engine works, including climate characteristics and the loads on the engines. In spite of the increase of the quantities of motor fuels, an attempt for reduction of the use of petroleum-based fuels can be successful if the combustion characteristics of the engines are improved. In this respect, the designers seek to reduce fuel consumption at preserved power of the facility, reduce their weight and improve the aerodynamic characteristics. In turn, the performance characteristics of the engines and their energy efficiency depend on the technical level of machine-building and motor-construction industries. The industries related to the production of construction materials and parts made of them also exert their influence.

Of all the measures aimed at reduction of fuel consumption described, an important role plays the implementation of controlling instrumentation in the organisation which has to be created for the operation of the technical means involved. In this respect, the cargo and passenger transportation should be optimised, high coefficient of loading should be sought, reduction of empty vehicle travelling to an acceptable minimum, rationalise the operations in individual production lines, etc. This inter-relationship between the operation conditions of heat aggregates, their low consumption of high-quality fuels would finally reflect on the operation costs of the aggregates. The structure, volume and quality of the motor fuels used determine the main requirements to the scale and technological commitment of their production. Further, this would determine the development of the transportation infrastructure connected with the distribution of the petroleum containing facilities, specialised vehicles for transportation of various fuels by railroad, sea or route, as well as the location of pipelines in country territory. Of course, each country has specific features related to its own needs for certain volume and structure of the fuels used and their quality which affects the development of the motor construction and oil refining industries. The ensuring of the enough fuels for the motor driven machines in a country is itself a complex task. Enormous investment of capital and human resources is necessary for the exploration,

extraction, production, and transportation and refining of petroleum, as well as building a distribution system for the dissemination of the consumer products. Investigations showed that major part of these investments is in the processes connected with the production and refining of petroleum to consumer products. According to the data of the International Bank for Development and Reconstruction (IBRD), the developing countries had invested about 460 bln USD in the period from 1985 to 1995 to satisfy the increasing demand on petroleum production and until 2005 – 720 bln USD. In the USA, about 24 bln USD were invested in 1985 for exploration and development of petroleum fields while in 2005 – 57 bln USD. For the same periods, the investments in petroleum refining industries were 1.5 and 17 bln USD, respectively, and more than half of them were devoted to motor fuels. In the developed countries, about 84% of the total investments in petroleum refining are made for production of motor fuels. Surveys showed that one of every 6 employees in the USA is directly or indirectly connected with the automotive industry and transportation[8]. At the same time, the statistical data reveal that, of the total consumption of motor fuels, 15% are used by aviation, 4% by railroad transport, 27% by shipping industry and the rest remains for road transport. In the European countries, about 85% of the total consumption are effected by road transport, 11% by aviation and the rest – by railroad and shipping. In Japan, the major part is also used for road transportation – 77%, the share of aviation is 7%, shipping – 10% and railroad – 4%. The road transport in Russia consumes about 72% of all the motor fuels produced. Therefore, it can be firmly stated that on world scale, the road transport industry is the main consumer of motor fuels and its development accompanied by proper controlling instrumentation exerts decisive effect on the general tendencies in the volume and structure of the production and consumption of the different types of motor fuels. For this reason, the economically developed countries put strong emphasise on the research and development work on the reduction of fuel consumption in combustion engines mounted in vehicles. The following main directions formed: increase of the effective efficiency coefficient of engines and gears, reduction of the total weight of vehicles, electronic control of engine operation, reduction of aerodynamic resistance of the design, reduction of the hydraulic resistances in the engine itself. All this is very closely related to the successful implementation of controlling instrumentation, as well as with the qualification of the personnel operating the vehicles, quality of the roads and the optimisation of the processes connected with the organisation and operation of transportation companies.

The measures taken in the different countries with respect to the most up-to-date achievements in the automotive industry controlling combined with deliberate changes in legislation related to the efficient use of petroleum-based fuels gave significant results. As can be seen from statistical data, the average consumption per car in the USA has fallen from 14.2 to 6.4 l/100 km for the period 1975–2005. This decrease is due mainly to the use of lighter materials in designs and improvements in the combustion process in the engines[9,10]. It has been established that the decreased consumption was effected by the following factors: about 30% – reduction of size and weight of

automobiles, about 20% – use of lighter construction materials in the design, about 15% – improved economic characteristics of combustion engines, 10% – improved aerodynamic properties of the vehicles, 10% – improved gearing and the remaining 15% – other organisational measures related to reasonable utilisation of the vehicles. As can be seen, the most important factor affecting fuel consumption of automotive industry is the reduction of the total weight of the vehicle. It is well known that each 100 kg of weight reduction practically gives 6–7% less fuel consumption. For this reason, many car manufacturers started production of front-wheel driven cars with reduced weight. According to the data for 2006, about 78% of the vehicles produced were front-wheel driven[11].

The design of new fuel delivery systems in the engines reduced benzene consumption by 15–20% and in diesel engines – by 25–30%. This accelerated the tendency of large scale shift to diesel engines in automotive industry. The only disadvantage here is the twice higher price of diesel engines and sophisticated technical servicing. Nevertheless, diesel driven vehicles increase their share, especially for trucks and trailers. Statistical data show that the world production of diesel engines increased by 9 bln USD per year for the period 1990–2000. About 24% of the total number of engines produced is used in cars, 42% – in trucks and the rest are used in agriculture, railroads and power generation. In 2005, the number of diesel engine cars reached total number of 35 mln. Diesel engines are preferred for trucks and trailers of medium and high power[12,13]. In this respect, the diesel fuel consumption on world scale increased – in USA only it increased from 100 mln t in 1990 to 137 mln t in 2000. This amount of diesel fuel was spread among the consumers as follows: 65% for trucks, 16% for cars, 12% for agriculture, and the rest – for other types of consumers[14]. This was considered enough to suppose that, despite the pursuit to design and produce less consuming diesel engines, the world scale diesel fuel consumption will increase due to the incessant increase of their number. The annual increase of this number was established to be 10 mln vehicles. Therefore, taking the total number of diesel driven vehicles in the world to be 520 mln, in 2010 they will be 570 mln. This rapid growth will inevitably give increased consumption of motor fuels. These changes will affect also the share of world scale petroleum consumption. In this respect, the predictions of Data Resources Co. are interesting so far as the actual state and expected development of energy industry in Europe for the period 1985–2015 is concerned[15]. It states that the needs of transportation for energy gradually increased by 1.7% annually from 1985 to 1990. The rise of petroleum prices slowed the rate of this growth in 2000 to 0.9% and in 2007 – to 0.7%. The growth of needs is expected to remain almost constant at 0.7% until 2025 and then the alternative energy sources will rapidly increase their share. It would satisfy the needs for energy and will push the development of transportation. The use of gasoline by vehicles was almost unchanged from 1985 to 1995 – about 630–650 mln t per year. Then it gradually fell to 600 mln t until 2005 despite the increase of the total number of vehicles from 340 to 520 mln for the same

period. A characteristic of this period is that the demand for lead-containing gasoline fell to almost zero at the expense of high-octane number lead-less fuels.

The fuel consumption of diesel driven vehicles also fell due to the measures taken in a number of countries. The data published show that until the end of the 1980's, the annual increase of diesel fuel consumption was about 3%, and then it began to fall by 1.7% annually until 1995 by to reach 1% in 2005. The expenses for fuel oils in power generation, commercial and domestic sectors also gradually decreased. Nevertheless, the demand for petroleum increased due to the increasing number of motor fuel consumers and its use in the developing petrochemical industry. For these reasons, a tendency of general increase of the total needs for petroleum-based fuels can be observed.

For the period until 2005, the volume and structure of the consumption of petroleum-based products show that the total consumption of petroleum middle distillates (kerosene, jet and diesel fuels) increased by 36% at generally stable structure of gasoline consumption of 29% of the total consumption of petroleum derivatives (including the wide low-octane fraction used by petrochemical synthesis). The general structure of the consumption of petroleum derivatives and its development in the period from 1985 to 2005 is given in Table 2 (mln t).

Table 2. General structure petroleum-derived consumption in the period 1895–2005

Product (mln t/year)	1985	1995	2005
Gasoline	649.5	628.1	730.7
Wide gasoline fraction	156.7	270.0	303.4
Kerosene	105.6	131.9	156.8
Diesel fuel	694.7	837.6	1098.7
Fuel oil	715.6	749.9	795.4
Other derivates	432.4	399.3	374.5

The general tendency which can be distinguished here is the change of the structure of motor fuel consumption with the highest increase observed is for middle distillate fuels and this is accompanied by the implementation of controlling instrumentation for process management. It should be noted that not all the quantities of diesel fuel and kerosene produced are used for transportation purposes. Significant portion of them is used as domestic fuel for generation of heat and energy. For instance, about one half of the diesel fuel produced in USA and Japan is used for transportation. In the European countries, about 2/3 of the middle distillate fuels are used for heating. In Japan, only 7 mln t of the kerosene produced in 2004 were used in aviation while the rest was used for domestic purposes[16]. Therefore, there are still reserves in many countries which could be used in the struggle for reduction of middle distillates consumption since major part of them are used for heating rather than for their main purpose.

Recently, the tendencies in the volume and structure of the controlling processes related to the consumption of motor fuels clearly show the dieselisation of automo-

tive transportation and significant growth of aviation services. As a result, the needs for diesel fuel and kerosene persistently grow. In the last decade only, the use of air transportation for cargo and passenger services grew by 20% compared to 1995. Nevertheless, due to the changes in the design of aircraft engines and devices and improved organisation of services, the kerosene consumption decreased by 4–5% during the same period[17].

CONCLUSIONS

1. Despite all this developments, a world tendency of growing needs for diesel and aviation fuels can be observed. Under the relatively stable quantities of refined petroleum, these increased needs can be satisfied only by shifting the refining industry towards secondary petroleum refining processes. It is necessary to improve the quality and performance characteristics of benzenes, diesel and jet fuels in order to secure the necessary amounts of them.

2. Simultaneously, the technological schemes of petroleum refining should be adapted with respect to secondary thermal and thermo-catalytic processes. Thus, additional amounts of motor fuels will be produced. At the same time, the research and development activities related to the production of alternative fuels from sources other than petroleum should continue.

REFERENCES

1. I. L. ALEXANDROV, A. A. BESCHINSKI: Global Energy Problem. Mysl Publ., Moscow, 2005, p. 217 (in Russian).
2. A. K. ANDRONOVA, E. D. PECHATNOVA: Operative Controlling, 'Delo i Servis' Publ. House, Moscow, 2006 (in Russian).
3. A. S. ASTAHOVA: World Energy Resources. Nedra, Moscow, 2004, p. 376 (in Russian).
4. J. H. VOLLMUTH: Controling-instrumente von A-Z. Gmbh&Co., Fachverlag, 1998.
5. A. A. BESCHINSKI, I. A. BASHMAKOV: Energy, Economics, Technology. Ecology, (7), 12 (2007).
6. V. I. EROHOV: Economics of Automotive Fuels. Transport Publ., Moscow, 2004, p. 301 (in Russian).
7. M. Ya. KON, V. G. SHERTUN: Oil Refining and Petrochemical Industry Abroad. Khimiya, Moscow, 2006, p. 137 (in Russian).
8. W. BEERNHARD, W. ZEE: Future Automotive Fuels, 2007, p. 211.
9. L. V. CARLEY: Motor Fuels from Alternative Sources. Mot. Serv. (USA), 2007, p. 72.
10. E. E. DAVID: A New Logistic in Biodiesel. Chem. Eng. Progr., **17**, 12 (2005).
11. P. N. DESPRAIRIES: Perspectives in Oil Transportation. Oil and Gas J., **87** (17), 107 (2003).
12. I. GIBSON: Some Approach in Controlling of Oils. Chemistry in Britain, **17** (2), 50 (2007).
13. A. M. GOLDSTEIN: Trends in Controlling Systems. Drevry Stad, (377), 6 (2005).
14. E. E. HEAVERICH: Oil and Gases – Primary Sources. 33 SAE Techn. Pap. Ser., 37 (2006).
15. L. KOSSWICZ: Economical Review for Energy Sources. Cosp. Paliw i energ., **33** (7), 47 (2006).
16. H. YAMATA: Usage of Petroleum Products in Japan. Revue de l'energie, (277), 157 (2006).
17. M. D. ROSE: Sources of Petroleum and Gas. Paip and Pap. Can., **87** (6), 70 (2007).

Received 19 October 2009
Revised 9 November 2009

EXPLORING QSAR OF 2,4-SUBSTITUTED 5-AZOLYLTHIOPYRIMIDINE ANALOGUES FOR SCREENING AGAINST ANTI-INFLUENZA VIRUS A

A. K. SRIVASTAVA, A. PANDEY*

QSAR Research Laboratory, Department of Chemistry, University of Allahabad, 211 002 Allahabad, India
E-mail: *avnipandey@rediffmail.com*

ABSTRACT

QSAR studies on the analogues of 2,4-substituted 5-azolylthiopyrimidines showing anti-influenza virus activity were performed. The anti-influenza activities of these analogues have been analysed in relation to their physicochemical properties and are found to be significantly affected by steric parameters – molecular weight (Mw), surface tension (St), density (D), parachor (Pc), information theoretic index (Id), electronic parameters – polarisability (Pz), electronegativity (χ_{eq}) and topological parameters – zero-, second- and fifth-order connectivities ($^{0}\chi$, $^{2}\chi$, $^{5}\chi$). Excellent results were obtained from multiparametric regression upon introduction of indicator parameters. It was found that the presence of 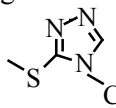 group at R_3-position was conducive for the activity, whereas the presence of methylthio group at R_2-position was detrimental for the activity. The results are critically discussed on the basis of regression data and cross-validation technique.

Keywords: QSAR, physiochemical properties, regression analysis, substituted 5-azolylthiopyrimidines analogues.

AIMS AND BACKGROUND

Pyrimidine exhibits important biological activity and is found as a core structure in a large variety of compounds[1]. The combinatorial approaches for the synthesis of this drug would help to speed up drug discovery. Recently, efficient methods have been developed to generate heterocycle library by three-component one-pot reaction[2]. The antiviral activity is associated with the presence of nitrogen heterocycle (pyrimidine derivatives)[3] or bis-heterocycle compounds[4]. This strategy would lead to explore a

* For correspondence.

convenient method in constructing novel bis-heterocycle library containing pyrimidine for antiviral screening.

These data prompted Gang Cheng and coworkers[5] to report a combinatorial synthesis of 2,4-substituted 5-azolylthiopyrimidine libraries using a sequential three-component, one-pot reaction and its anti-influenza virus activity.

The current study represents the QSAR analysis of 2,4-substituted 5-azolylthiopyrimidine analogues using a number of structural parameters with different dummy indicator parameters as predictor variables.

EXPERIMENTAL

QSAR studies were performed on the compounds listed in Table 1, where the biological activity CC_{50} is cytotoxicity which is measured as the logarithm of 50% cytotoxic concentration in the Madin-Darby Canine kidney (MDCK) cells. All the QSAR reported here were derived by us and were not reported with the original data set taken from the literature as reference. We have used the Hansch analysis[6] for developing these models.

An attempt has been made to correlate the activities of these compounds with physicochemical parameters. The molecular weight (Mw)[7], surface tension (St)[7], density (D)[7], parachor (Pc)[7], information theoretic index (Id)[7], polarisability (Pz)[7] and electronegativity (χ_{eq})[7] were calculated by ACD Lab software. The zero-, second- and fifth-order connectivities ($^0\chi$, $^2\chi$, $^5\chi$) for a set of substituted 5-azolylthiopyrimidine analogues were calculated by DRAGON software[8–23].

Indicator parameters[24] are the dummy parameters sometimes used for accounting those structural features not covered in any molecular descriptor used. The details of such parameters, used in the present study are given in the results and discussion section (Table 1).

The multi-regression analysis used to derive the correlation was executed with the SPSS (Statistical package for the social sciences), 7.5 version programme.

RESULTS AND DISCUSSION

The series of substituted 5-azolylthiopyrimidine derivatives, their inhibitory activities, physicochemical parameters and indicator parameters are reported in Table1.

Table 1. Biological activity and physicochemical data for substituted pyrimidines

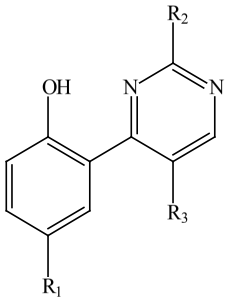

S.No	R_1	R_2	R_3	pCC_{50}	Mw	St	Pz	D	χ_{eq}	Pc	$^0\chi$	$^2\chi$	$^5\chi$	Id	I_1	I_2
1	2	3	4	5	6	7	8	9	10	11	12	13	14	15	16	17
1	H	CH_3	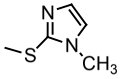	6.287	298.363	52.800	33.870	1.330	2.383	602.600	14.820	9.172	4.911	4.392	0	1
2	H	C_6H_5	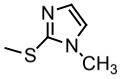	5.523	360.432	53.800	42.060	1.300	2.381	748.400	17.933	11.225	6.438	4.706	0	1
3	H	4-pyridinyl	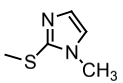	5.253	361.420	57.500	41.450	1.360	2.398	729.500	17.933	11.225	6.438	4.706	0	1
4	H	4-Cl C_6H_4	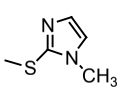	5.307	394.877	54.900	43.890	1.380	2.401	777.200	18.803	11.847	6.662	4.696	0	1
5	H	*tert*-butyl	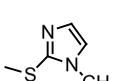	5.756	340.443	46.200	39.410	1.230	2.348	718.300	17.320	11.130	5.278	4.546	0	1
6	H	4-$NH_2C_6H_4$	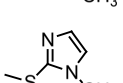	5.329	375.447	58.600	42.820	1.370	2.385	755.500	18.803	11.847	6.662	4.800	0	1

to be continued

Continuation of Table 1

1	2	3	4	5	6	7	8	9	10	11	12	13	14	15	16	17
7	H	NH_2	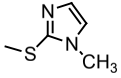	6.113	299.351	63.300	32.870	1.450	2.404	578.700	14.820	9.172	4.911	4.458	0	1
8	CH_3O	H	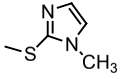	6.294	314.362	53.300	34.420	1.360	2.405	621.800	15.527	9.341	5.132	4.407	0	1
9	CH_3O	*tert*-butyl	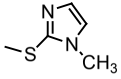	5.494	370.469	44.800	41.720	1.240	2.355	768.500	18.897	11.932	5.829	4.606	0	1
10	CH_3O	methylthio	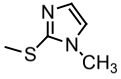	4.300	360.454	53.400	39.270	1.380	2.392	702.400	17.104	10.144	5.602	4.522	1	1
11	Cl	*tert*-butyl	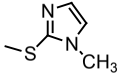	5.472	374.888	47.400	41.240	1.310	2.366	747.100	18.190	11.763	5.715	4.546	0	1
12	CH_3	*tert*-butyl	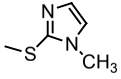	5.513	354.469	44.200	41.160	1.210	2.339	749.400	18.190	11.763	5.715	4.546	0	1
13	H	*tert*-butyl		5.655	327.404	82.800	35.420	1.380	2.374	715.400	16.449	10.612	4.986	4.546	0	0
14	H	*tert*-butyl	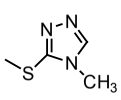	5.672	341.432	49.200	38.790	1.290	2.363	699.400	17.320	11.130	5.278	4.546	0	0
15	H	*tert*-butyl	H	4.852	228.290	44.200	26.670	1.106	2.329	531.900	12.466	7.915	3.543	4.063	0	0
16	Cl	*tert*-butyl	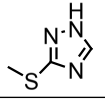	4.423	361.849	84.700	37.330	1.450	2.395	725.500	17.320	11.245	5.423	4.593	0	0

Table 2. Autocorrelation matrix between physicochemical and indicator parameters

	Mw	St	Pz	D	χ_{eq}	Pc	$^{0}\chi$	$^{2}\chi$	$^{5}\chi$	Id	I_1	I_2
Mw	1.000											
St	–0.148	1.000										
Pz	0.929	–0.394	1.000									
D	–0.156	0.750	–0.404	1.000								
χ_{eq}	–0.138	0.461	–0.296	0.877	1.000							
Pc	0.923	–0.116	0.910	–0.371	–0.403	1.000						
$^{0}\chi$	0.948	–0.265	0.962	–0.388	–0.369	0.965	1.000					
$^{2}\chi$	0.885	–0.179	0.893	–0.419	–0.484	0.957	0.965	1.000				
$^{5}\chi$	0.830	–0.206	0.891	–0.079	0.104	0.736	0.809	0.698	1.000			
Id	0.788	0.058	0.821	–0.005	0.022	0.779	0.811	0.763	0.906	1.000		
I_1	0.111	–0.069	0.018	0.167	0.166	–0.031	–0.039	–0.211	–0.028	–0.127	1.000	
I_2	0.100	–0.665	0.276	–0.265	0.050	–0.035	0.102	–0.048	0.362	0.058	0.134	1.000

The autocorrelation between the used parameters is shown in Table 2. The results show that all the physicochemical parameters are orthogonal and can be subjected to regression analysis with indicator parameters.

The statistically significant models obtained are as follows:

$$pCC_{50} = -0.013\ (\pm 0.005)\ Mw - 0.020\ (\pm 0.010)\ St - 1.181\ (\pm 0.515)\ I_1 + 11.269 \quad (1)$$

$n = 15,\ R = 0.936,\ R^2 = 0.876,\ R^2_A = 0.842,\ se = 0.225,\ F_{(3,11)} = 25.886,\ Q = 4.160$

$$pCC_{50} = -0.110\ (\pm 0.046)\ Pz - 0.028\ (\pm 0.013)\ St - 1.342\ (\pm 0.584)\ I_1 + 11.419 \quad (2)$$

$n = 15,\ R = 0.916,\ R^2 = 0.839,\ R^2_A = 0.795,\ se = 0.256,\ F_{(3,11)} = 19.146,\ Q = 3.578$

$$pCC_{50} = -3.554\ (\pm 2.192)\ D - 0.443\ (\pm 0.162)\ {}^2\chi - 1.471\ (\pm 0.575)\ I_1 + 15.170 \quad (3)$$

$n = 15,\ R = 0.923,\ R^2 = 0.851,\ R^2_A = 0.811,\ se = 0.246,\ F_{(3,11)} = 20.995,\ Q = 3.752$

$$pCC_{50} = -9.049\ (\pm 9.843)\ \chi_{eq} - 0.428\ (\pm 0.211)\ {}^2\chi - 1.504\ (\pm 0.721)\ I_1 + 31.793 \quad (4)$$

$n = 15,\ R = 0.875,\ R^2 = 0.766,\ R^2_A = 0.702,\ se = 0.308,\ F_{(3,11)} = 12.011,\ Q = 2.841$

$$pCC_{50} = -3.297\ (\pm 2.373)\ D - 0.007\ (\pm 0.003)\ Pc - 1.172\ (\pm 0.623)\ I_1 + 14.785 \quad (5)$$

$n = 15,\ R = 0.906,\ R^2 = 0.821,\ R^2_A = 0.773,\ se = 0.269,\ F_{(3,11)} = 16.870,\ Q = 3.368$

$$pCC_{50} = -3.293\ (\pm 2.662)\ D - 0.292\ (\pm 0.142)\ )\ {}^0\chi - 1.183\ (\pm 0.694)\ I_1 + 15.019 \quad (6)$$

$n = 15,\ R = 0.882,\ R^2 = 0.778,\ R^2_A = 0.718,\ se = 0.300,\ F_{(3,11)} = 12.863,\ Q = 2.940$

$$pCC_{50} = -0.013\ (\pm 0.005)\ Mw - 1.230\ (\pm 0.610)\ I_1 + 0.492\ (\pm 0.380)\ I_2 + 9.576 \quad (7)$$

$n = 15,\ R = 0.910,\ R^2 = 0.828,\ R^2_A = 0.781,\ se = 0.266,\ F_{(3,11)} = 17.645,\ Q = 3.421$

$$pCC_{50} = -0.335\ (\pm 0.187)\ {}^2\chi - 1.636\ (\pm 0.728)\ I_1 + 0.401\ (\pm 0.444)\ I_2 + 8.931 \quad (8)$$

$n = 15,\ R = 0.874,\ R^2 = 0.764,\ R^2_A = 0.699,\ se = 0.310,\ F_{(3,11)} = 11.862,\ Q = 2.819$

$$pCC_{50} = -0.241\ (\pm 0.136)\ {}^0\chi - 1.435\ (\pm 0.718)\ I_1 + 0.503\ (\pm 0.450)\ I_2 + 9.347 \quad (9)$$

$n = 15,\ R = 0.872,\ R^2 = 0.761,\ R^2_A = 0.695,\ se = 0.312,\ F_{(3,11)} = 11.646,\ Q = 2.795$

$$pCC_{50} = -0.548\ (\pm 0.324)\ {}^5\chi - 1.471\ (\pm 0.736)\ I_1 + 0.725\ (\pm 0.492)\ I_2 + 8.116 \quad (10)$$

$n = 15,\ R = 0.866,\ R^2 = 0.749,\ R^2_A = 0.681,\ se = 0.319,\ F_{(3,11)} = 10.960,\ Q = 2.715$

$$pCC_{50} = -2.787\ (\pm 1.676)\ ID - 1.537\ (\pm 0.748)\ I_1 + 0.476\ (\pm 0.463)\ I_2 + 17.964 \quad (11)$$

$n = 15,\ R = 0.863,\ R^2 = 0.744,\ R^2_A = 0.674,\ se = 0.323,\ F_{(3,11)} = 10.669,\ Q = 2.672$

where n is the number of data points, R – the correlation coefficient, R^2 – the coefficient of determination, R^2_A – the adjusted R^2, se – the standard error of estimate, F – the F ratio[25], Q – the quality of fit[26,27], data within the parenthesis are the confidence interval at 95% level. Compound No 15 was taken as outlier as it exhibited no inhibition for influenza A virus.

It may be inferred that negative coefficients of the parameters – Mw, St, Pc, Id, D, Pz, χ_{eq}, ${}^0\chi$, ${}^2\chi$, ${}^5\chi$ (equations (1)–(11)) suggest that substituents which are smaller, less bulkier, less polar, less electronegative with less vertices and less branching are

good for the activity. In equations (1) to (11), the coefficient of I_1 is negative and hence the presence of CH_3S group at R_2-position should be avoided whereas I_2 has positive coefficient implying that 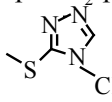 group at R_3-position should be preferable.

Predicted and residual values for the derived QSAR models are given in Table 3. Predicted values are the calculated activities of the equation and the residual values are the difference between the observed biological activities and the calculated activities and are found to be low. The calculated *F* value is greater than *F* theoretical value ($F_{(3,11)}$ = 3.59) for all the significant equations. The plots of observed pCC_{50} versus predicted pCC_{50} based on equations (1), (2 and (3) are shown in Fig. 1 and the predicted R^2 were found to be fairly large.

Table 3. Comparison between observed and predicted activities and their residual values for equations (1), (2) and (3)

S. No	Observed	Equation (1)		Equation (2)		Equation (3)	
		predicted	residual	predicted	residual	predicted	residual
1	6.287	6.310	–0.024	6.251	0.036	6.379	–0.092
2	5.523	5.473	0.050	5.325	0.198	5.576	–0.053
3	5.253	5.388	–0.135	5.290	–0.037	5.636	–0.110
4	5.307	4.998	0.309	5.094	0.214	5.016	0.291
5	5.756	5.885	–0.129	5.825	–0.069	5.867	–0.111
6	5.329	5.182	0.147	5.109	0.220	5.052	0.278
7	6.113	6.093	0.020	6.072	0.041	5.953	0.160
8	6.294	6.090	0.204	6.177	0.117	6.198	0.096
9	5.494	5.516	–0.022	5.610	–0.115	5.476	0.018
10	4.300	4.300	0.000	4.300	0.000	4.300	0.000
11	5.472	5.407	0.065	5.591	–0.119	5.302	0.170
12	5.513	5.739	–0.226	5.687	–0.174	5.658	–0.144
13	5.655	5.343	0.312	5.256	0.399	5.563	0.092
14	5.672	5.813	–0.142	5.810	–0.139	5.654	0.018
15	4.852	7.401	–	7.277	–	7.732	–
16	4.423	4.853	–0.430	4.994	–0.571	5.034	–0.611

The observed activities are the biological activities CC_{50}, which are measures of cytotoxicity, predicted values are the calculated activities of the equations and residual values are the difference between the observed biological activities and the calculated activities.

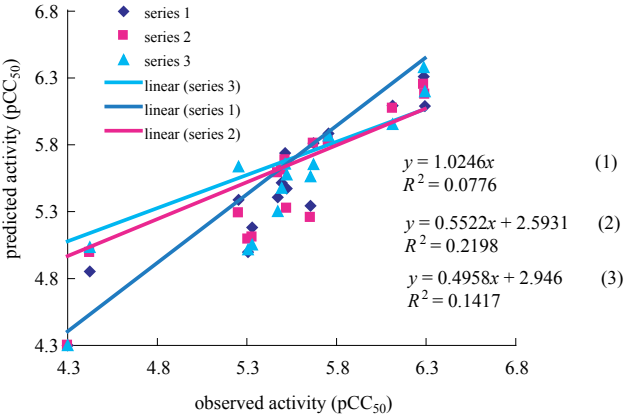

Fig. 1. Plot of comparision between observed and predicted activities for equations (1), (2) and (3)

CROSS-VALIDATION

The cross-validation analysis was performed using leave-one-out (LOO) method[28], in which one compound is removed from the data set and the activity is correlated using the rest of the data set. The cross-validated R^2 was found to be very close to the value of R^2 for the entire data set and hence these models can be termed as statistically significant.

Cross-validation provides the values of PRESS, SSY and R^2_{cv} and PSE from which we can test the predictive power of the proposed model. The meanings of these cross-validated parameters are given as footnote to Table 4. It is argued that PRESS is a good estimate of the real predictive error of the model and if it is smaller than SSY the model predicts better than chance and can be considered statistically significant. Furthermore, the ratio PRESS/SSY can be used to calculate approximate confidence intervals of prediction of new compound. To be a reasonable QSAR model PRESS/SSY should be smaller than 0.4 and for our models the value of this ratio which is smaller than 0.1 indicates that they are excellent models. Also, if PRESS value is transformed in a dimensionless term by relating it to the initial sum of squares, we obtain R^2_{cv}, i.e. the complement to the traces on of unexplained variance over the total variance. The PRESS and R^2_{cv} have good properties. However, for practical purposes of end users the use of square root of PRESS/n, which is called predictive square error (PSE), is more directly related to the uncertainty of the predictions. The PSE values also support our results. The calculated cross-validated parameters confirm the validity of the models.

Table 4. Cross-validation parameters and predictive error of coefficient of correlation (PE) for the proposed models

Equation No	*n*	Parameters	PRESS	SSY	PRESS/SSY	R^2cv	PSE	*R*	$1-R^2$	PE	6PE
(1)	15	Mw+St+I_1	0.555	3.917	0.142	0.858	0.192	0.936	0.124	0.021	0.126
(2)	15	Pz+St+I_1	0.719	3.753	0.192	0.808	0.219	0.916	0.161	0.028	0.168
(3)	15	D+ $^2\chi$ +I_1	0.665	3.807	0.175	0.825	0.211	0.923	0.149	0.026	0.156
(4)	15	χ_{eq} + $^2\chi$ +I_1	1.046	3.426	0.305	0.695	0.264	0.875	0.234	0.040	0.240
(5)	15	D +Pc+I_1	0.798	3.674	0.217	0.783	0.231	0.906	0.179	0.031	0.186
(6)	15	D+ $^0\chi$ +I_1	0.992	3.480	0.285	0.715	0.257	0.882	0.222	0.037	0.222
(7)	15	Mw+I_1+I_2	0.769	3.703	0.208	0.792	0.226	0.910	0.172	0.030	0.180
(8)	15	$^2\chi$ +I_1+I_2	1.056	3.416	0.309	0.691	0.265	0.874	0.236	0.041	0.246
(9)	15	$^0\chi$ +I_1+I_2	1.071	3.401	0.315	0.685	0.267	0.872	0.239	0.041	0.246
(10)	15	$^5\chi$ +I_1+I_2	1.121	3.351	0.335	0.665	0.273	0.866	0.251	0.043	0.258
(11)	15	Id+I_1+I_2	1.144	3.328	0.334	0.656	0.276	0.863	0.256	0.044	0.264

PREDICTIVE ERROR OF COEFFICIENT OF CORRELATION (PE)

The predictive error of coefficient of correlation (PE)[29,30] is yet another parameter used to decide the predictive power of the proposed models. We have calculated PE value of all the proposed models and they are reported in Table 4. It is argued that of

(i) R < PE, then correlation is not significant;

(ii) R > PE; several times (at least three times), then correlation is indicated; and if

(iii) R > 6PE, then the correlation is definitely good.

For all the models developed the condition R > 6PE is valid and hence they can be assumed to have good predictive power.

The data presented in Table 4 indicate that in all the cases, R is much larger than 6PE indicating that all the proposed models have represented high degree of correlation.

CONCLUSIONS

After discussing all the QSAR models, some points may be kept in mind for further drug designing:

1. The values of activities and parameters should be of large range. This large range of variation in activity helps in obtaining significant models with high values of regression coefficient and low values of standard error of estimate, in the case of parameters the values of different calculated parameters are also in wide range as given in Table 1.

2. Smaller, less dense, less bulky, less electronegative, less polar groups with fewer vertexes and less branching are conducive for the activity.

3. In the present series, we prefer the use of 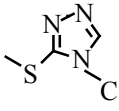 group at R_3-position whereas CH_3S group at R_2-position should be strictly avoided for rationale drug designing.

REFERENCES

1. U. GHOSH, D. GANESSUNKER, V.J. SATTIGERI, K.E. CARLSON, D. J. MORTENSEN, B. S. KATZENLLENBOGEN, J. A. KATZENLLENBOGEN: Estrogenic Diazenes: Heterocyclic Non-steriodal Estrogens of Unusual Structure with Selectivity for Estrogen Receptor Subtypes. Bioorg. Med. Chem., **11**, 629 (2003).
2. F. XIE, S. LI, D. BAI, L. LOU, Y. HU: Three Component, One-pot Synthesis of 2,4,5-substituted Pyrimidines Library for Screening against Human Hepatocellular Carcinoma BEL-7402 Cells. J. Comb. Chem., **9**, 12 (2007).
3. E. de CLERCQ: Antiviral Drugs in Current Clinical Use. J. Clin. Virol., **30**, 115 (2004).
4. W.-L. WANG, D.-Y. YAO, M. GU, M.-Z. FAN, J.-Y. LI, Y.-C. XING, F.-J. NAN: Synthesis and Biological Evaluation of Novel Bisheterocycle-containing Compounds as Potential Anti-influenza Virus Agents. Bioorg. Med. Chem. Lett., **15**, 5284 (2005).
5. G. CHENG, S. LI, J. LI, Y. HU: Three-component, One-pot Synthesis of Novel 2,4-substituted 5-Azolylthiopyrimidine Library for Screening against Anti-influenza Virus A. Bioorg. Med. Chem. Lett., **18**, 1177 (2008).
6. (a) C. HANSCH, A. LEO: Exploring QSAR – Fundamentally and Application in Chemistry and Biology. Amer. Chem. Soc., Washington, D. C. (1995); (b) C. HANSCH, A. LEO, D. HOCHMAN: Exploring QSAR – Hydrophobic, Electronic and Steric Constant. Amer. Chem. SOC., Washington, D. C. 1995.
7. ACD-LAB Software for Calculating the Referred Physicochemical Parameters. Chem Sketch www.acdlabs.com/acdlabs-rss-feed.xml
8. DRAGON Software for Calculation of Topological Indices: www.disal.unimib.it
9. A. K. SRIVASTAVA, A. NATH, S. CHAURASIA, V. K. PATHAK, A. PANDEY: QSAR Based Modeling of Neurokinin-1 Receptor Antagonists as Antidepressant Drugs. J. Saudi Chem. Soc., **12**, 329 (2008).
10. A. K. SRIVASTAVA, ARCHANA, M. JAISWAL: Quantitative Structure Activity Relationship Studies on a Series of 1,3-diaryl-4,5,6,7-tetrahydro-2H-isoindole Derivatives as Potent and Selective COX-2 Inhibitors. J. Indian Chem. Soc., **84**, 260 (2007).
11. A. K. SRIVASTAVA, A.VERMA: QSAR study of 2-subtituted-4-aryl Oxazole Bezenesulphonamide. A New Class of β_3 Adrenenergic Receptor Agonists. Oxid. Commun., **29** (1), 8 (2006).
12. A. K. SRIVASTAVA, ARCHANA, M. JAISWAL: Quantitative Structure – Activity Relationship Studies on a Series of *p*-Arylthio Cinnamides as Antagonists of Biochemical ICAM-1/LFA-1 Interaction in Relation to Antiinflammatory Activity. Oxid. Commun., **31** (1), 44 (2008).
13. A. K. SRIVASTAVA, A. KHAN, A. TRIPATHI, S. CHAURASIA: A QSAR Study on Benzooxazinones Analogues of Efarirenz for the Discovery of Potent HIV-1 Reverse Transcriptase Inhibitors. J. Saudi. Chem. Soc., **9**, 571 (2005).
14. A. K. SRIVASTAVA, M. JAISWAL, ARCHANA: QSAR Studies on Indole Substituted Potent Human Histamine H_4 Antagonists: Role of Physicochemical and Statistical Parameters. J. Saudi. Chem. Soc., **12**, 221 (2008).

15. P. V. KHADIKAR, M. JAISWAL, M. GUPTA, D. MANDOLOI, R. S. SISODIA: QSAR Based Modeling of a New Class of RNA Polymerase Inhibitors. J. Indian Chem. Soc., **85**, 627 (2008).
16. A. K. SRIVASTAVA, S. CHAURASIA, A. NATH, A. PANDEY: Quantitative Structure – Activity Relationship (QSAR) Studies on a Series of Thiol-based Saha Analogues as Potent Histone Deacetylase (HDAC) Inhibitors. J. Saudi Chem. Soc., **12**, 281 (2008).
17. A. K. SRIVASTAVA, ARCHANA, M. JAISWAL: Exploring QSAR of Selective as 8-substituted Analogues of 3-(3-Cyclopentyloxy-4-methoxy-benzyl)-8 Isopropyl Adenine. J. Saudi Chem. Soc., **12**, 227 (2008).
18. A. K. SRIVASTAVA, S. CHAURASIA, A. NATH, ARCHANA: Quantitative Structure Activity Relationship Studies on a Novel Series of Phthalazinone as Potent Poly (ADA-ribose) Polymerase Inhibitors. Proc. Nat. Acad. Sci. India Sect. A, **78**, Part 1 (2008).
19. A. K. SRIVASTAVA, S. CHAURASIA, A. NATH, M. K. SRIVASTAVA, A. PANDEY: Quantitative Structure Activity Relationship Studies on a Series of Tetrahydroquinoline-based Farnesyltransferase Inhibitors: Oxid. Commun., **30** (4), 778 (2007).
20. A. K. SRIVASTAVA, V. K. PATHAK, ARCHANA, M. JAISWAL: QSAR Based Modeling of a New Class of RNA Polymerase Inhibitors. J. Indian Chem. Soc., **85**, 627 (2008).
21. J. SINGH, V. K. AGARWAL, S. SINGH, P. V. KHADIKAR: Use of Topological as well as Quantum Chemical Parameters in Modelling Antimalarial Activity of 2,4-diamino-6-quinazoline Sulphonamides. Oxid. Commun., **31** (1), 17 (2008).
22. J. SINGH, V. K. DUBEY, V. K. AGARWAL, P. V. KHADIKAR: QSAR Study on Octanol-Water Partitioning: Dominating Role of Equalized Electro Negativity. Oxid. Commun., **31** (1), 27 (2008).
23. A. K. SRIVASTAVA, A. SRIVASTAVA, ARCHANA, M. JAISWAL: Role of Physicochemical Parameters in Quantitative Structure Activity Relationship Based Modeling of CYP26A1 Inhibitory Activity. J. Indian Chem. Soc., **85**, 721 (2008).
24. J. SINGH, V. K. AGARWAL, S. SINGH, P. V. KHADIKAR: Use of Topological as well as Quantum Chemical Parameters in Modeling Antimalarial Activity of 2,4-diamino-6-quinoline Sulphonamides. Oxid. Commun., **31** (1), 17 (2006).
25. M. V. DIUDEA (Ed.): QSPR/QSAR Studies for Molecular Descriptors. Nova Science, and Hunting don, New York, 2000.
26. L. POGLIANI: From Connectivity Indices to Semiempirical Connectivity Terms. Recent Trends in Graph. Chem. Rev., **100**, 3827 (2000).
27. L. POGLIANI: Modeling with Special Descriptor Derived from a Medium-sized Set of Connectivity Indices. J. Phys. Chem., **100**, 18065 (1996).
28. R. D. CRAMER, III, J. D. BUNCE, D. E. PATTERSON: Cross Validation, Bootstrapping and Partial Least Squares Compared with Multiple Regression in Conventional QSAR Studies. Quant. Struct. Act. Relat., **7**, 18 (1988).
29. J. SINGH, V. K. DUBEY, V. K. AGARWAL, P. V. KHADIKAR: QSAR Study on Octanol-Water Partitioning Dominating Role of Equalized Electronegativity. Oxid. Commun., **31** (1), 27 (2008).
30. S. CHATTERJEE, A. S. HADI, B. PRICE: Regression Analysis by Example. 3rd ed. Wiley VCH, New York, 2000.

Received 16 May 2009
Revised 18 July 2009

Oxidation Communications 33, No 3, 631–651 (2010)

QSAR STUDIES ON SOME PROTEASE INHIBITORS INCORPORATING SULPHONYL-L-ALANINE HYDROXAMATE MOIETIES

J. SINGH[a], K. SINGH [b], B. SHAIK[b], N. SINGH[c], V. K. AGRAWAL[d]*

[a]*Delhi Technological University, Bavana Road, 110 042 Delhi, India*
[b]*QSAR and Computer Chemical Laboratories, A.P.S. University, 486 003 Rewa, India*
[c]*Department of Chemistry, Radharama Institute of Technology and Science, 462 02l Bhopa, India*
[d]*Research Division, Laxmi Fumigation and Pest Control Pvt. Ltd., 3 Khatipura, 452 007 Indore, India*
E-mail: *vijay-agrawal@lycos.com*

ABSTRACT

Effort has been made to use topological indices for the QSAR modelling of the inhibition of *Clostridium histolyticum* collagenase obtained using carboxylic acid and their corresponding hydroxamates. Good results are obtained using some topological indices along with indicator parameters.

Keywords: CA inhibitors, topological indices, the Wiener index, the Schiff bases, QSAR, equalised electronegativity.

AIMS AND BACKGROUND

Scozzafava and Supuran[1] have developed new ChC (*C. histolyticum* collagenase) inhibitors with a motive to use them as pharmacological agents for the treatment of corneal keratitis. It was reported[2–4] that the collagenase inhibitor would kill the bacteria present on the cornea as well as the protective collagen shield will help in the speedy recovery of the wound. Because of the double benefits of such compounds the new potent protease inhibitors were synthesised by Scozzafava and Supuran[1] incorporating sulphonyl-L-alanine hydroxamate moieties.

Earlier, we have investigated QSAR modelling of the sulphanilamide Schiff base inhibitors of carbonic anhydrase[5–12] developed by Scozzafava and Supuran using various topological indices including the Wiener index. The results presented therein indicted that we can use such distance-based topological indices successfully in drug designing.

* For correspondence.

Prompted by the above results we have also used topological indices for modelling inhibitors of carbonic anhydrase. In addition, we have recently modelled carbonic anhydrase inhibition activity of sulphonamides using molecular negentropy. Earlier, we have reported QSAR studies on carbonic anhydrase inhibition of ureido and thioureido derivatives of aromatic/ heterocyclic sulphonamides using topological indices[12]. Also, using topological indices we have reported QSAR studies on various sulphonamides having potential biological activities[12].

In this work the attempt has been made to use topological indices for the QSAR study of the inhibition of *Clostridium histolyticum* collagenase (ChC) using carboxylic acid and their corresponding hydroxamate[1]. The carboxylic acids chosen have the following structural feature:

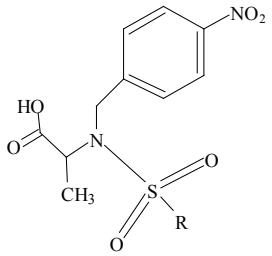

Fig. 1. General structure of carboxylic acid used in the present investigation

The hydroxamate of the aforementioned carboxylic acids has the following structure:

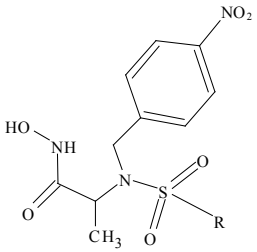

Fig. 2. Hydroxamates used in the present study

Both of them lead to ChC inhibitors incorporating alkyl-aryl-sulphonamido-L-alanine hydroxamates as well as aryl-sulphonylamino-arolureido-L-alanine hydroxamate moieties. Consequently, the following structural elements in the design of the *Clostridium histolyticum* (ChC) inhibitors are obtained[1]:

(i) a strong zinc-binding function (of the carboxylic acid or hydroxamate acid type);

(ii) a small group in α to it;

(iii) the already optimised benzyl group at the S_2' site converted to a 4-nitrobenzyl;

(iv) variable alkyl/aryl sulphonoyl-; aryl-sulphonyl-uredio-, arylureido; aryl sulphenyl moieties at S_1'.

EXPERIMENTAL

The structural details of the aforementioned series of compounds are given in Tables 1 and 2. As stated above, Table 1 gives general scheme obtaining hydroxamate moieties. Table 2 gives the structural details of 98 compounds used in the present study. This Table 2 also records the activity in their log units and the magnitude of 4 indicator parameters used. These values have been taken from the work of Scozzafava and Supuran[1]. The details of the indicator parameters are given as footnote to Table 2. Table 3 records the values of the topological indices: W, $^1\chi$, J, Sz, lg RB along with the value of equalised electronegativity (χ_{eq}). Needless to record that all the topological indices were obtained from their hydrogen-suppressed graphs in that all the carbon-hydrogen as well as hetero-atom-hydrogen bonds were suppressed. The correlation matrix for the correlation of the parameters used is given in Table 4.

Table 1. Structural details of protease inhibitors used in the present investigation

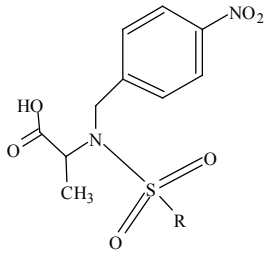

structure I (compounds **1**–**35**)

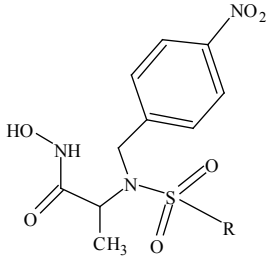

structure II (compounds **36**–**70**)

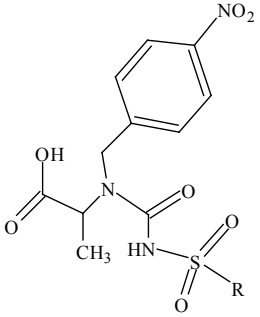

structure III (compounds **71**–**74**)

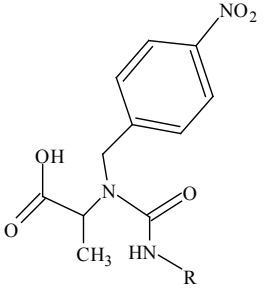

structure IV (compounds **75**–**80**)

to be continued

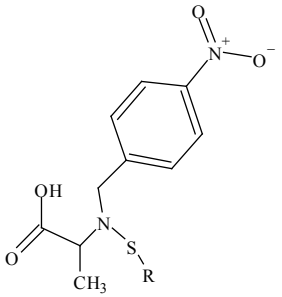

structure V (compounds **81**–**83**)

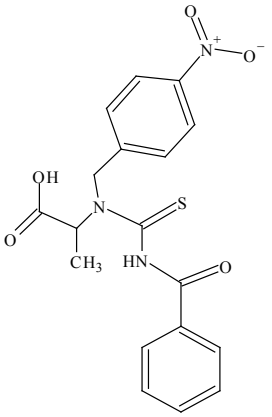

structure VI (compounds **84**)

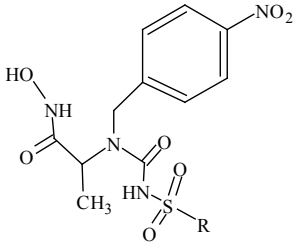

structure VII (compounds **85**–**88**)

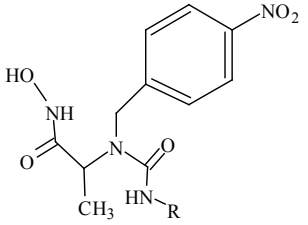

structure VIII (compounds **89**–**94**)

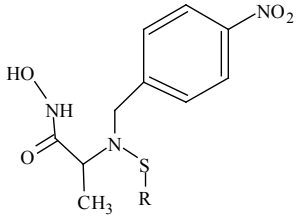

structure IX (compounds **95**–**97**)

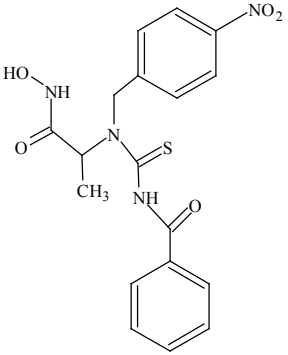

structure X (compounds **98**)

Table 2. Activity of compounds and indicator parameters of various compounds used in the present study

Compd. No	R	lg K_i	IP_1	IP_2	IP_3	IP_4
1	2	3	4	5	6	7
1	CH_3	1.2553	0	0	0	0
2	CF_3	0.6721	0	0	0	0
3*	CCl_3	0.7076	0	0	0	0
4	n-C_4F_{9-}	0.3617	0	0	0	0
5	n-C_8F_{17}	0.2553	0	0	0	0
6	Me_2N	1.5563	0	0	0	0
7*	C_6H_5	1.3222	0	0	0	0
8	$PhCH_2$	1.1761	0	0	0	0
9	4-F–C_6H_4	1.0000	1	0	0	0
10	4-Cl–C_6H_4	0.9542	1	0	0	0
11	4-Br–C_6H_4	1.0000	1	0	0	0
12	4-I–C_6H_4	1.0792	1	0	0	0
13	4-CH_3–C_6H_4	1.1139	1	0	0	0
14	4-O_2N–C_6H_4	0.7243	1	0	0	0
15	3-O_2N–C_6H_4	0.7404	0	0	1	0
16	2-O_2N–C_6H_4	0.6812	0	0	0	0
17	3-Cl-4-O_2N–C_6H_3	0.5185	0	0	0	1
18	4-AcNH–C_6H_4	0.4914	1	0	0	0
19	4-BocNH–C_6H_4–	0.3802	1	0	0	0
20	3-BocNH–C_6H_4–	0.4150	0	0	1	0
21	4-Ac–C_6H_4–	0.3222	1	0	0	0
22*	C_6H_5–	–0.3979	0	0	0	0
23*	3-CF_3–C_6H_4	–0.5229	0	0	1	0
24	2,5-$Cl_2C_6H_3$	0.5563	0	0	0	1
25	4-CH_3O–C_6H_4–	0.7160	1	0	0	0
26	2,4,6-$(CH_3)_3$–C_6H_2–	0.7782	0	0	0	0
27	4-CH_3O-3-BocNH–C_6H_3	0.3222	0	0	0	1
28	2-HO-3,5-Cl_2–C_6H_2–	0.3979	0	0	0	0
29	3-HOOC–C_6H_4–	0.3010	0	0	1	0
30*	4-HOOC–C_6H_4	0.1461	1	0	0	0
31	1-naphthyl	0.0792	0	0	0	0
32	2-naphthyl	0.1139	0	0	0	0
33	5-Me_2N-1-naphthyl	0.0414	0	0	0	0
34*	2-thienyl	0.3222	0	0	0	0
35	quinoline-8-yl	0.0792	0	0	0	0
36	CH_3	1.8808	0	1	0	0
37	CF_3	1.8751	0	1	0	0
38	CCl_3	1.7160	0	1	0	0
39	n-C_4F_9	1.0414	0	1	0	0

to be continued

Continuation of Table 2

1	2	3	4	5	6	7
40	*n*-C_8F_{17}	0.8451	0	1	0	0
41	Me_2N	1.8388	0	1	0	0
42	C_6H_5	1.7324	0	1	0	0
43*	$PhCH_2$	1.6990	0	1	0	0
44	4-F–C_6H_4	1.5441	1	1	0	0
45	4-Cl–C_6H_4	1.5052	1	1	0	0
46	4-Br–C_6H_4	1.4771	1	1	0	0
47	4-I–C_6H_4	1.5682	1	1	0	0
48	4-CH_3–C_6H_4	1.5563	1	1	0	0
49	4-O_2N–C_6H_4	1.0000	1	1	0	0
50	3-O_2N–C_6H_4	1.0792	0	1	1	0
51	2-O_2N–C_6H_4	1.1139	0	1	0	0
52	3-Cl-4-O_2N–C_6H_3	0.9542	0	1	0	1
53	4-AcNH–C_6H_4	1.0414	1	1	0	0
54	4-BocNH–C_6H_4–	1.0000	1	1	0	0
55	3-BocNH–C_6H_4–	0.9031	0	1	1	0
56	4-Ac-C_6H_4–	0.9542	1	1	0	0
57	C_6H_5–	0.6990	0	1	0	0
58	3-CF_3–C6H4	0.7782	0	1	1	0
59	2,5-$Cl_2C_6H_3$	1.1139	0	1	0	1
60	4-CH_3O–C_6H_4–	1.3222	1	1	0	0
61	2,4,6-$(CH_3)_3$–C_6H_2–	1.2304	0	1	0	0
62	4-CH_3O-3-BocNH–C_6H_3	0.9031	0	1	0	1
63	2-HO-3,5-Cl_2–C_6H_2–	1.0792	0	1	0	0
64	3-HOOC–C_6H_4–	0.9542	0	1	1	0
65	4-HOOC–C_6H_4	0.7782	1	1	0	0
66	1-naphthyl	0.8451	0	1	0	0
67	2-naphthyl	0.9031	0	1	0	0
68	5-Me_2N-1-naphthyl-	0.8451	0	1	0	0
69	2-thienyl	1.0414	0	1	0	0
70	quinoline-8-yl	0.9031	0	1	0	0
71	4-F–C_6H_4–	0.5185	1	0	0	0
72	4-Cl–C_6H_4–	0.3802	1	0	0	0
73	4-CH_3–C_6H_4–	0.3979	1	0	0	0
74	2-CH_3–C_6H_4–	0.4914	0	0	0	0
75	4-F–C_6H_4–	0.7324	1	0	0	0
76	3-Cl–C_6H_4–	0.7853	0	0	1	0
77	4-Cl–C_6H_4–	0.8129	1	0	0	0
78	2,4-F_2–C_6H_3–	0.7924	0	0	0	1
79	3,4-Ci_2–C_6H_3–	0.6990	0	0	0	1
80	1-naphthyl	0.6628	0	0	0	0

to be continued

Continuation of Table 2

1	2	3	4	5	6	7
81	4-O_2N–C_6H_4–	0.7404	1	0	0	0
82	4-O_2N–C_6H_4–	0.7993	1	0	0	0
83	2,4-$(O_2N)_2$–C_6H_3–	0.7076	0	0	0	1
84*	struc. No 6	–0.0458	0	0	0	0
85	4-F–C_6H_4–	0.9542	1	1	0	0
86	4-Cl–C_6H_4–	0.8451	1	1	0	0
87	4-CH_3–C_6H_4–	1.0792	1	1	0	0
88	2-CH_3–C_6H_4–	0.9031	0	1	0	0
89	4-F–C_6H_4–	1.0792	1	1	0	0
90	3-Cl–C_6H_4–	1.1461	0	1	1	0
91	4-Cl–C_6H_4–	1.2553	1	1	0	0
92	2,4-F_2–C_6H_3–	1.1761	0	1	0	1
93	3,4-Ci_2–C_6H_3–	1.1139	0	1	0	1
94	1-naphthyl	1.0000	0	1	0	0
95	4-O_2N–C_6H_4–	1.0410	1	1	0	0
96	4-O_2N–C_6H_4–	0.8460	1	1	0	0
97	2,4-$(O_2N)_2$–C_6H_3–	0.9542	0	1	0	1
98	struc. No 10	0.7782	0	1	0	0

IP_1 = 1, if 4th substituted benzene ring is present in the parent structure (I to X) at R, otherwise 0; IP_2 = 1, if -NHOH group is present in parent structure, otherwise 0; IP_3 = 1, if halogen is present at R in the parent structures, otherwise 0; IP_4 = 1, if -SO_2R is directly attached with N of the parent structure, otherwise 0; * indicates serious outliers.

Table 3. Calculated values of molecular descriptor (W, $^1\chi$, J, Sz, χ_{eq} and lg RB) used in the present study

Compd. No	W	$^1\chi$	J	Sz	lg RB	χ_{eq}
1	2	3	4	5	6	7
1	844	9.1249	2.5940	1096	249.0273	2.4577
2	1180	10.3749	2.8341	1486	345.6985	2.5795
3	1180	10.3749	2.8341	1486	345.6985	2.5350
4	2710	14.1249	3.3312	3178	755.8829	2.7012
5	6304	19.1249	3.6992	6988	1615.6900	2.8104
6	1066	10.0683	2.7421	1354	312.7817	2.4361
7	1492	11.7301	2.0524	2032	427.7411	2.4415
8	1711	12.2032	2.0018	2278	479.7202	2.4249
9	1673	12.1239	2.0572	2297	473.2324	2.4741
10	1673	12.1239	2.0572	2297	473.2324	2.4631
11	1673	12.1239	2.0572	2297	473.2324	2.4591
12	1673	12.1239	2.0572	2297	473.2324	2.4572
13	1673	12.1239	2.0572	2297	473.2324	2.4249
14	2089	13.0346	2.0521	2881	573.8986	2.4961

to be continued

Continuation of Table 3

1	2	3	4	5	6	7
15	2032	13.0346	2.1066	2767	567.0104	2.4961
16	1975	13.0515	2.1685	2653	559.0753	2.4961
17	2262	13.4453	2.1001	3122	620.7579	2.5183
18	2640	14.0178	1.9940	3600	694.8716	2.4584
19	3506	15.2022	1.9783	4718	885.2424	2.4178
20	3354	15.2022	2.0677	4414	870.0491	2.4178
21	2350	13.5178	2.0253	3226	632.3981	2.4587
22	2321	13.8003	2.2639	3185	652.4866	2.6125
23	2224	13.3353	2.1327	3024	616.1906	2.4577
24	1802	12.5346	2.1341	2456	512.3981	2.4858
25	1880	12.6619	2.0491	2588	523.2189	2.4415
26	1971	12.9453	2.1744	2693	557.5104	2.3981
27	3838	16.1509	2.1497	5082	993.6246	2.4122
28	1971	12.9453	2.1723	2693	557.8713	2.503
29	2032	13.0346	2.1066	2767	567.0104	2.4769
30	2089	13.0346	2.0521	2881	573.8986	2.4769
31	2162	13.7133	1.7427	3204	606.3585	2.4296
32	2162	13.7133	1.7427	3204	606.3585	2.4296
33	2815	15.0346	1.7845	4217	770.7914	2.4053
34	1333	11.2301	2.0390	1700	385.7337	2.4621
35	2528	13.7032	1.8541	3176	656.5821	2.4456
36	966	9.6629	2.6263	1236	282.4225	2.4563
37	1323	10.9129	2.8754	1647	384.9314	2.5720
38	1323	10.9129	2.8754	1647	384.9314	2.7011
39	2934	14.6629	3.3761	3420	814.8544	2.6890
40	6678	19.6629	3.7352	7380	1704.922	2.7960
41	1202	10.6063	2.7818	1508	350.0686	2.4383
42	1653	12.2681	2.0813	2220	471.3841	2.4419
43	1884	12.7412	2.0339	2478	525.9172	2.4260
44	1653	12.2681	2.0813	2220	471.3841	2.4728
45	1653	12.2681	2.0813	2220	471.3841	2.4623
46	1653	12.2681	2.0813	2220	471.3841	2.6076
47	1653	12.2681	2.0813	2220	471.3841	2.4567
48	1653	12.2681	2.0813	2220	471.3841	2.4260
49	2282	13.5726	2.085	3110	624.6401	2.4953
50	2222	13.5726	2.1382	2990	617.4559	2.4953
51	2162	13.5895	2.1985	2870	609.1923	2.4953
52	2464	13.9833	2.1323	3362	673.6971	2.5158
53	2860	14.5558	2.0290	3862	750.8303	2.4593
54	3767	15.7402	2.0127	5030	949.0381	2.4198
55	3607	15.7402	2.1016	4710	933.1678	2.4198
56	2556	14.0558	2.0594	3471	685.7119	2.4584
57	2526	14.3384	2.2928	3426	706.9861	2.6045
58	2424	13.8733	2.1643	3259	668.9391	2.5134

to be continued

Continuation of Table 3

1	2	3	4	5	6	7
59	1980	13.0726	2.1638	2664	560.3179	2.4832
60	2062	13.1999	2.0813	2803	571.5624	2.4419
61	2158	13.4833	2.2041	2912	607.615	2.4001
62	4112	16.6889	2.1818	5405	1061.444	2.4134
63	2158	13.4833	2.202	2912	607.9883	2.4997
64	2222	13.5726	2.1382	2990	617.4559	2.4758
65	2282	13.5726	2.0850	3110	624.6401	2.4758
66	2359	14.2513	1.7634	3445	658.7784	2.4304
67	2359	14.2513	1.7634	3445	658.7785	2.4304
68	3044	15.5726	1.8054	4502	830.3099	2.4079
69	1485	11.7681	2.066	1872	427.1796	2.4606
70	2359	14.2513	1.7634	3445	658.7785	2.4471
71	2362	13.5077	1.9897	3076	635.6031	2.4896
72	2362	13.5077	1.9897	3076	635.6031	2.4795
73	2362	13.5077	1.9897	3076	635.6031	2.4431
74	2318	13.5246	2.0250	2988	630.0172	2.4431
75	1792	12.2738	1.9049	2416	491.3092	2.4557
76	1773	12.2738	1.9235	2378	489.0477	2.4451
77	1792	12.2738	1.9049	2416	491.3092	2.4451
78	1956	12.6845	1.9489	2628	535.1728	2.4879
79	1974	12.6845	1.9304	2664	537.4937	2.4662
80	2332	13.8631	1.5986	3374	631.0488	2.4151
81	1833	12.2738	1.8651	2553	496.3129	2.4616
82	1731	12.2906	1.9733	2349	483.6462	2.4616
83	2336	13.5951	2.0208	3206	633.4279	2.5183
84*	1986	12.7906	1.9112	2580	539.9017	2.4279
85	2570	14.0458	2.0230	3314	689.2737	2.4893
86	2570	14.0458	2.0230	3314	689.2737	2.4796
87	2570	14.0458	2.0230	3314	689.2737	2.4446
88	2524	14.0626	2.0574	3222	683.5054	2.4446
89	1970	12.8118	1.9388	2624	538.1123	2.4569
90	1950	12.8118	1.9569	2584	535.7555	2.4468
91	1970	12.8118	1.9388	2624	538.1123	2.4468
92	2143	13.2225	1.9823	2846	584.1732	2.4874
93	2162	13.2225	1.9642	2884	586.5995	2.4668
94	2539	14.4011	1.6215	3625	684.6548	2.4177
95	2014	12.8118	1.8992	2770	543.4708	2.4623
96	1906	12.8286	2.0049	2554	530.1799	2.4623
97	2543	14.1331	2.0530	3452	687.0603	2.4301
98	2166	13.3286	1.9562	2787	587.8035	2.5158

Table 4. Correlation matrix for the correlation of molecular descriptors and their correlation with lg K_i

	lg K_i	W	$^1\chi$	J	Sz	lg RB	IP_1	IP_2	IP_3	IP_4	χ_{eq}
lg K_i	1.0000										
W	–0.3348	1.0000									
$^1\chi$	–0.3885	0.9564	1.0000								
J	0.1524	0.3034	0.0941	1.0000							
Sz	–0.3828	0.9796	0.9814	0.1445	1.0000						
lg RB	–0.3386	0.9984	0.9629	0.3122	0.9788	1.0000					
IP_1	0.1047	–0.0850	–0.0788	–0.2495	–0.0713	–0.1040	1.0000				
IP_2	0.6120	0.0980	0.1569	0.0386	0.0986	0.1072	0.0000	1.0000			
IP_3	–0.1453	0.0616	0.0835	–0.0521	0.0748	0.0629	–0.2569	0.0000	1.0000		
IP_4	–0.0321	0.1036	0.1255	–0.0777	0.1296	0.1006	–0.2846	0.0000	–0.1259	1.0000	
χ_{eq}	–0.0471	0.3720	0.2438	0.7960	0.2392	0.3894	–0.1596	0.0465	–0.0657	–0.0261	1.0000

During the regression analysis compounds **3**, **7**, **22**, **23**, **30**, **34**, **43** and **84** were found to be serious outliers, hence they were deleted from further analysis. Some of these compounds were found to be least active during the experiments performed by Supuran et al.[1]. Compound **3** has trichloro attachement whereas compounds **7** and **22** are having phenyl group attached at *R*. Similarly in compounds **23** and **43** phenyl group with CH_3 behaves also as a outlier. At this stage we do not have convincing reasons why these compounds behave differently but this behaviour may be because of their structures and groups attached to them.

The results of variety of statistical analyses are presented in Table 5. Finally, Table 6 records the comparison of the calculated and observed activities using the best model. The residues, i.e. the differences between the observed and calculated activities are also presented in Table 6. The predictive correlation coefficient (R_{pred}^2) is obtained from the graph between observed and calculated activity (Fig. 3).

Table 5. Regression parameters and quality of correlation for modelling lg K_{Ii} activity

Model No	Parameter used	A_i = 1,2,3,4……..	$^1\chi$	R^2	R	Se	F- ratio	Q=R/se
1	2	3	4	5	6	7	8	9
1	$^1\chi$	–0.1446(±0.0152)	2.5299	0.6922	0.8320	0.2289	97.843	3.6348
	IP_2	0.5537(±0.0487)						
2	$^1\chi$	–0.4325(±0.0764)	4.9645	0.7372	0.8586	0.2127	80.424	4.0367
	Sz	$4.5606\times10^{-4}(\pm1.1886\times10^{-4})$						
	IP_2	0.6075(±0.0474)						
3	$^1\chi$	–0.1516(±0.0140)	2.116	0.7435	0.8623	0.2102	83.104	4.1023
	J	0.2406(±0.0580)						
	IP_2	0.5466(±0.0448)						
4	W	$4.6518\times10^{-4}(\pm8.3184\times10^{-5})$	4.7024	0.7743	0.8799	0.1971	98.352	4.4642
	$^1\chi$	–0.3883(±0.0455)						
	Ip_2	0.5962(±0.0427)						
5	$^1\chi$	–0.4113(±0.0488)	4.7914	0.7759	0.8809	0.1964	99.264	4.4852
	lg RB	$0.0021(\pm3.6352\times10^{-4})$						
	IP_2	0.5914(±0.0424)						
6	$^1\chi$	–0.4545(±0.0860)	5.2795	0.7769	0.8814	0.1972	74.000	4.4696
	J	–0.0616(±0.1007)						
	lg RB	$0.0024(\pm6.7505\times10^{-4})$						
	IP_2	0.5995(±0.0446)						
7	$^1\chi$	–0.4152(±0.0487)	4.7911	0.7807	0.8836	0.1955	75.662	4.5197
	lg RB	$0.0021(\pm3.6329\times10^{-4})$						
	IP_1	0.0584(±0.0428)						
	IP_2	0.5931(±0.0422)						

to be continued

Continuation of Table 5

1	2	3	4	5	6	7	8	9
8	$^1\chi$	–0.4306(±0.0879)	4.9675	0.7808	0.8837	0.1966	59.858	4.4949
	J	–0.0222(±0.1054)						
	lg RB	0.0022(±6.8838×10^{-4})						
	IP_1	0.0555(±0.0451)						
	IP_2	0.5960(±0.0445)						
9	$^1\chi$	–0.4222(±0.0491)	4.8402	0.7835	0.8852	0.1954	60.814	4.5302
	lg RB	0.0022(±3.6568×10^{-4})						
	IP_1	0.0732(±0.0450)						
	IP_2	0.5961(±0.0422)						
	IP_4	0.0674(±0.0645)						
10	$^1\chi$	–0.4737(±0.0576)	6.8657	0.7892	0.8884	0.1928	62.884	4.6079
	lg RB	0.0026(±4.5319×10^{-4})						
	IP_1	0.0499(±0.0424)						
	IP_2	0.6058(±0.0422)						
	χ_{eq}	–0.6507(±0.3549)						
11	$^1\chi$	–0.4435(±0.0695)	7.1864	0.7907	0.8892	0.1933	52.261	4.6001
	Sz	–1.4423×10^{-4}(±1.8481×10^{-4})						
	lg RB	0.0031(±7.7715×10^{-4})						
	IP_1	0.0517(±0.0426)						
	IP_2	0.5991(±0.0431)						
	χ_{eq}	–0.8888(±0.4686)						
12	$^1\chi$	–0.3784(±0.0886)	6.7670	0.7941	0.8911	0.1917	53.350	4.6484
	J	0.1972(±0.1399)						
	lg RB	0.0019(±6.8784×10^{-4})						
	IP_1	0.0696(±0.0444)						
	IP_2	0.5894(±0.0435)						
	χ_{eq}	–1.1104(±0.4804)						
13	W	–0.5518(±0.0722)	8.3871	0.7967	0.8926	0.1904	54.226	4.6880
	$^1\chi$	0.0074(±0.0028)						
	lg RB	0.0813(±0.0456)						
	IP_1	0.6031(±0.0417)						
	IP_2	–1.1090(±0.4368)						
	χ_{eq}	–0.0010(±5.7892×10^{-4})						
14	W	–0.0012(±5.9446×10^{-4})	8.7310	0.8022	0.8957	0.1890	47.521	4.7392
	$^1\chi$	–0.5776(±0.0737)						
	lg RB	0.0085(±0.0028)						
	IP_1	0.1102(±0.0491)						
	IP_2	0.6063(±0.0414)						
	IP_4	0.0976(±0.0646)						
	χ_{eq}	–1.1903(±0.4368)						

Table 6. Estimated value of lg K_i from model No 14 and comparison with observed value

Compd. No	Observed lg K_i	Estimated lg K_i	Residual
1	2	3	4
1	1.2553	1.603	–0.3477
2	0.6721	1.140	–0.4679
3	0.7076	–	–
4	0.3617	0.413	–0.0513
5	0.2553	0.232	0.0233
6	1.5563	1.350	0.2063
7	1.3222	–	–
8	1.1761	0.747	0.4291
9	1.0000	0.836	0.1640
10	0.9542	0.849	0.1052
11	1.0000	0.854	0.1460
12	1.0792	0.856	0.2232
13	1.1139	0.895	0.2189
14	0.7243	0.622	0.1023
15	0.7404	0.524	0.2164
16	0.6812	0.518	0.1632
17	0.5185	0.529	–0.0105
18	0.4914	0.442	0.0494
19	0.3802	0.346	0.0342
20	0.4150	0.296	0.1190
21	0.3222	0.560	–0.2378
22	–0.3979	–	–
23	–0.5229	–	–
24	0.5563	0.745	–0.1887
25	0.7160	0.732	–0.0160
26	0.7782	0.688	0.0902
27	0.3222	0.301	0.0212
28	0.3979	0.566	–0.1681
29	0.3010	0.547	–0.246
30	0.1461	–	–
31	0.0792	0.384	–0.3048
32	0.1139	0.384	–0.2701
33	0.0414	0.236	–0.1946
34	0.3222	–	–
35	0.0792	0.342	–0.2628
36	1.8808	2.032	–0.1512
37	1.8751	1.600	0.2751
38	1.7160	1.446	0.2700
39	1.0414	0.946	0.0954
40	0.8451	0.838	0.0071

to be continued

Continuation of Table 6

1	2	3	4
41	1.8388	1.790	0.0488
42	1.7324	1.296	0.4364
43	1.6990	–	–
44	1.5441	1.370	0.1741
45	1.5052	1.382	0.1232
46	1.4771	1.209	0.2681
47	1.5682	1.389	0.1792
48	1.5563	1.426	0.1303
49	1.0000	1.110	–0.1100
50	1.0792	1.013	0.0662
51	1.1139	1.008	0.1059
52	0.9542	1.026	–0.0718
53	1.0414	0.938	0.1034
54	1.0000	0.857	0.1430
55	0.9031	0.811	0.0921
56	0.9542	1.053	–0.0988
57	0.6990	0.824	–0.1250
58	0.7782	1.004	–0.2258
59	1.1139	1.230	–0.1161
60	1.3222	1.211	0.1112
61	1.2304	1.174	0.0564
62	0.9031	0.831	0.0721
63	1.0792	1.059	0.0202
64	0.9542	1.037	–0.0828
65	0.7782	1.133	0.3548
66	0.8451	0.880	–0.0349
67	0.9031	0.880	0.0231
68	0.8451	0.749	0.0961
69	1.0414	1.396	–0.3546
70	0.9031	0.860	0.0431
71	0.5185	0.541	–0.0225
72	0.3802	0.553	–0.1728
73	0.3979	0.597	–0.1991
74	0.4914	0.484	0.0074
75	0.7324	0.777	–0.0446
76	0.7853	0.684	0.1013
77	0.8129	0.789	0.0239
78	0.7924	0.658	0.1344
79	0.6990	0.681	0.0180
80	0.6628	0.313	0.3498
81	0.7404	0.761	–0.0206

to be continued

Continuation of Table 6

1	2	3	4
82	0.7993	0.771	0.0283
83	0.7076	0.458	0.2496
84	–0.0458	–	–
85	0.9542	1.035	–0.0808
86	0.8451	1.046	–0.2009
87	1.0792	1.088	–0.0088
88	0.9031	0.976	–0.0729
89	1.0792	1.247	–0.1678
90	1.1461	1.154	–0.0079
91	1.2553	1.259	–0.0037
92	1.1761	1.138	0.0381
93	1.1139	1.159	–0.0451
94	1.0000	0.804	0.1960
95	1.0410	1.232	–0.1910
96	0.8460	1.244	–0.3980
97	0.9542	1.057	–0.1028
98	0.7782	0.947	–0.1688

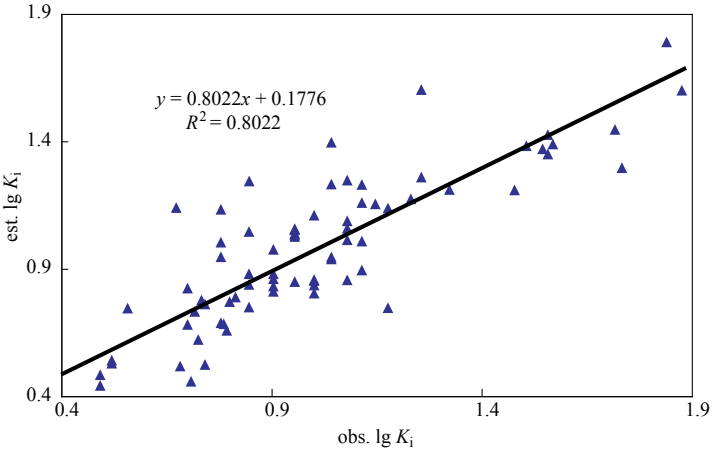

Fig. 3. Correlation of observed and estimated lg K_i using model No 14

RESULTS AND DISCUSSION

A perusal of Table 2 shows that all the derivatives possessed inhibitory constants in the range of 5 –12 nM against ChC, while the range for hydroxamate moieties is found as 15–30 nM. Table 3 shows that the magnitude of all the topological indices increases with the increase in the size, shape and bulk of the compounds used.

The correlation matrix as recorded in Table 4 is important in the sense that it represents interrelationship between the two variables as well as the relationship of the parameters with the activity. In addition, one can use the correlation matrix for investigating multicollinearity. Any data in the correlation matrix with a value greater than 0.4 is usually indicative of multi-collinearity. The value 0.9 indicates high collinearity.

A perusal of Table 4 yields the following information:

(i) W is highly correlated with $^1\chi$, Sz and lg RB;

(ii) $^1\chi$ is highly correlated with Sz, lg RB;

(iii) J is correlated with χ_{eq};

(iv) Sz is highly correlated with W, $^1\chi$ and lg RB;

(v) lg RB is highly correlated with W, Sz, $^1\chi$;

(vi) J is non-correlated with any of the topological indices used;

(vii) Except the indicator parameter IP_2 no other indicator parameters or topological indices correlates well with the activity.

From the above results we conclude the following:

(i) No one-variable model is possible for modelling the activity;

(ii) If any two or more topological indices among W, Sz, $^1\chi$ and lg RB are present in the model, then the model may suffer from the defect due to colinearity;

(iii) J, χ_{eq}, IP_1, IP_3 and IP_4, can be very conveniently used for obtaining multiple parametric model so that no multi-colinearity defect will be present;

(iv) Presence of hydroxamate acid function namely –NHOH is very much beneficial for the exhibition of the activity.

With the aforementioned information we have subjected the data to regression analysis following maximum R^2 method[13]. The results are presented in Table 5 and give the following informations:

(i) There are six one-variable models none of which yield statistically significant results;

(ii) All the one-variable models have equally good statistics;

(iii) The Balaban index J fails to correlate with the activity;

(iv) There are six two-variable models and all of them are statistically significant;

(v) Among the 4 bi-parametric model the model containing $^1\chi$ and IP_2 gave the best results. This model is found as below:

$$\lg K_i = -0.1446\ (\pm 0.0152)\ ^1\chi + 0.5537\ (\pm 0.0487)\ IP_2 + 2.5299 \qquad (1)$$

$$n = 98,\ R = 0.8320,\ \text{se} = 0.2289,\ F = 97.843.$$

The negative coefficient of $^1\chi$ indicates that first order branching is not favourable for the exhibition of the activity. The coefficient of the indicator parameter IP_2 is positive. This indicator accounts for the presence/absence of hydroxamic function –NHOH. The positive coefficient of IP_2 indicates that hydroxamic function is ben-

eficial for the exhibition of the activity. That is, compared to carboxylic acid their hydroxamates are more active;

(vi) Similar to two-parametric models we have 4 three-parametric models for modelling the activity. All these models are significantly better than the two-variable models discussed above. Though more or less all the 4 tri-parametric models appear to be equally good, the model containing $^1\chi$, lg RB and IP_2 gave better results. This model is found as below:

$$\lg K_i = -0.4113\ (\pm 0.0488)\ ^1\chi + 0.0021\ (\pm 3.6352\times10^{-4})\ \lg RB + 0.5914\ (\pm 0.0424)\ IP_2 + 4.7914 \quad (2)$$

$$n = 90,\ R = 0.8809,\ \text{se} = 0.1964,\ F = 99.264.$$

The coefficients of both $^1\chi$ and IP_2 are the same as in equation (1) and, therefore, they carry same physical significance. The topological index lg RB also accounts for branching and like $^1\chi$ its coefficient should have been negative. The change in sign is probably due to high collinearity between $^1\chi$ and lg RB. It is worthy to mention that by the introduction of lg RB in equation (1) the quality of regression is increased from $R = 0.8320$ to $R = 0.8809$. Thus, lg RB is responsible for the improvement of the quality of regression;

(vii) There are two four-parametric models with slight improvement in the quality of correlation. Here, the model containing $^1\chi$, lg RB, IP_1 and IP_2 is found to give better results:

$$\lg K_i = -0.4152\ (\pm 0.0487)\ ^1\chi + 0.0021\ (\pm 3.6329\times10^{-4})\ \lg RB + 0.0058\ (\pm 0.0428)\ IP_1 + 0.5931\ (\pm 0.0422)\ IP_2 + 4.7911 \quad (3)$$

$$n = 90,\ R = 0.8836,\ \text{se} = 0.1955,\ F = 75.662.$$

The physical significance of the parameters $^1\chi$, lg RB and IP_2 is the same as discussed above. A slight improvement in the quality of regression is due to the addition of IP_1 whose coefficient is positive. Since IP_1 stands for the aromatic nucleus at R, the positive coefficient indicates that the presence of aromatic nucleus at R is favourable for the exhibition of the activity;

(viii) There are 3 five-parametric models all having slightly better statistics than the models discussed above. Out of the 3 five-parametric models, the model containing $^1\chi$, lg RB, IP_1, IP_2 and χ_{eq} is found to yield better results. The improvement is due to added χ_{eq} parameter whose coefficient in the model is negative. This indicates that the electronegativity is not favourable for the exhibition of the activity. This model is found as below:

$$\lg K_i = -0.4737\ (\pm 0.0576)\ ^1\chi + 0.0026\ (\pm 4.5319\times10^{-4})\ \lg RB + 0.0499\ (\pm 0.0424)\ IP_1 + 0.6058\ (\pm 0.0422)\ IP_2 - 0.6507\ (\pm 0.3549)\ \chi_{eq} + 6.8657 \quad (4)$$

$$n = 90,\ R = 0.8884,\ \text{se} = 0.1928,\ F = 62.884.$$

The physical significance of the terms involved in equation (4) is discussed above;

(ix) Successive regression analysis yielded 3 six-parametric models all with improved statistics and yielding the best six-paremetric model containing $^1\chi$, lg RB, χ_{eq}, IP_1, IP_2 and W as the correlating parameters. This model is found as below:

$$\lg K_i = -0.0074\ (\pm 0.0028)\ ^1\chi + 0.0813\ (\pm 0.0456)\ \lg RB + 0.6031\ (\pm 0.0417)\ IP_1 - 1.1090\ (\pm 0.4368)\ IP_2 - 0.0010\ (\pm 5.7892\times10^{-4})\ \chi_{eq} - 0.5518\ (\pm 0.0722)\ W + 8.3871 \quad (5)$$

$$n = 90,\ R = 0.8926,\ se = 0.1904,\ F = 54.226.$$

Once again the physical significance of the parameters $^1\chi$, lg RB, χ_{eq}, IP_1 and IP_2 is the same as discussed above. The improvement in the quality of correlation is due to the addition of W, the negative coefficient of W may be attributed for the high colinearity between $^1\chi$ and W. Otherwise it carries the same physical significance as that of $^1\chi$;

(x) Finally, the stepwise regression gave the seven-parametric model containing W, $^1\chi$, lg RB, IP_1, IP_2, IP_4 and χ_{eq}. This model is found as below:

$$\lg K_i = -0.0012\ (\pm 5.9446\times10^{-4})\ W - 0.5776\ (\pm 0.0737)\ ^1\chi + 0.0085\ (\pm 0.0028)\ \lg RB + 0.1102\ (\pm 0.0491)\ IP_1 + 0.6063\ (\pm 0.0414)\ IP_2 + 0.0976\ (\pm 0.0646)\ IP_4 - 1.1904\ (\pm 0.4368)\ \chi_{eq} + 8.7310 \quad (6)$$

$$n = 90,\ R = 0.8957,\ se = 0.1890,\ F = 47.521.$$

The improvement in the quality of correlation is due to the added indicator parameter IP_4. This indicator parameter is due to presence/absence of $-SO_2R$ directly attached to N of the parent structure. Thus, the presence of $-SO_2R$ at N of the parent structure is favourable for the exhibition of the activity.

PREDICTIVE POWER OF THE MODELS

In order to estimate the predictive power of the models, we have calculated the Pogliani quality factor[14] Q which is defined as the ratio of correlation coefficient to that of standard error of estimation. That is, $Q = R/\text{se}$ indicating that higher the R, lower the se, higher will be Q. High value of Q indicates high quality of the model. The Q values calculated for each of the proposed models are given in Table 5 indicating that the model expressed by equation (6) has the highest predictive power.

In order to confirm our findings we have calculated lg K_i from equation (6) and compared them with the observed values of lg K_i. Such a comparison is given in Table 6. The residue, i.e. the difference between the observed and calculated lg K_i indicates this to be the best model.

In order to confirm predictive power of the model we have calculated predictive correlation coefficient (R_{pred}^2) from the plot of observed lg K_i against calculated lg K_i and is found to be 0.8022 ($R_{pred}^2 = 0.8022$). Such correlation is demonstrated in Fig. 3.

The Wiener index (*W*). The Wiener index (W) is widely used topological index[15]. It is based on the vertex-distances of the respective molecular graph.

Molecular graph can be denoted by *G* and having $v_1, v_2, v_3, ..., v_n$ as its vertices. Let $d(v_i,v_j|G)$ stands for the shortest distance between the vertices v_i and v_j. Then the Wiener index is defined as:

$$W = W(G) = 1/2 \sum_{i=1}^{n} \sum_{j=1}^{n} d(v_i,v_j|G) \tag{7}$$

The Szeged index (Sz). Let e be an edge of the molecular graph *G*. Let $n_1(e|G)$ be the number of vertices of *G* lying closer to one end of *e*; let $n_2(e|G)$ be the number of vertices of *G* lying closer to the other end of *e*. Then the Szeged index[16,17] (Sz) is defined as:

$$Sz(G) = Sz = \sum_{e} n_1(e|G)\, n_2(e|G) \tag{8}$$

with the summation going over all the edges of *G*.

In cyclic graphs, there are edges equidistant from both the ends of edge *e*; by definition of Sz such edges are not taken into account.

First order connectivity index ($^1\chi$). The connectivity index $\chi = \chi(G)$ of a graph *G* is defined by Randic[18] as under:

$$\chi = \chi(G) = \sum_{ij} [\delta_i\, \delta_j]^{-0.5} \tag{9}$$

where δ_i and δ_j are the valence of a vertex *i* and *j*, equal to the number of bonds connected to the atoms *i* and *j*, in *G*.

lg RB. The lg RB has been calculated by the method as described in literature[19–21].

The Balaban index (J). The Balaban index, J (the average distance sum connectivity index) is defined[22] by:

$$J = J(G)\ \frac{M}{\mu + 1} \sum_{\text{bonds}} (d_i\, d_j)^{-1/2} \tag{10}$$

where *M* is the number of bonds in a graph *G*, μ – the cyclomatic number of *G* and d_i's(i=1,2,3,...,N) – the distance sums (distance degrees) of atoms in *G* such that

$$d_i = \sum_{j=1}^{N} (D)_{ij} \tag{11}$$

The cyclomatic number μ of *G* indicates the number of independent cycles in *G* and is equal to the minimum number of cuts (removal of bonds) necessary to convert

a polycylic structure into an acyclic structure:

$$\mu = M - N + 1. \quad (12)$$

One way to compute the Balaban index (J) for hetero-system is to modify the elements of the distance matrix for hetero-system as follows:

(i) The diagonal elements:

$$(D)_{ij} = 1 - (Z_c/Z_i) \quad (13)$$

where $Z_c = 6$ and Z_i = atomic number of the given element.

(ii) The off-diagonal elements:

$$(D)_{ij}\, d_i = \sum_r k_r \quad (14)$$

where the summation is over all bonds. The bond parameter k_r is given by:

$$k_r = 1/b_r\, (Z_c^2/Z_i\, Z_j)$$

where b_r is the bond weight with values: 1 for single bond, 2 for double bond, 1.5 for aromatic bond and 3 for triple bond.

Regression analysis. Modelling is performed using maximum R^2 method following step-wise regression analysis[13].

REFERENCES

1. A. SCOZZAFAVA, C. T. SUPURAN: Protease Inhibitors: Synthesis of *Clostridium histolyticum* Collagenase Inhibitors Incorporating Sulfonyl-Alanine Hydroxamate Moieties. Bioorg. Med. Chem. Letters, **10**, 499 (2000).
2. J. J. REIDY, B. M. GEBHARDT, H. E. KAUFMAN: The Collagen Shield. A New Vehicle for Delivery of Cyclosporin A to the Eye. Cornea, **9** (3), 196 (1990).
3. M. R. SAUSCH, T. P. O'BRIEN, J. D. DICK, J. D. GOTTSCH: Topical Ciprofloxacin Treatment of *Pseudomonas keratitis* in Rabbits. Arch. Opthalmol., **106**, 279 (1988).
4. M. T. DORIGO, R. De NATALE, P. A. MIGLIOLI: Collagen Shields Delivery of Netilmicin: A Study of Ocular Pharmacokinetics. Chemotherapy, **41**, 1 (1995).
5. V. K. AGRAWAL, P. V. KHADIKAR: Modelling of Carbonic Anhydrase Inhibitory Activity of Sulfonamides Using Molecular Negentropy. Bioorg. Med. Chem. Letters, **13** , 447 (2003).
6. V. K. AGRAWAL, R. SHARMA, P. V. KHADIKAR: QSAR Studies on Carbonic Anhydrase Inhibitors: A Case of Ureido and Thioureido Derivatives of Aromatic/Heterocyclic Sulfonamides. Bioorg. Med. Chem., **10**, 2993 (2002).
7. A. SAXENA, V. K. AGRAWAL, P. V. KHADIKAR: Estimation of Antitumor Activity of Sulfonimidamide Analogous of Oncolytic Sulfonylureas. Oxid. Commun., **26** (1), 9 (2003).
8. P. V. KHADIKAR, B. W. CLARE, A. T. BALABAN, C. T. SUPURAN, V. K. AGRAWAL, J. SINGH, A. K. JOSHI, M. LAKHWANI: QSAR Modeling of Carbonic Anhydrase-I, -II and -IV Inhibitory Activities: Relative Correlation Potential of Six Topological Indices. Revue. Roumaine de Chimie, **51**, 703 (2006).
9. A. SCOZZAFAVA, C. T. SUPURAN: Protease Inhibitors: Synthesis of *Clostridium histolyticum* Collagenase Inhibitors Incorporating Sulfonyl-L-Alanine Hydroxamate moieties. Bio. Med. Chem. Lett., **10**, 499 (2000).

10. J. SINGH, S. SINGH, S. THAKUR, M. LAKHWANI, P. V. KHADIKAR, V. K. AGRAWAL, C. T. SUPURAN: QSAR Study on Murine Recombinant Isozyme mCAXIII: Topological vs Structural Descriptors. ARKIVOC, **XIV**, 103 (2006).
11. V. K. AGRAWAL, M. BANERJI, M. GUPTA, J. SINGH, P. V. KHADIKAR, C. T. SUPURAN: QSAR Study on Carbonic Anhydrase Inhibitors: Water-soluble Sulfonamides Incorporating β-Alanyl Moieties, Possessing Long Lasting-intra Ocular Pressure Lowering Properties – A Molecular Connectivity Approach. Eur. J. Med. Chem., **40**, 1002 (2005).
12. V. K. AGRAWAL, J. SINGH, A. PANDEY, P. V. KHADIKAR: Modeling of Inhibitory Activities of Sulfanil-Amide Schiff's Bases Using Physicochemical Properties. Oxid. Commun., **29** (4), 803 (2006).
13. S. CHATERJEE, A. S. HADI, B. PRICE: Regression Analysis by Examples. 3rd ed. Wiley, New York, 2000.
14. L. POGLIANI: Structure-Property Relationships of Amino Acids and Some Dipeptides. Amino Acids, **6**, 141 (1994).
15. H. WIENER: Structural Determination of Paraffins Boiling Points. J. Am. Chem. Soc., **69**, 17 (1947).
16. P. V. KHADIKAR, S. KARMARKAR, V. K. AGRAWAL, J. SINGH, A. SHRIVASATAVA, I. LUKOVITS, M. V. DIUDEA: Szeged Index – Applications for Drug Modeling. Letters Drug Design Discovery, **2**, 606 (2005).
17. M. V. DIUDEA (Ed.): QSPR/QSAR Studies by Molecular Descriptors. Babes-Bolyai University, Cluj, Romania, 2000.
18. M. RANDIC: On Characterization of Molecular Branching. J. Am. Chem. Soc., **97**, 6609 (1975).
19. L. B. KIER, L. H. HALL: Molecular Connectivity in Structure-Activity Relationship. Wiley, New York, 1986.
20. L. B. KIER, L. H. HALL: Molecular Structure Description. Academic Press. New York, 1999.
21. R. TODESCHINI , V. COSONNI: Handbook of Molecular Descriptors. Wiley-VCH, Weinheim, 2000; M. KARELSON: Molecular Descriptors in QSAR/QSPR. J. Wiley & Sons, New York, 2000.
22. A. T. BALABAN: Highly Discriminating Distance-based Topological Indices. Chem. Phys. Lett., **89** , 399 (1982); J. DEVILLERS, A. T. BALABAN: Topological Indices and Related Descriptors in QSAR and QSPR. Gordon and Breach, The Netherlands, 1999, p. 871.

Received 23 December 2008
Revised 4 February 2009